Title
DESIGN AND OPERATION OF MINIMALLY ACTUATED MEDICAL EXOSKELETONS FOR INDIVIDUALS WITH PARALYSIS

Author
Tung, Wayne Yi-Wei

Publication Date
2013

Peer reviewed|Thesis/dissertation

Design and Operation of Minimally Actuated Medical Exoskeletons for Individuals with Paralysis

By

Wayne Yi-Wei Tung

A dissertation submitted in partial satisfaction of the

requirements for the degree of

Doctor of Philosophy

in

Engineering – Mechanical Engineering

in the

GRADUATE DIVISION

of the

UNIVERSITY OF CALIFORNIA, BERKELEY

Committee in charge:

Professor Homayoon Kazerooni, Chair
Professor Hari Dharan
Professor Ruzena Bajcsy

Fall 2013

Design and Operation of Minimally Actuated Medical Exoskeletons for Individuals with Paralysis

By

Wayne Yi-Wei Tung

Abstract

Design and Operation of Minimally Actuated Medical Exoskeletons for
Individuals with Paralysis

by

Wayne Yi-Wei Tung

Doctor of Philosophy in Engineering – Mechanical Engineering

University of California, Berkeley

Professor Homayoon Kazerooni, Chair

Powered lower-extremity exoskeletons have traditionally used four to ten powered degrees of freedom to provide ambulation assistance for individuals with spinal cord injury. Systems with numerous high-impedance powered degrees of freedom commonly suffer from cumbersome walking dynamics and decreased utility due to added weight and increased control complexity. This work proposes a new approach to powered exoskeleton design that minimizes actuation and control complexity through embedding intelligence into the hardware. Two novel, minimally actuated exoskeleton systems (the Austin and the Ryan) are presented in this dissertation. Unlike conventional powered exoskeletons, the presented devices use a single motor for each exoskeleton leg in conjunction with a unique hip-knee coupling system to enable their users to walk, sit, and stand. The two types of joint coupling systems used are as follows.

The Austin Exoskeleton employs a bio-inspired mechanical joint coupling system designed to mimic the biarticular coupling of human leg muscles. This system allows a single actuator to power both hip and knee motions simultaneously. More specifically, when the mechanical hamstring and rectus femoris of the exoskeleton are activated, power from the hip actuator is transferred to the knee, generating synchronized hip-knee flexion and extension. The coupling mechanism is switched on and off at specific phases of the gait (and the sit-stand cycle) to generate the desired joint trajectories. The device has been proven to be successful in assisting a complete T12 paraplegic subject to walk, sit, and stand.

The Ryan Exoskeleton (also called the Passive Knee Exoskeleton) uses dynamic joint coupling. Dynamic joint coupling refers to a method of generating knee rotation through deliberate swinging of the hip joint. This minimalistic system is the first powered exoskeleton that weighs less than 20 pounds and has a compact form factor that more closely resembles a reciprocating

gait orthosis than a conventional exoskeleton. The Passive Knee Exoskeleton has been validated by several SCI test pilots with injury levels ranging from T5 to T12. The lightweight, ambulation-centric assistive device have been tested to be able to comfortably reach an average ambulation speed of 0.27 m/s and have demonstrated high levels of maneuverability. The dynamic joint coupling paradigm has been proven to be effective especially for newly injured individuals who have not yet developed significant amounts of joint contracture or sustain high levels of spasticity.

Overall, this dissertation focuses on the design and operation of the Austin and Ryan Exoskeletons.

Table of Contents

List of Figures

List of Tables

Acknowledgements

First and foremost, I want to thank my research advisor, Professor Homayoon Kazerooni, for making this amazing five-year journey possible. I feel extremely blessed to have a mentor who has not only been a great source of inspiration for my work but has also kindly encouraged me and looked out for my best interest every step along the way. His guidance and support over the years mean a great deal to me and I am truly grateful for his hospitality and kindness.

I would also like to express my gratitude to the members of my dissertation committee and qualifying committee: Professor Hari Dharan, Professor Ruzena Bajcsy, Professor David Rempel, Professor Dennis Lieu, and Professor Kyriakos Komvopoulos. I really appreciate the countless hours they have spent patiently helping me and guiding me over the years.

I want to thank all of my colleagues and friends in the Robotics and Human Engineering Laboratory who have made my Ph.D. journey extremely fun and memorable. In particular, I want to thank Michael McKinley, Minerva Pillai, Jason Reid, Yoon Jeong, and Josh Cherian for laboring with me for countless hours and through numerous late nights in the basement of Etcheverry Hall. Their excellence, dedication, and camaraderie have made all of the amazing projects of Kaz Lab possible. I am honored to have had the opportunity to work with every single one of them.

I am also grateful for the hard work and friendship of the newer generation of HEL: Dong-Jin Hyun, Lee-Huang Chen, Stephen McKinley, Kyunam Kim, Patrick Barnes, Nick Um, Christina Yee, Brad Perry, and Meiting Wu. My appreciation further extends to all of the HEL undergrads. Specifically to Alex Wen, Nate Poon, Daniel Driver, Mimi Lan, Matt Fisher, Chris Guichet, Leonard Carrier, Jonathan McKinley, Leo Qu, and Yasemin Sarigul-Klijn. They have provided tremendous help in machining, maintaining hardware, and performing many other tasks. My sincere gratitude also goes to the test pilots who have patiently worked with us and provided invaluable feedback along the way.

I want to thank my family, especially my parents, for their support and encouragement over the years. I am thankful for their unconditional love and their selfless dedication to me every step along the way. My gratitude towards them goes beyond what words can express. My appreciation further extends out to all of my aunts and uncles, especially Uncle Harry. They have collectively taught me at a young age to appreciate the importance of education and have truly been an invaluable source of guidance and encouragement for me.

Above all, I want to thank God for all of His blessings. He alone has made everything possible and I am grateful for His infinite love and mercy.

Chapter 1
Introduction

1.1 Motivation

According to the National Spinal Cord Injury Statistical Center (NSCISC), in 2012 there are approximately 270,000 individuals in the United States who are suffering from Spinal Cord Injury (SCI), with an estimated 12,000 new injuries sustained each year [1]. Out of this number, an estimated 43% result in paraplegia (116,000 total and 5160 per year). Depending on the severity of the injury, SCI can cost between $300,000 and $950,000 within the first year of the injury, and between $40,000 and $165,000 each year after that [2].

The prevalence and the nature of this type of injury have summoned much national attention, specifically due to the injury's immediate debilitating effects and its tendency to have detrimental long term economic and health consequences. Although, the loss of mobility and accessibility have been surveyed to be the primary concerns amongst persons with paraplegia, the primary physical injury is only the beginning of a larger medical problem of a significant increase in risk of incurring secondary injuries [3]. Due to the inability to stand and walk, and the extensive amount of time SCI patients commonly spend sitting in wheelchairs, these individuals are at a drastically higher risk for developing many severe health predicaments [4], including the following:

- Acute pressure ulcer development
- Bone density loss and osteoporosis
- Muscular atrophy, muscle spasticity, decreased joint range of motion
- Increased incidence of urinary tract infection
- Reduced digestive and bowel function
- Impaired respiratory and cardiovascular functions

Studies have shown that being in an upright position several hours a day can greatly decrease the likelihood for SCI patients to sustain secondary injuries as well as significantly increasing the overall quality of life and life expectancy [5]. For this reason, physicians and therapists commonly recommend rehabilitation therapy or various types of lower extremity orthoses or assistive equipments (such as the standing frame) for SCI patients after their initial injury. Recent advancements in robotic technologies combined with the high financial cost associated with rehabilitation and secondary injury medical treatments have incentivized the development of powered medical exoskeleton systems designed to improve the health conditions of SCI patients. The refinement of this technology to further enhance system ease of use, reduce hardware weight, and reduce device cost is gradually leading to the feasibility of widespread commercialization of this technology in the world market.

1.2 Exoskeleton Prior Art

<u>Passive Orthoses</u>

Passive lower limb orthoses are some of the earliest instruments designed aiming towards restoring bipedal mobility for individuals suffering from lower extremity paralysis. Today, these passive orthoses are still the most common type of assistive devices for paraplegics and they are frequently recommended by physicians and therapists as means to avert the onset of secondary injuries. The most basic type of passive orthotics is the long leg braces, also known as knee-ankle-foot orthoses (KAFOs). As shown in Figure 1-1, these braces are rigidly fastened to the user's legs with the intention to lock both the knee joints and the ankle joints against knee flexion, dorsiflexion, and plantar flexion. With these joint degrees of freedom constrained and with the assistance of crutches, walkers, or parallel bars, the user can achieve a quasi bipedal gait by swinging one leg in front of the other, utilizing a great deal of upper body strength and abdominal control, if unimpaired after the injury.

Figure 1-1: Examples of common passive orthoses.
[a] Long leg braces (Left)   [b] RGO (Right)

A slightly more advanced variation of the long leg braces called the reciprocating gait orthoses (RGO) includes a torso unit as shown in Figure 1-1b. The most distinguishing feature of the RGO is the metal link mounted at the back of the torso unit which acts as a transmission system that reciprocally couples the motion of the two hip joints. In other words, this passive transmission system pairs the motion of the hip joints such that when one leg goes through hip extension the other leg is driven to go through hip flexion, and vice versa. This feature is particularly helpful for paraplegic individuals with less upper body control because the act of leaning forward over the stance leg helps generate forward propulsion for the swing leg. With the RGO mechanism, a longer stride length can be attained while reducing the energy expenditure associated with manual leg swing. For additional information on the RGO, the reader is referred to [6–8].

The RGO, as well as other types of passive orthoses, are commonly prescribed and highly recommended by doctors due to the wide variety of health benefits they provide [9]. The relatively lower cost of passive orthotics (ranging from $4,000 to $10,000) makes these devices more practical for personal ownership and increases the accessibility and the likelihood of post-injury rehabilitation. In contrast to periodic visits to rehabilitation centers, personal rehabilitation orthotics can be less expensive, more convenient, and can be used at one's own privacy.

In spite of the aforementioned benefits, passive orthosis also has its limitations. Studies have shown that ambulation with the assistance of the RGO is still largely energetically inefficient (requiring approximately 14 times more work in comparison to normal ambulation) [10,11]. Performance issues such as rapid user fatigue and sluggish ambulation rate have contributed to a low long-term adoption rate of the RGO. An extensive study conducted by Sykes et al. has shown that only 29 percent of RGO users continued usage after an average of 5.4 years [12]. It is interesting that despite a relatively high level of reported perceived improvements in physical health through usage (approximately 65 percent), a much smaller fraction actually commits to long-term and persistent use. This shows that the benefits of passive rehabilitation devices can often be outweighed by their shortcomings and additional performance improvements must be made to achieve a higher long-term adoption rate.

Powered Exoskeletons

While the concept of a low-cost personal rehabilitation device is highly appealing, the current state of the abovementioned passive orthoses technology does not quite have the level of performance that would instigate more widespread use. In the effort to improve ambulation efficiency, several research groups began developing powered exoskeleton systems with actuators for locomotion assistance. Some of the earliest attempts date back to the early 1970s and the technology continued to progress along with the advancement of peripheral technologies (actuators, sensors, batteries, computers, etc.) [13–18].

Powered exoskeleton technology has made tremendous grounds in the recent years with several systems emerging in the commercial market having the potential for personal ownership. Figure 1-2 shows four of the most well-known powered exoskeletons today: the eLEGS, ReWalk, Vanderbilt Exoskeleton, and the Rex. The eLEGS is a device that is currently being developed by Ekso Bionics located in Berkeley, California (formerly known as Berkeley Bionics). This device evolved from several military exoskeletons of UC Berkeley's Berkeley Robotics and Human Engineering Laboratory, namely, the Human Universal Load Carrier (HULC) and the Berkeley Lower Extremity Exoskeleton (BLEEX) [19–21]. This medical device uses four electric motors to power the knee and the hip joint motion along the sagittal plane while constraining all other joint degrees of freedom [22]. With balance aids such as crutches or walkers, paralyzed individuals can use the device to achieve locomotion without experiencing high level of fatigue as observed with passive orthotic users. The ReWalk by Argo Medical Technologies and the Vanderbilt University Exoskeleton also operate in a similar fashion, utilizing hip and knee actuations [23–25]. The biggest difference between these three devices is in the user interface, which varies from one or a combination of push buttons, crutch position sensors, torso orientation sensors, and ground reaction force sensors.

(a) eLEGS **(b) ReWalk** **(c) Vanderbilt** **(d) Rex**

Figure 1-2: Powered Exoskeleton Systems

The Rex exoskeleton, on the other hand, operates on a completely different paradigm. This system, made by a New Zealand based company called Rex Bionics, utilizes a total of ten joint actuators to power the hip, the knee, and the ankle along both the frontal and sagittal planes [26]. The more elaborate actuation scheme generates a very slow and controlled walking gait by putting the user through a series of quasi-statically balanced postures. Balancing aids are not necessary to operate the Rex, as shown in Figure 1-2d, however, there are tradeoffs such as drastically slower ambulation and increase in overall device weight [27].

Table 1-1 summarizes and compares some of the specifications of the aforementioned devices. (Numbers shown in the table are accurate as of October 2012)

	Device Name	Powered Degrees of Freedom	Device Weight	Approximate Cost
1	Rex	10 (2 Hip, 1 Knee, 2 Ankle)	85 Pounds	$150,000
2	eLEGS	4 (1 Hip, 1 Knee)	45 Pounds	$100,000
3	ReWalk	4 (1 Hip, 1 Knee)	45 Pounds	$100,000
4	Vanderbilt	4 (1 Hip, 1 Knee)	27 Pounds	N/A
5	RGO	0	15 Pounds	$10,000

Table 1-1: Exoskeleton system specification summary and comparison

Functional Electrical Stimulation (FES) and FES Hybrids

Another type of mobility technology uses Functional Electrical Stimulation (FES). FES employs electric stimulation to activate leg muscle contractions [28]. When muscle activation is synchronized properly, this method has shown the capacity to enable paraplegics to ambulate with the assistance of walkers. There are several advantages with FES.

1. The patient's muscles are used in powering the gait, which has many health benefits such as increased blood circulation, increase bone loading, decrease in muscle atrophy, and so forth.
2. The use of FES can be more convenient since it does not require the donning and doffing of exoskeleton bracing.
3. The use of leg muscles eliminates the need for external actuation, which decreases the overall weight of the system.

Despite these advantages, FES has a major setback of causing rapid muscle fatigue, which drastically limits the effectiveness of most FES-aided systems [29]. In the effort to address this limitation, several research groups have developed FES hybrid systems that utilize FES in combination with passive orthosis [30,31]

1.3 Research Objective and Thesis Contributions

As shown in Table 1-1, there is a drastic increase in weight and cost going from a passive orthotic device to a powered exoskeleton. It shows that in the effort to actuate and improve the performance of passive orthotics, powered exoskeleton developers have lost some of the most desirable properties of passive orthoses. For instance, one of the main motivations behind adding actuation and improve operation efficiency was to promote more widespread use, however, a tenfold increase in device cost will most likely generate the opposite effect due to the decreased accessibility. Additionally, tripling and quintupling the device weight (and thus the device size) will also drastically decrease the maneuverability and portability of the system, which in turn affects the level of user independence.

In light of this, the research objective is to explore the feasibility of other methods of actuation that could potentially be more effective in providing gait assistance while maintaining the recognized positive attributes of passive orthoses.

The author's work can be categorized into the following sections.

1.3.1 Austin Exoskeleton: Minimize Actuation through Hip-Knee Coupling

The Austin Project began with an objective to build a simpler and lighter powered exoskeleton that only needs to perform a single task: generate a basic forward walking gait. Due to the cyclic nature of the human gait and the impracticality of using the exoskeleton for elaborate lower extremity motions, actuating both the hip and knee joints appears to be redundant. A bio-inspired joint coupling system that simulates biarticular leg muscles was implemented and has been proven to be effective in eliminating the requirement of knee actuation for gait assistance. Additionally, the joint coupling system has also shown the capability to assist the user for sitting and standing operations.

1.3.2 Ryan Exoskeleton: Minimize Actuation through Dynamic Coupling

The Ryan exoskeleton was inspired by the gait mechanics of bilateral above-knee amputees. It has been observed that bilateral transfemoral amputees using unactuated knee-ankle prosthetics were able to attain a high level of bipedal mobility and achieving an extremely independent lifestyle. From this observation, it naturally invokes the question of whether knee actuation is essential for powered exoskeletons and whether the same passive-knee ambulation strategy will be effective for paraplegics. The Ryan Exoskeleton utilizes a novel exoskeleton actuation paradigm which takes advantage of dynamic joint coupling to eliminate the need for knee actuation. This system became the first powered exoskeleton that weighs less than 20 pounds and has a compact form factor that more closely resembles an RGO than the conventional exoskeletons.

Chapter 2

Austin Exoskeleton: Biomimetic Actuation

The Austin Exoskeleton is based on a bio-inspired joint motion coupling system that uses a single actuator to power both the hip and knee joint. To facilitate the description of the coupling system, one must first understand the concept of hip-knee coupling. The role hip-coupling and biarticular muscles in human ambulation are described in the first section. After establishing a basic understanding of the concept of hip-knee coupling, the paper then begins the description of gait generation and the joint coupling system hardware. The third section explains how the joint coupling system is used for sitting and standing. The last section will go though the design details of critical exoskeleton components.

2.1 Hip-Knee Coupling and Biarticular Muscles

Hip-knee joint coupling describes the motion where the knee flexes simultaneously with hip flexion and extends simultaneously with hip extension (see Figure 2-1). This coupling behavior has been observed in a wide variety of natural human motions (e.g., walking, sitting, standing, and stair-climbing) [32]. Biarticular muscles such as the hamstring and the rectus femoris have been shown to play a major role in generating this coupled motion. Biarticular muscles differ from monoarticular muscles such that they span over two joints instead of just one, and this unique characteristic allows them to transfer power from one of its spanned joint to another.

Various examples of this biarticular muscle power transfer and coupling motion are described in the literature during human walking [33–36], running and jumping [37–39], and sitting and standing [40]. The direction of power transfer by the biarticular muscles in the lower extremity has been described in [41] to go from the proximal joint to the distal joints, in other words, from hip to knee and from knee to ankle. The coupling mechanism proposed in this paper will be later shown to be consistent with this description.

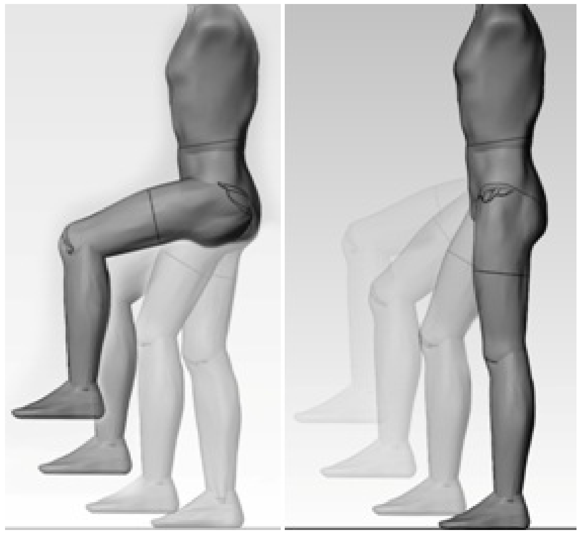

**Figure 2-1: Hip-Knee joint coupling demonstration
Coupled Flexion (Left) Coupled Extension (Right)**

To more clearly illustrate the relationship between joint power transfer and joint coupling, Figure 2-2 shows a simulated human leg motion with an activated hamstring during hip flexion. The simulation was generated by constraining the hamstring to a fixed length while flexing the hip manually. The incremental motion demonstrates how a fixed-length hamstring can generate knee flexion and transfer power from the hip to the knee. The hip and knee angles of the simulated coupling motion are plotted in Figure 2-3. It can be insightful to view the simulation data as a set of joint-angle combinations that produces a specific hamstring length. The chosen starting position dictates the hamstring length of the simulation and a different initial position will generate a series of different leg motions. The gait generation strategy proposed in this paper will take advantage of this behavior to generate a variety of leg motions.

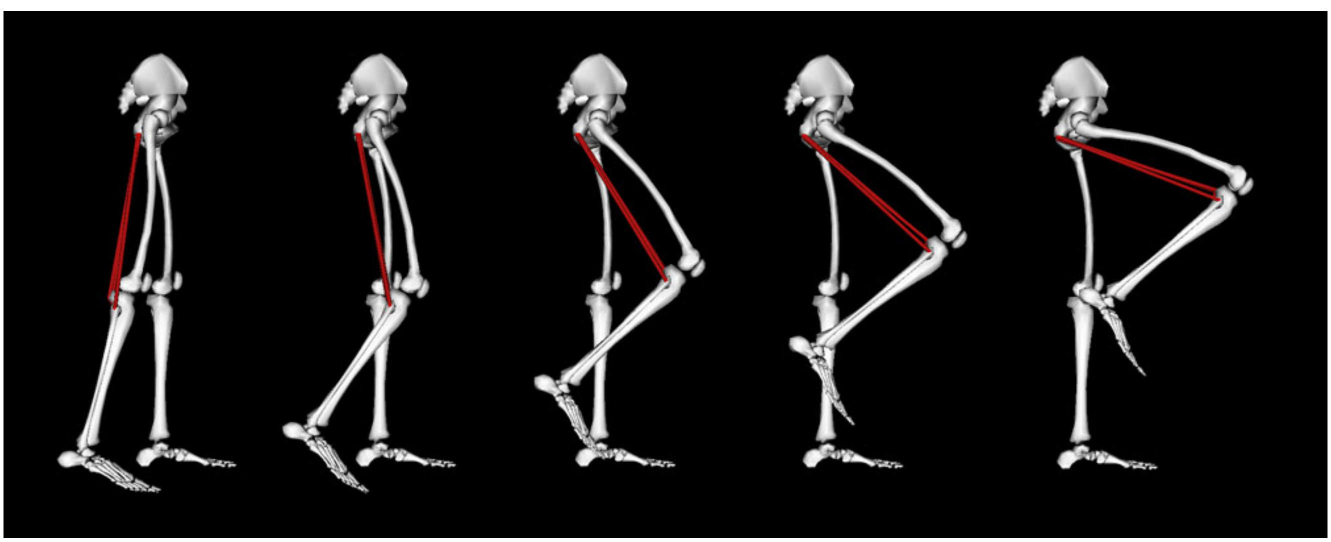

Figure 2-2: Leg motion with fixed hamstring length and hip flexion

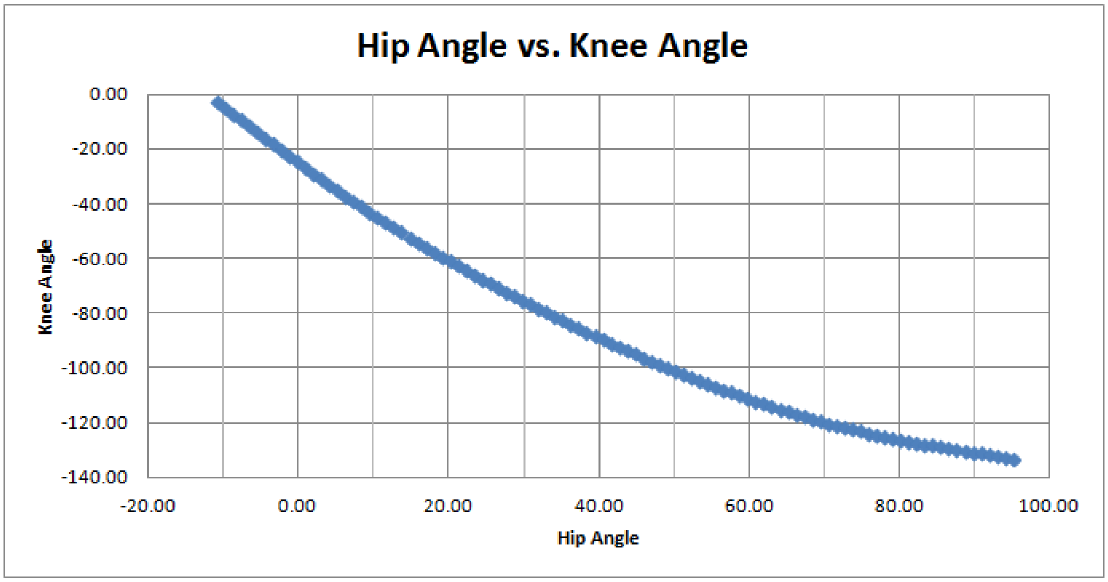

Figure 2-3: Plot of hip and knee angles during coupled hip-knee flexion

2.2 Gait Generation

In the design of an assistive medical exoskeleton device, the primary objective is to provide user-independence, which requires the basic capability of walking and sitting-standing. This section will elaborate on the role of hip-knee coupling during human walking.

2.2.1 Joint Coupling Walking Mechanics

The human gait is most commonly divided into two phases: stance and swing [42]. The stance phase represents the percentage of the gait cycle when the foot is contacting the ground, and the swing phase represents the percentage of the gait cycle when the foot is not contacting the ground. Figure 2-4a shows the traditional two phases of the gait cycle and the corresponding event description.

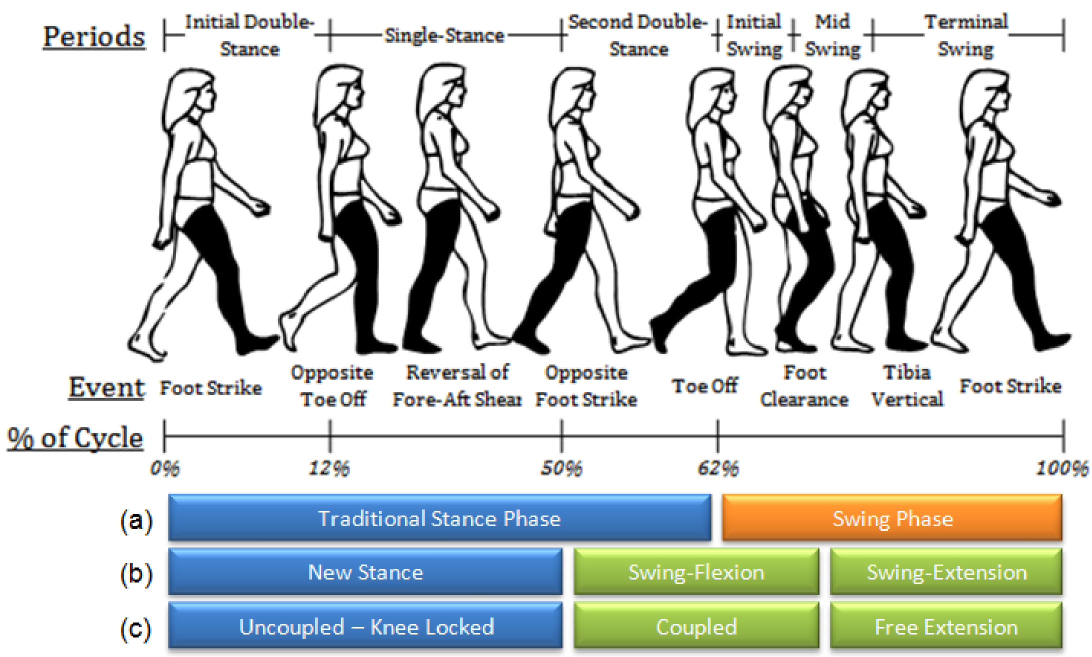

Figure 2-4: Illustration of normal walking cycle events
a) Traditional Gait Cycle Description. b) New Three-Phase Gait Cycle Description
c) Coupling Activation Timing. Image adapted from [42]

To help illustrate the role of hip-knee coupling during walking, it is useful to adopt a new gait cycle description, one that further divides the swing phase into two sub-phases: Swing-Flexion and Swing-Extension. The new three-phase cycle can be described as below:

- PHASE I – New Stance
  This phase is approximately the same as the traditional stance description. During stance, the person's foot is in contact with the ground and the leg is weight bearing. The hip goes through extension while the knee can be approximated to be locked and unpowered. The major difference of this new stance description is that it terminates at maximum hip extension, right before the knee begins to flex (at the onset of Second Double Stance). This stance modification is important for systems without ankle actuation. Reader is referred to Figure 2-4b.

- PHASE II – Swing-Flexion
  Immediately after stance, the gait transitions into the Swing-Flexion phase where the hip reaches maximum extension and begins to flex. In this phase, the knee also flexes to guarantee toe clearance. Recall from the previous section, this phase matches the description of the coupled flexion motion as illustrated in Figure 2-2. This phase begins at maximum hip extension and ends at maximum knee flexion (or maximum toe clearance).

- PHASE III – Swing-Extension
  At maximum knee flexion, the gait goes into the Swing-Extension phase where the knee re-extends to get ready for foot strike. This phase begins at maximum toe clearance and ends at foot strike.

2.2.2 Gait Generation through Hip-Knee Coupling

A new gait generation strategy was proposed based on the three-phase gait cycle where traditional knee actuators are replaced by a joint coupling system. Through this system, the knee motion becomes a function of the hip motion, and the knee is only powered to perform the coupled motion. In this design, the knee has two states: Coupled and Uncoupled.

1. ***Coupled State:*** In the Coupled state, the knee will flex and extend with the hip, powered by a coupling mechanism that transfers power from the hip to the knee. The coupling hardware will be described in full detail in the next section.

2. ***Uncoupled State:*** In the Uncoupled state, the knee default to a locked configuration which requires no power and is completely passive.

A walking gait is generated through toggling between the coupled and uncoupled state, in the following sequence. Refer to Figure 2-4c for graphical depiction.

- STEP I: During stance, the hip-knee coupling system is deactivated and the knee stays locked while the hip goes through extension.

- STEP II: Transitioning into Swing-A, the coupling system engages and activates coupled hip-knee flexion in the same manner as observed in natural human gait.

- STEP III: At the point of maximum toe clearance, the coupling system is deactivated – releasing the shank to be swung forward, the knee extends, locks, and gets ready for stance.

This sequence is repeated for continuous walking cycle.

2.2.3 Exoskeleton Hardware Overview

The AUSTIN exoskeleton suit is shown in Figure 2-5. It consists of two legs and a torso which the user is strapped to by six human machine interface components: shoulder straps, corset, lower back support, thigh straps, knee braces, and foot braces. There are three major functionality hardware components: 1) hip actuation, 2) hip-knee coupler system, and 3) controllable locking knee. A simple wireless user interface that consists of two push buttons is installed on the handle of the stability aids, which is used to operate the exoskeleton. Electrical components such as the computer, wireless communication chip, amplifiers, and batteries are located on the back of exoskeleton as shown in Figure 2-6.

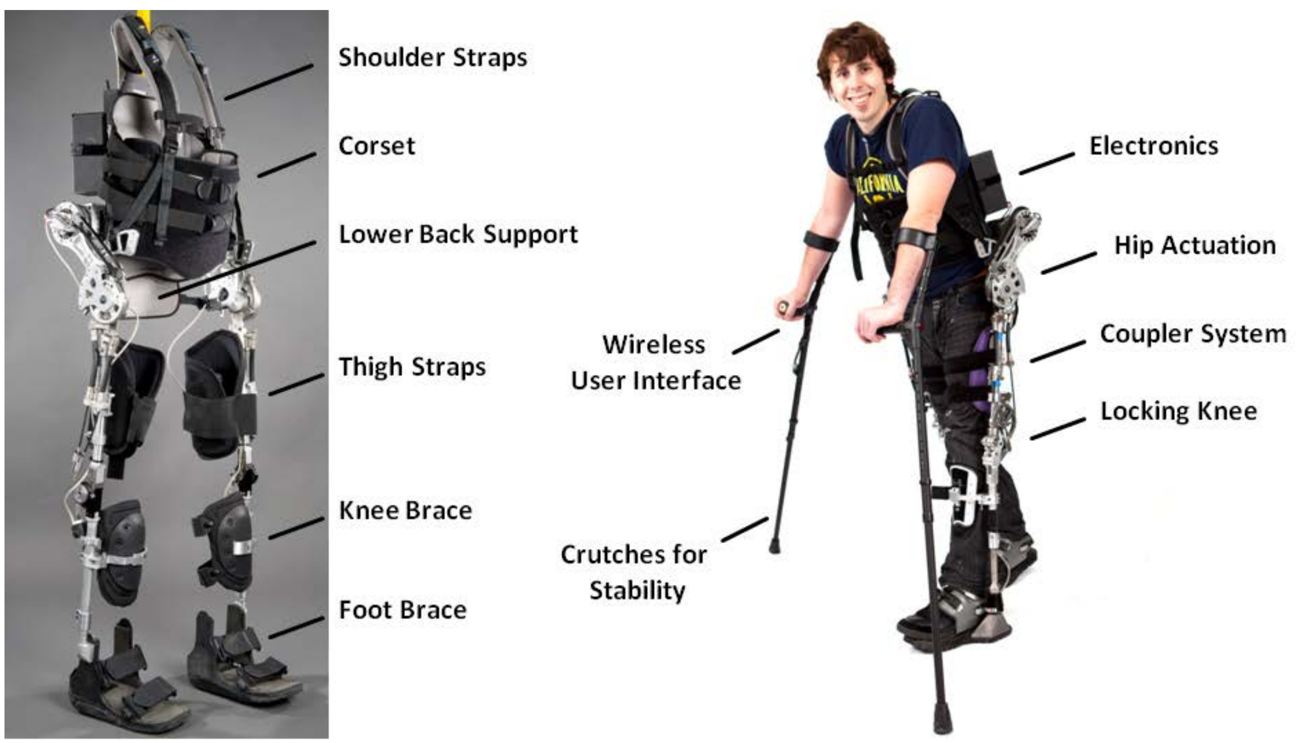

Figure 2-5: AUSTIN exoskeleton suit hardware overview

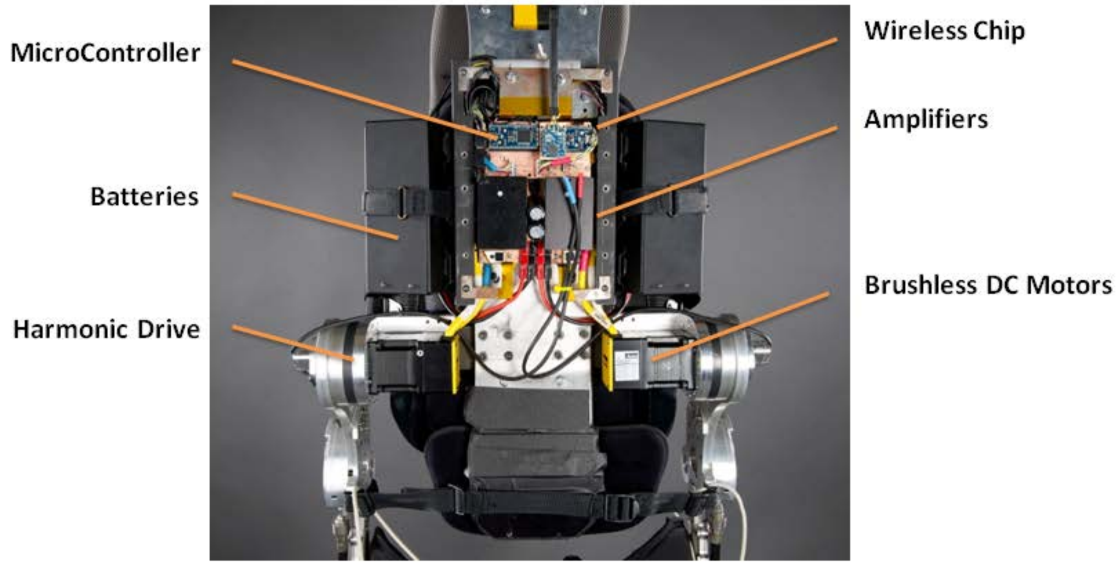

Figure 2-6: AUSTIN Exoskeleton Suit Rear View

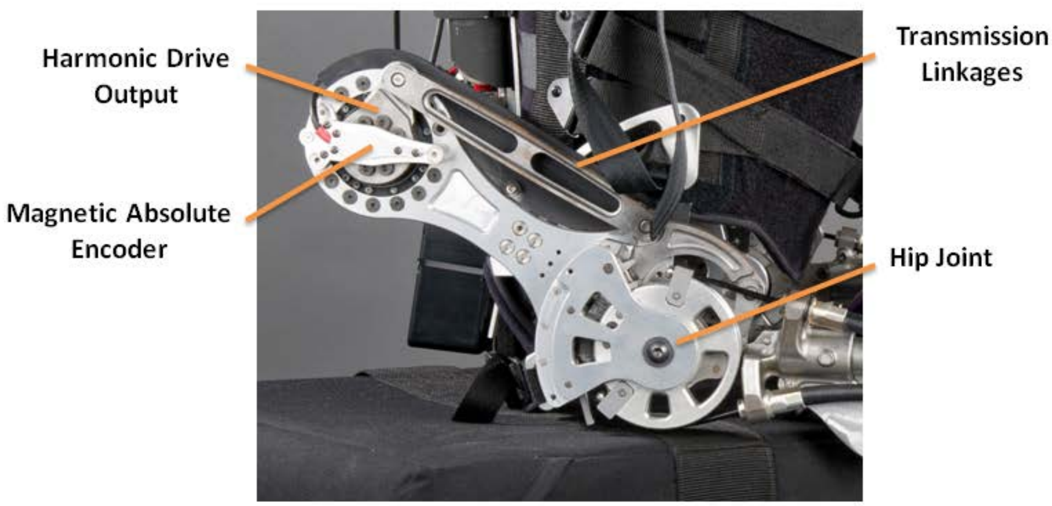

Figure 2-7: Motor to Hip Joint Transmission System

2.2.4 Gait Generation Hardware Description

The powered exoskeleton system designed to execute the proposed gait generation strategy consists of three major components:

1) Hip actuation
2) Hip-knee coupling mechanism
3) Controllable locking knee

2.2.4.1 Hip Actuation

The hip actuation component is used to provide powered rotation for the hip joint along the sagittal plane for hip flexion and extension. This maneuver is achieved with a 300W Parker BE231D brushless DC motor mounted at the lower back of the exoskeleton, as shown in Figure 2-6. The motor is connected to a 160-to-1 gear reduction harmonic drive. At the output of the harmonic drive, a transmission linkage system (shown in Figure 2-7 and Figure 2-8) transfers the motor torque to the hip with a 1-to-2 gear increase, which totals to a net 80-to-1 gear reduction from the motor to the hip joint. This actuation system is capable of providing 53 Nm of continuous hip torque and approximately 160 Nm of maximum intermittent torque. The exoskeleton hip joint was designed to permit 20° of hip extension and 110° degrees of hip flexion (measured with respect to the vertical axis). All other hip joint degrees of freedom are constrained to the neutral standing position.

The motor configuration of this design was chosen to minimize the hip width of the exoskeleton, which only amounts to 1.5 inches on each side of the user's hip. An alternative motor configuration uses a low-profile (but larger diameter) motor-harmonic drive package that is mounted directly at the hip. The "pancake-style" motor assembly requires less hardware as it forgoes the transmission system that transfers torque from the lower back to the hip joint; however, it also produces a wider exoskeleton hip profile.

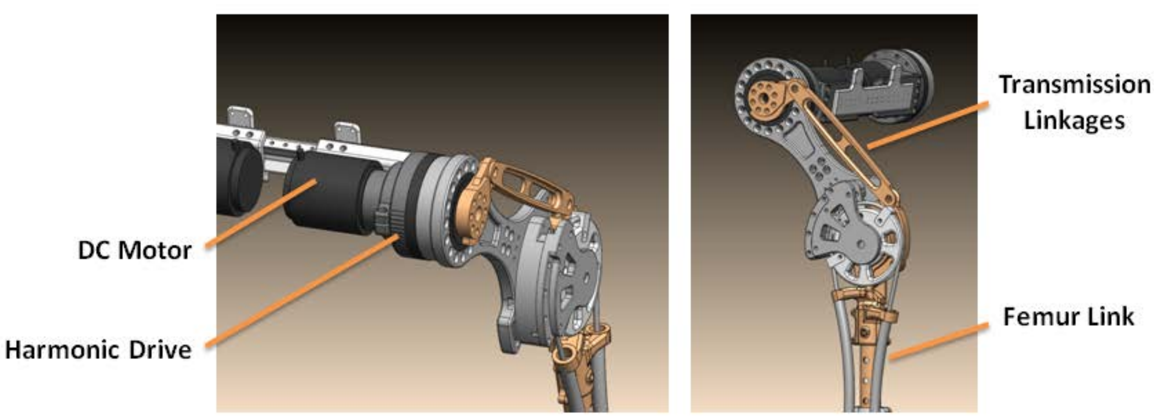

Figure 2-8: AUSTIN Hip Actuation Assembly

2.2.4.2 Coupling Mechanism

As shown in Figure 2-9, the coupling mechanism is located next to the femur-link of the exoskeleton. It consists of a larger 4-inch diameter pulley at the hip (hip pulley) and a smaller 2-inch diameter pulley at the knee (knee pulley). The hip pulley is allowed to freely rotate coaxially to the hip joint. The knee pulley is fastened to the tibia link of the exoskeleton so that rotation of the knee pulley generates knee rotation. The two pulleys are connected to each other by a pair of wire ropes. In this configuration, rotating the hip pulley would drive the knee to rotate at twice the angular velocity (due to the 2-to-1 diameter ratio of the two pulleys).

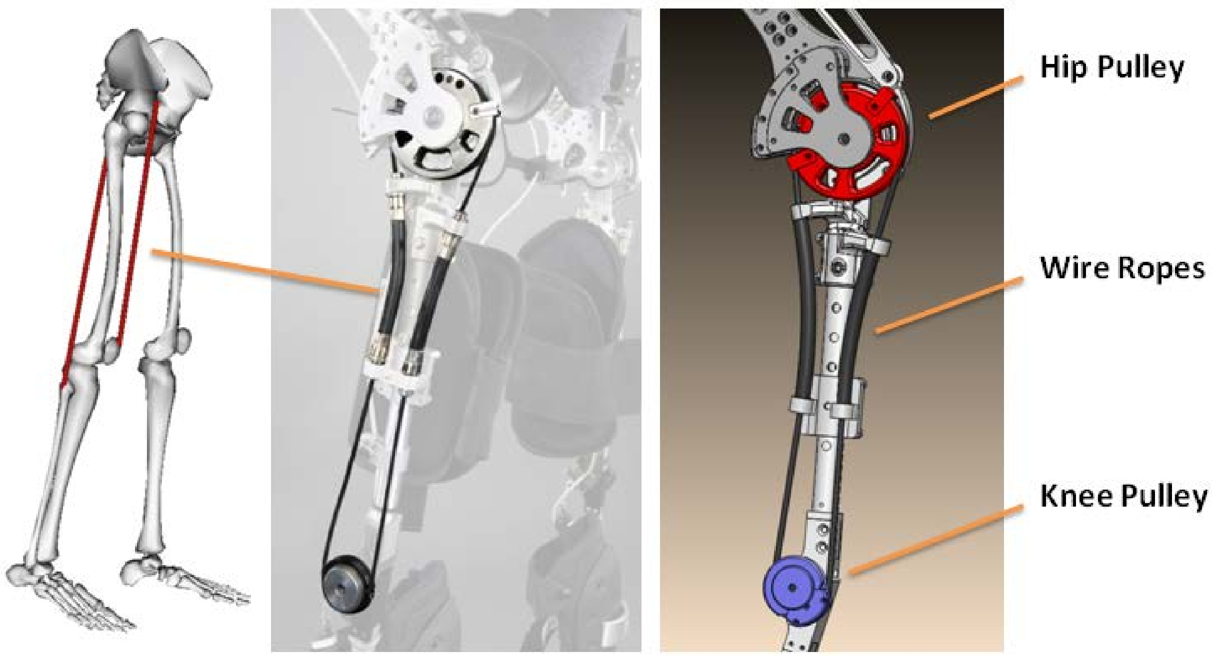

Figure 2-9: Coupling Mechanism Comparison to Biarticular Leg Muscles

Coupled motion of the exoskeleton leg is generated when a mechanical break (see Section 2.4.3) fixes the hip pulley relative to the torso of the exoskeleton. In this state, the hip pulley becomes analogous to the pelvis where the hamstring and rectus femoris are attached, see Figure 2-9. The two wire ropes connected to the pulleys now span across both the hip joint and the knee joint, acting as two antagonistic biarticular muscles with approximately infinite stiffness. In the same fashion as their biological analogues, the wire ropes can now generate knee flexion during hip flexion and generate knee extension during hip extension. Figure 2-10 provides a pictorial demonstration of the two states of the coupling system. The ratio of knee and hip rotation is determined by the relative diameter ratio of the coupler pulleys. The coupling ratio of the present device is 2-to-1, such that the knee will rotate two degrees for every one degree of rotation at the hip. This coupling ratio was chosen based on analysis of clinical gait data. Design of a more sophisticated and nonlinear coupling ratio will be discussed in Section 0.

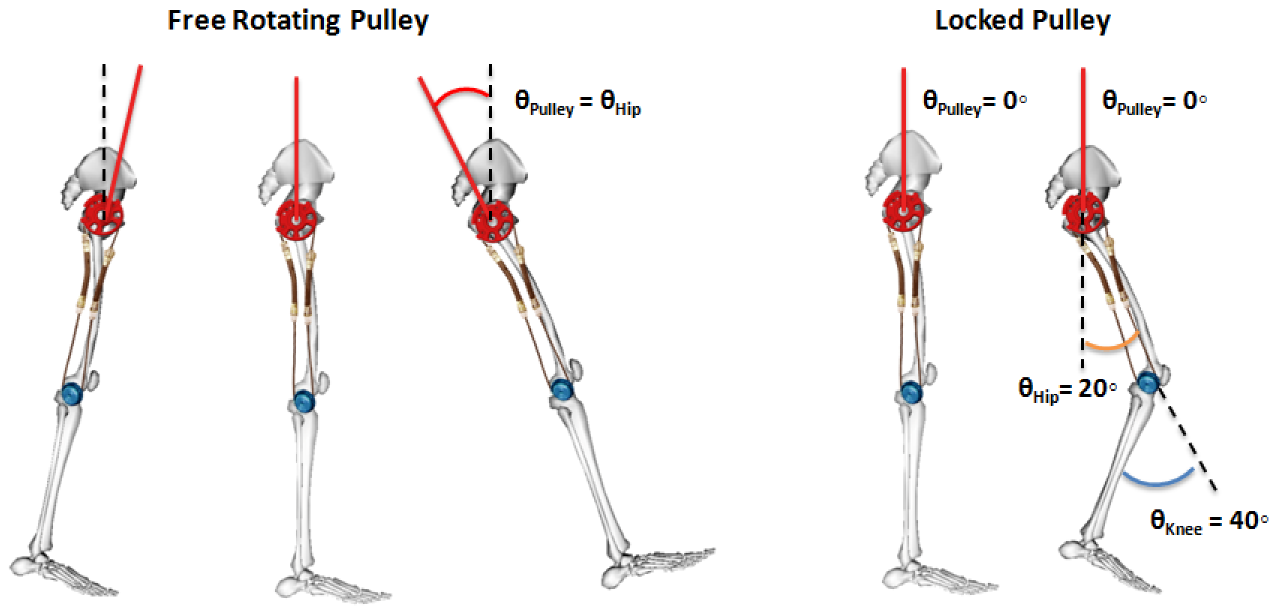

Figure 2-10: Hip-Knee Coupling System Operation Demonstration

2.2.4.3 Controllable Locking Knee

The exoskeleton knee plays a critical role in this gait generation system since the locking and unlocking behavior of the knee needs to operate in concert with the hip-knee coupling mechanism. The knee has three basic functions:

1. The knee automatically locks against flexion at heel strike and throughout stance phase.
2. The knee smoothly unlocks when the coupling mechanism gets activated during Swing-Flexion phase.
3. The knee is free to extend when the coupling mechanism gets deactivated during Swing-Extension phase.

The knee design went through several iterations until reaching optimal performance. The latest knee design utilizes an off-the-shelf one-way locking gas spring controlled by a cam coupled to the knee pulley, as shown in Figure 2-11 and Figure 2-12. In addition to the three basic functions, the locking gas spring knee has the added capability to lock against flexion at all angles while permitting free extension, which is valuable for stumbling recovery. The spring constant of the joint can also be adjusted to provide different amounts of knee extension assistance (particularly for individuals with knee joint contractures or spasticity). The reader is referred to Section 2.4.1 for more detailed discussion of the four knee design revisions.

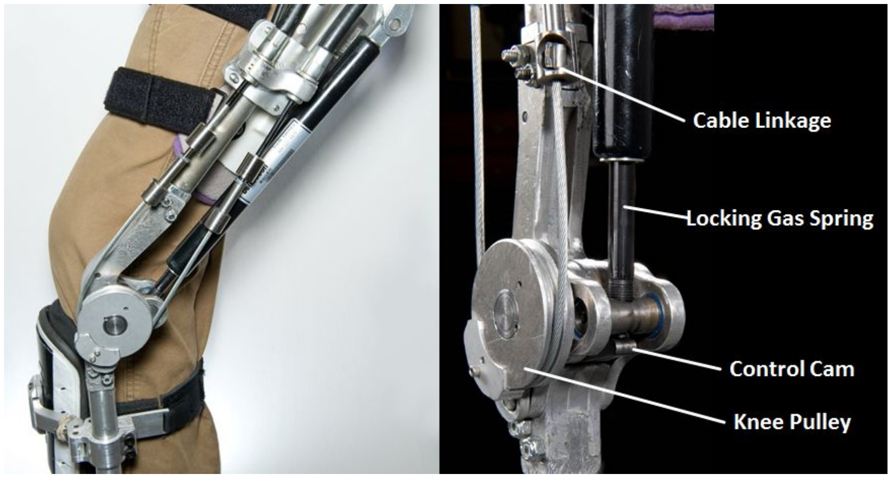

Figure 2-11: One-Way Locking Gas Spring Knee [43]

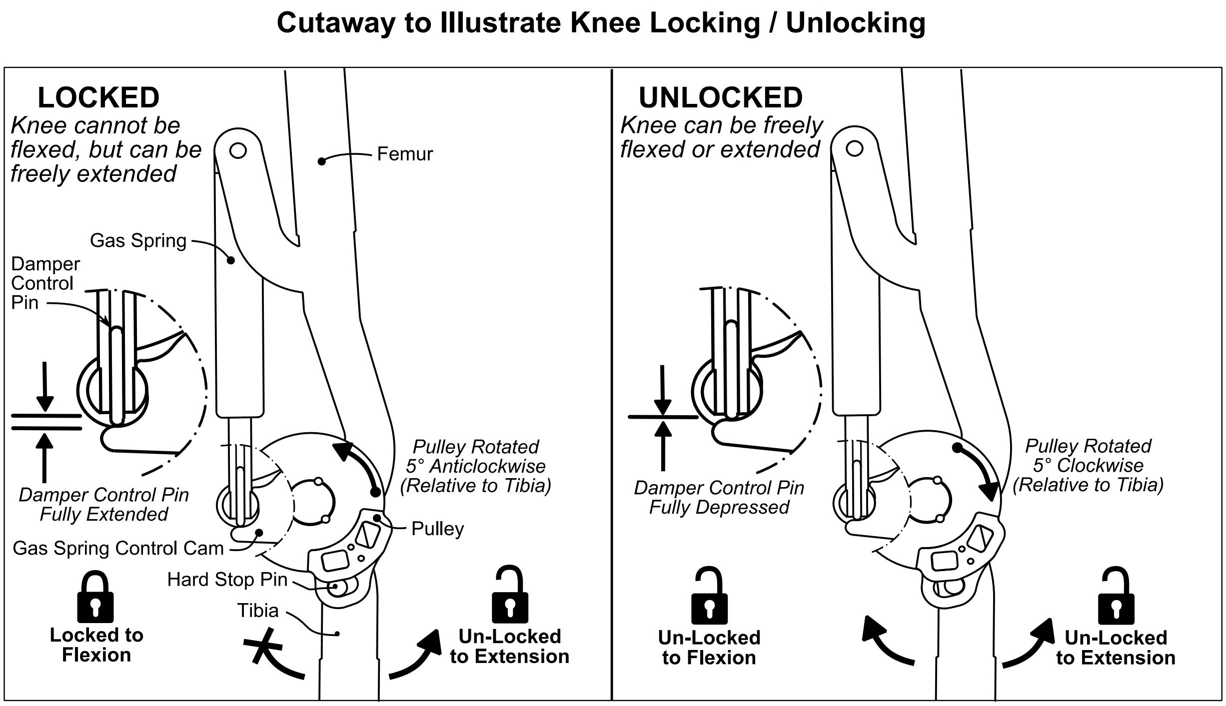

Figure 2-12: One-Way Locking Gas Spring Knee Operation

2.2.5 Generation of Coupling Gait Trajectory

As previously described, the walking gait of the exoskeleton is generated through the activation and deactivation of the hip-knee coupling system, in other words, through engaging and disengaging the hip pulley. The synchronization of the pulley engagement as a function of hip angle defines the gait trajectory. Three independent clinical gait analysis (CGA) data by Winter, Kirtley, and Linskell were used as reference to determine the optimal level-ground walking trajectory [44–47]. The analysis presented in this section will be based primarily on Winter's data since it is generally regarded as the biomechanical standard.

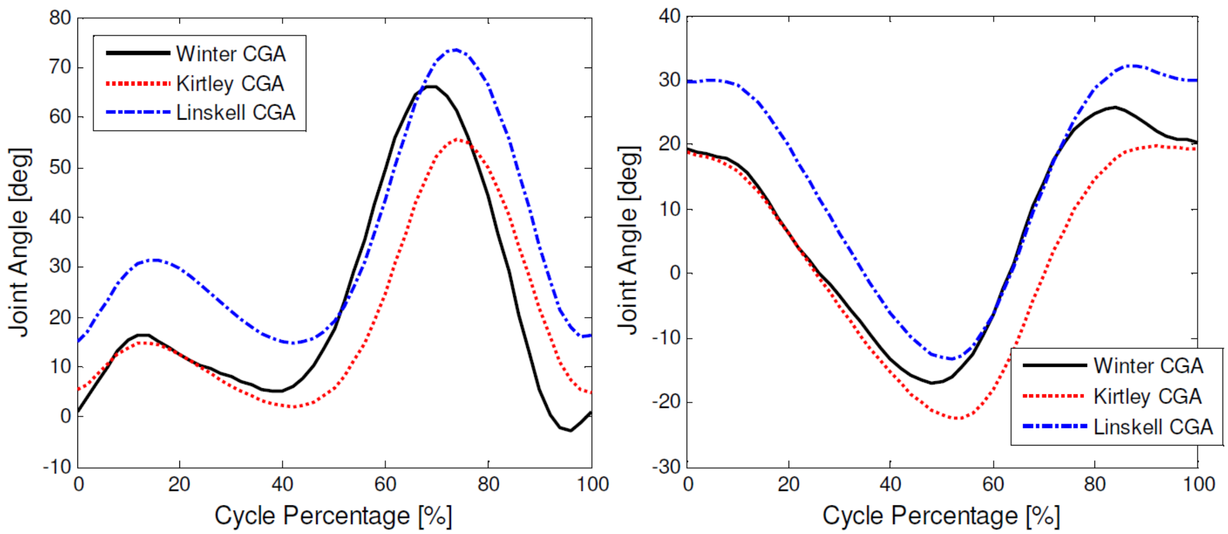

(A) (B)

Figure 2-13: Winter, Kirtley, and Linskell CGA data at the (A) knee and (B) hip

Figure 2-14 illustrates the sign convention used to represent the CGA data. The CGA data is collected with the torso lining up with the vertical axis. Hip angle is measured with respect to the torso, and hence a zero hip angle signifies that the thigh is in line with the torso. Hip extension from the torso axis is defined as negative hip angle, and hip flexion forward from the torso axis is defined as positive hip angle. Knee angle is referenced with respect to the thigh, where full knee extension is zero degrees and positive knee angle represents knee flexion. Negative knee angle equates to hyperextension of the knee joint, which is prohibited by the exoskeleton hardware.

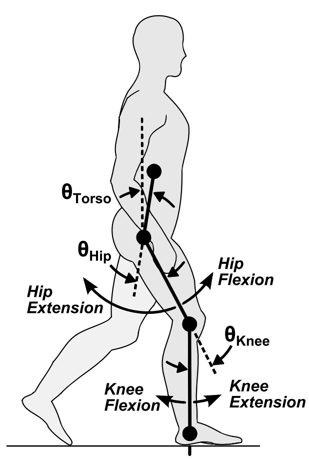

Figure 2-14: Joint Angle Definition

The coupling gait trajectory can be determined by superimposing the hip joint data on top of the knee joint data, which reveals regions of stance, swing-flexion, and swing-extension. Figure 2-15 shows the superimposed Winter CGA data and the corresponding gait phase.

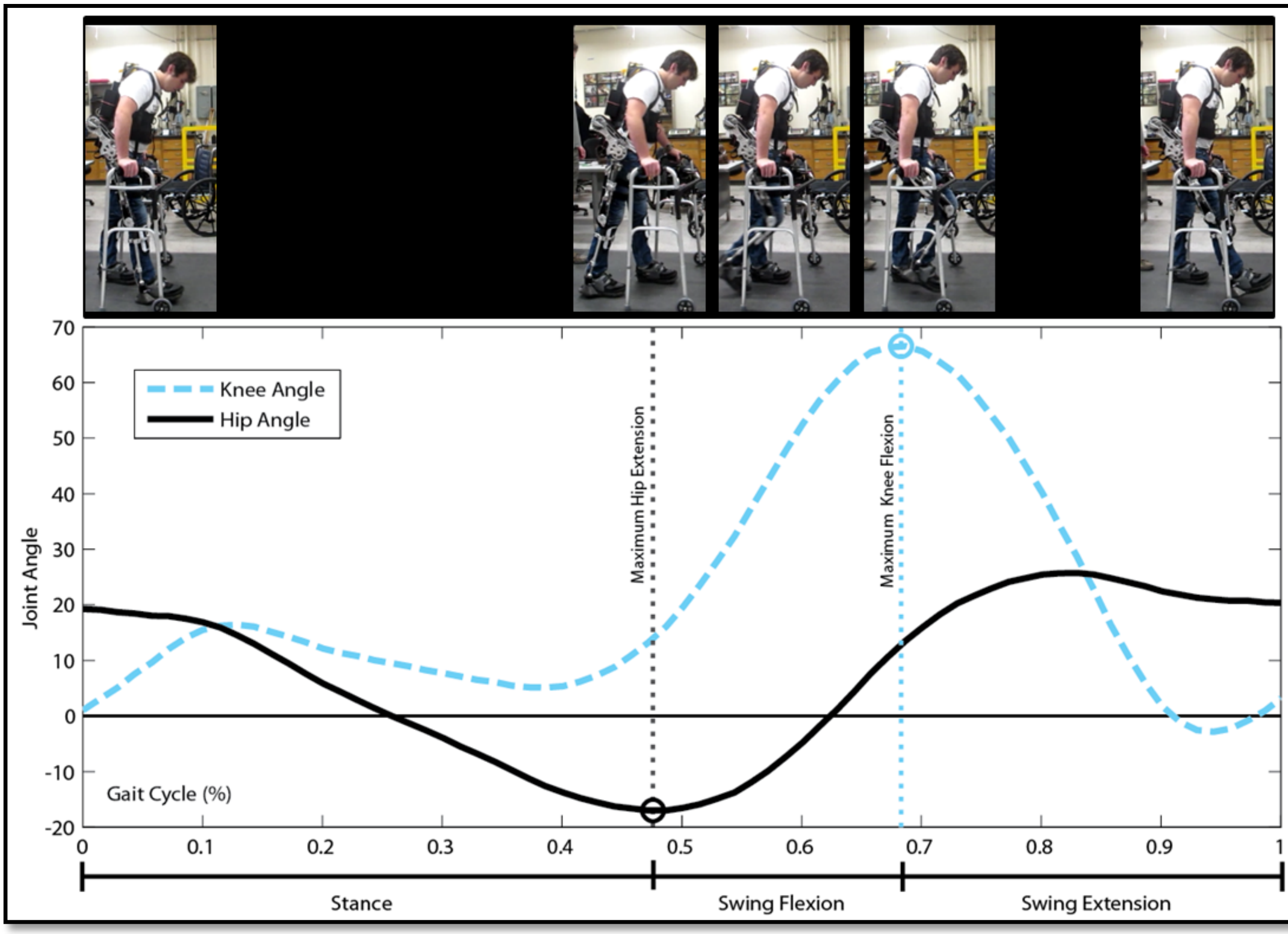

Figure 2-15: Winter's CGA data with Frames of Exoskeleton Gait

The two vertical dashed lines in Figure 2-15 mark the point of maximum hip extension and maximum knee flexion. The segment between the dotted lines represents the Swing-Flexion phase of the gait cycle where the hip and the knee are both flexing. Based on the CGA data, the Swing-Flexion phase of the gait begins when the hip is extended to approximately -17° and ends after approximately 30° of hip flexion when the hip angle reaches +13°. In this time interval, the knee is flexed 60° as a result of joint coupling.

At maximum knee flexion, the coupling system can be deactivated, thus allowing the knee to freely re-extend with the assistance from gravitational force and the knee extension spring. As shown in the Swing-Extension segment of Figure 2-15, knee angle returns to zero while the hip joint can be controlled to follow an independent and arbitrary trajectory.

During stance phase, the hip can be driven to follow a desired trajectory while the knee remains uncoupled (knee angle remains constant). It is possible to design a knee that allows slight knee flexion during stance phase as observed in the stance phase of Figure 2-15. The reader is referred to Section 2.4.1 for more detail on knee designs.

2.2.6 ***Preliminary Walking Experiments***

Preliminary experiments have been conducted with the AUSTIN exoskeleton to assess the feasibility of using hip-knee coupling for ambulation assistance. The test pilot is a 21-year-old male (6'2", 200 pounds) with a complete T12 injury sustained 3 years prior to the experiment. The subject has been in a wheelchair ever since initial injury and has not had any previous training on orthotic usage. As recommended by doctors, the subject used a standing frame (at least 4 hours a week) for 2 months prior to initial testing in order to avoid getting dizziness from not being used to being in a standing position.

Point tracking data of the subject walking with the exoskeleton was collected for comparison with published CGA data.

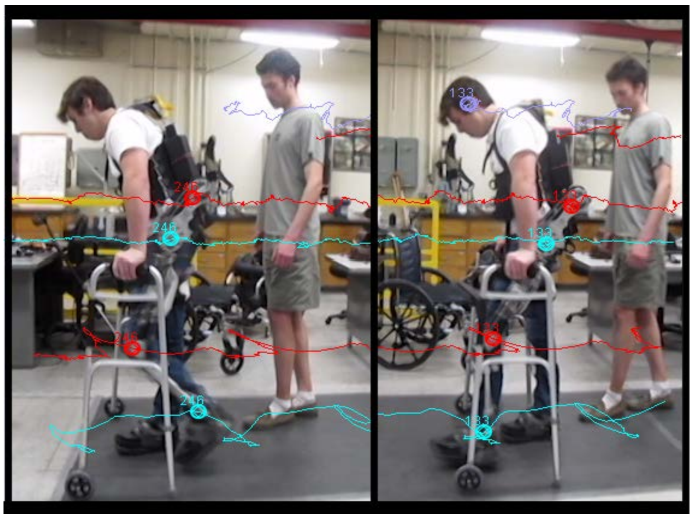

Figure 2-16: Point Tracking Frames from Software Tracker© Video from a Canon PowerShot SX40 HS

During the active mechanical gait cycle, the device exhibits similar gait characteristics to healthy walking. Point tracking data of two steps are plotted in Figure 2-17 with markers indicating the moment of "heel-off" for each step. Figure 2-17 provides a direct comparison between CGA data and the full gait cycle of the AUSTIN system. During double stance, the paraplegic pilot must actively shift their weight to the new stance foot before the next step is triggered. This balancing phase extends the stance period for the exoskeleton gait and can be seen in the extended pre-heel- off period in Figure 2-17. With experience and confidence, the length of the balance phase can be reduced.

Figure 2-18 highlights the region in which mechanical gait generation is active (showing only the region between heel off and heel strike) so that a direct comparison can be made to the CGA reference data. As expected, the mechanical gait generator produces a swing phase gait trajectory similar to the CGA reference.

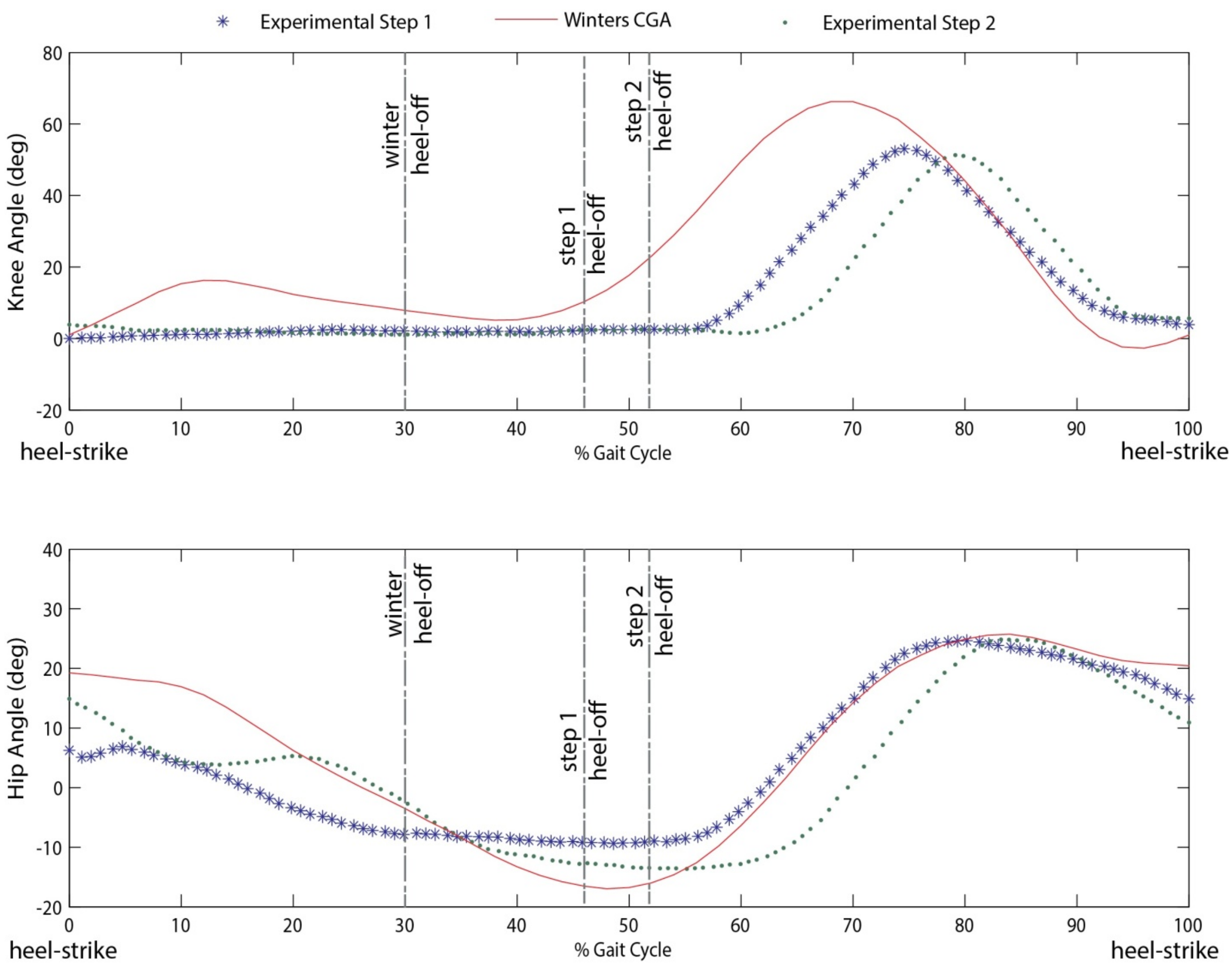

Figure 2-17: Point Tracking Knee and Hip Angles while using the Exoskeleton Starting and ending with heel strike.

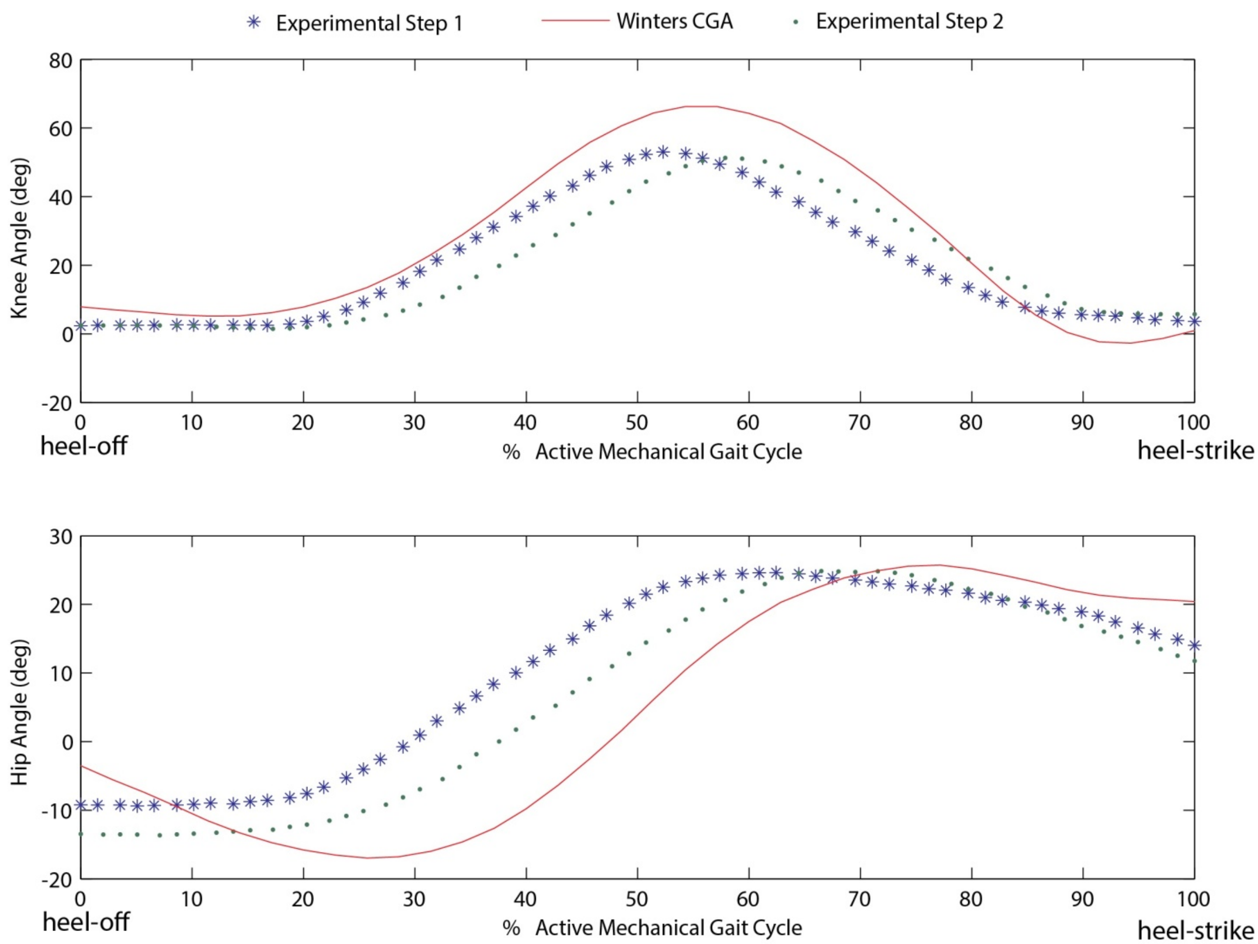

Figure 2-18: Hip and Knee Angles from Heel-off to Heel-strike

The knee and hip are decoupled during Swing-Extension. The location of release is adjustable in the mechanical gait generator and would allow tuning of the gait for a variable stride length and toe clearance.

2.3 Sitting and Standing

In addition to ambulation, the gait generation coupling mechanism is also used to provide assistance for sitting and standing operations.

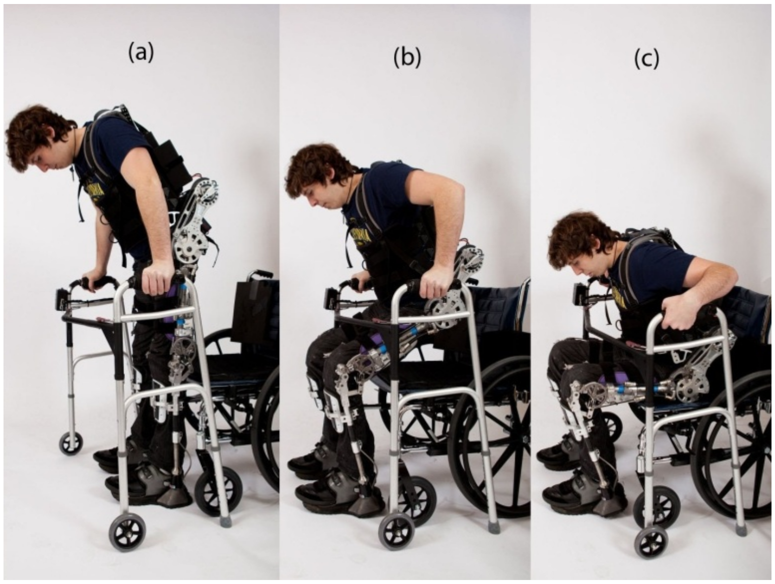

Figure 2-19: Sitting and Standing Sequence

As a finite state machine, the sitting procedure can only be initiated after the user commands the system to terminate the gait and to bring the feet together into a standing position. Once the sitting procedure is triggered, the exoskeleton flexes both hips forward 45° while leaving the coupling mechanisms deactivated and the knees locked. Since the weight of the user is distributed through both legs, the hip rotation results in the rotation of the torso in a forward bending motion. At the end of the 45° bend, as shown in Figure 2-19a, the coupling mechanisms are engaged while the hips continue to flex 55°. During the 55° of hip flexion, the coupling system generates 110° of knee flexion, and brings the user to a seated position, as depicted in Figure 2-19b and Figure 2-19c. Once the user is in the seat, the hips are then re-extended 10° to bring the torso back to a comfortable sitting position. The standing process is simply the reversal of the sitting procedure.

2.4 Exoskeleton Design Discussion

2.4.1 Knee Designs

The exoskeleton knee design plays a critical role in the operation of the exoskeleton system since the locking and unlocking behavior of the knee needs to work in tandem with the coupling mechanism to accommodate for the different phases of the gait cycle.

2.4.1.1 First Revision: Adapted Prosthetic Safety Knee

The first exoskeleton knee was designed with two very basic functionality requirements. 1) The knee has to lock during stance phase since the leg is weight bearing, and 2) the knee has to unlock during swing phase so that the coupling mechanism can take over the motion of the knee joint. An off-the-shelf prosthetic knee by Ottobock called the "Safety Knee" was chosen to perform this task. The Safety Knee utilizes a mechanism similar to that of a c-clamp such that when load is present across the exoskeleton knee joint, that load is used to clamp down and lock the exoskeleton knee (see Figure 2-20). This design was able to accomplish the objective of locking the knee joint during stance and allows free rotation during swing given that the user is able to properly load the leg during stance and unload the leg during swing.

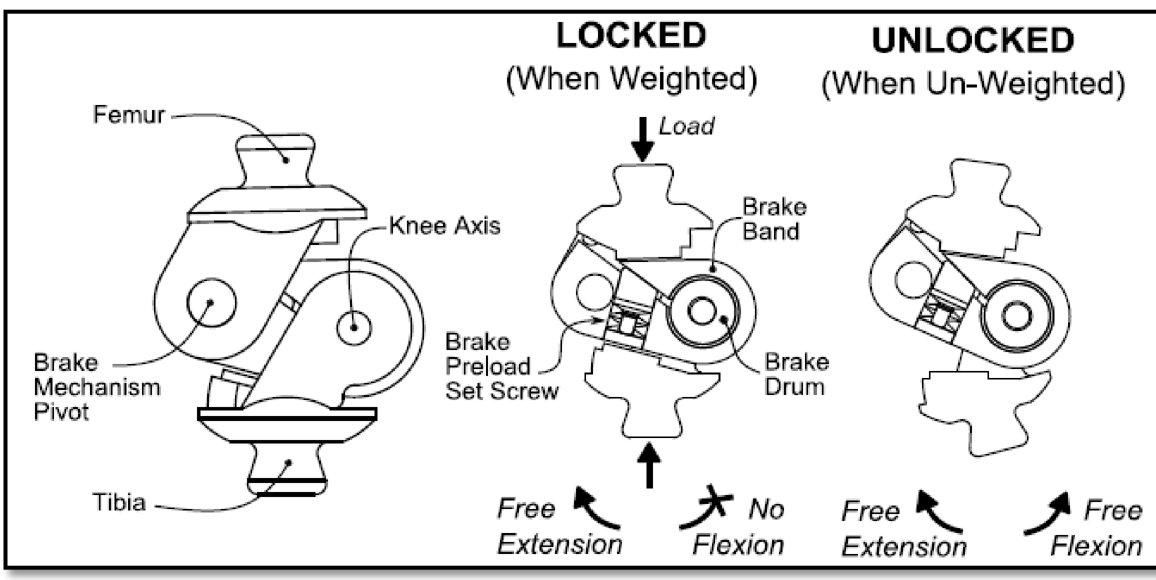

Figure 2-20: Safety Knee Locked and Unlocked Configuration [43].

After several months of testing with paralyzed subjects, it was concluded that those suffering from paraplegia do not have enough control of their weight distribution to use the Safety Knees effectively. It would require an excessive amount of training and tuning of the knees to obtain satisfactory results.

2.4.1.2 <u>Second Revision: Single-Pawl Lock Knee</u>

The second revision of the exoskeleton knee was designed to operate without relying on the user's ability to appropriately distribute his or her weight. A single-pawl-lock knee was designed such that a spring-loaded pawl on the femur engages onto the tibia and locks the knee when the knee gets to a fully extended position. As shown in Figure 2-21, the release mechanism of the pawl is connected to the knee pulley so that the pawl gets released whenever the coupling mechanism is activated.

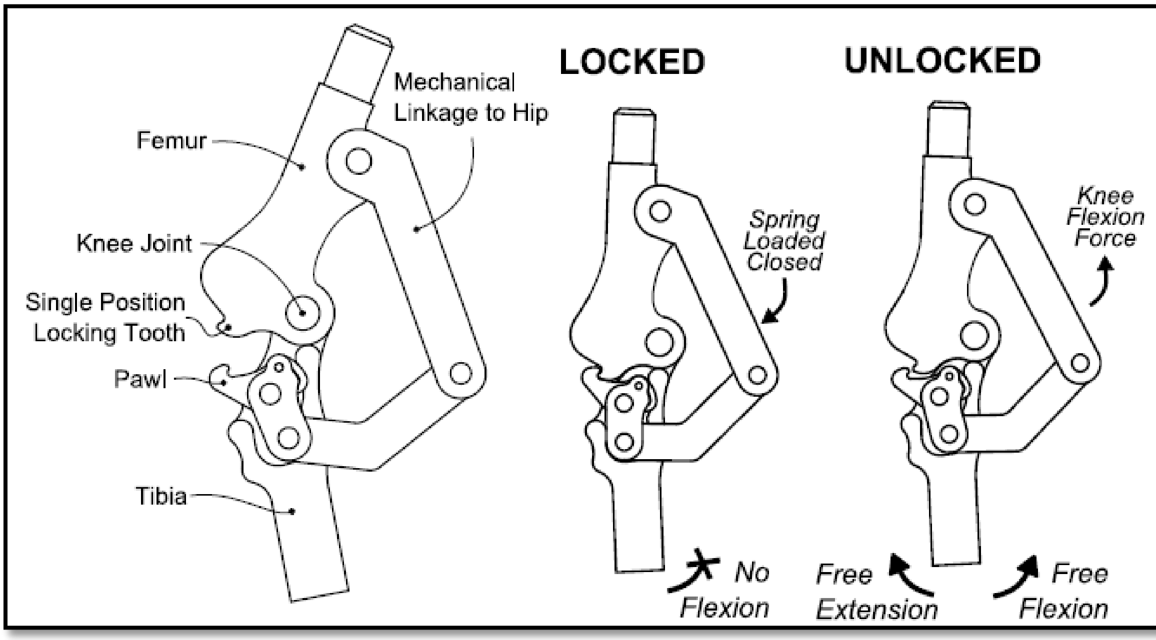

Figure 2-21: Single-Pawl-Lock Exoskeleton Knee Construction.
Figure from [43]

The single-pawl-lock knee provided great performance as long as the knee returns to the fully extended position at the end of the swing phase. However, full extension of the knee for every step cannot be guaranteed since there will always be instances of which the user's foot scrapes the ground during swing or bump into unexpected objects. Such unexpected toe drag would often prevent full extension of the knee joint and result in an unlocked knee going into stance. The uncertainty of whether the knee is locked for every step prompted the design of the third knee revision.

2.4.1.3 <u>Third Revision #1: One-Way-Clutch Ratchet Knee</u>

The third revision of the exoskeleton knee operates in a similar fashion as the second revision except that it was designed to be able to lock at all angles. This knee revision no longer has to be in the fully extended position to lock, which is extremely useful in unexpected scenarios when the user foot-strikes while the knee is not fully extended. The "lock-at-all-angles" feature drastically increased the overall safety of the system and it has also been shown to be catalytic in providing improved pilot confidence and comfort while operating the device. Furthermore, the locking of the exoskeleton knee was designed to only prohibit joint flexion while still allowing incremental extension of the knee. In other words, in the scenario which the user foot-strikes with a bent knee, it is possible to straighten out the knee without risking further bending the joint.

Figure 2-22 illustrates the construction of the one-way-clutch ratchet knee. The knee joint consists of a pawl mounted on the exoskeleton tibia and a circular ratchet mounted over a one-way bearing that is rotating on the femur shaft. The circular ratchet and the one-way bearing are orientated to lock in the direction of knee flexion. The pawl is spring-loaded to engage with the circular ratchet which would lock the joint against flexion but still allows free extension via the one-way bearing. A pawl control pin located on the knee pulley is used to release the pawl whenever the coupling mechanism is activated and the knee pulley is driven to rotate in the flexion direction.

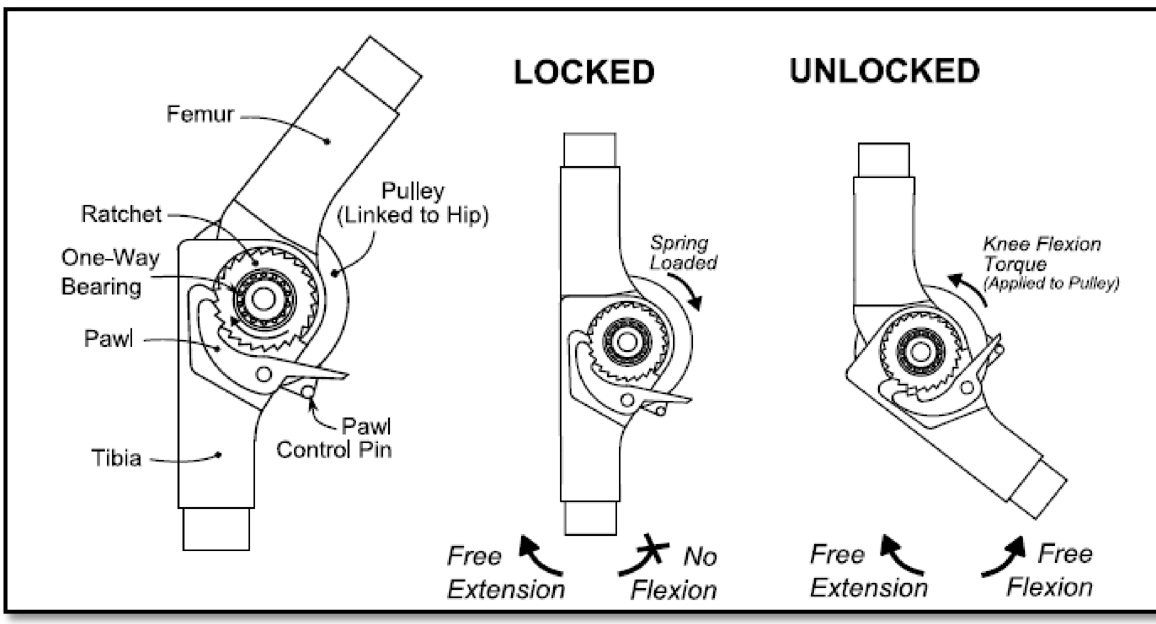

Figure 2-22: One-Way-Clutch Ratchet Knee Construction.
Figure from [43]

The incorporation of a one-way bearing is significant because, unlike a pure ratchet design, the one-way bearing provides an infinitesimal locking increment with minimal backlash. Furthermore, the ratchet teeth engagement geometry and the magnitude of the pawl spring loading were designed so that the pawl engagement force is large enough to rotate the ratchet upon contact. This specification guarantees that the knee actually locks on contact even if the pawl is initially positioned to land on the top of a ratchet tooth.

While the one-way-clutch knee provided very reliable and safe locking performance, the design had an unexpected issue with unlocking. It was observed that the exoskeleton user has to substantially unload the torque at the knee that was about to be unlocked in order to successfully unlock the joint. Originally, this feature was deemed as a safety feature which would prevent the user from collapsing as a result of unlocking the knee before shifting weight off of the swing leg. However, it became obvious that degree of unloading is important since it is unrealistic and energetically inefficient to completely unload the swing leg during ambulation. Furthermore, other factors such as patient knee joint contracture can also cause flexion torques at the knee which resists joint unlocking.

Large friction forces at the locking interface of the pawl and the ratchet is the cause of the system's inability to unlock the joint. It can be observed from Figure 2-22 that the friction forces are proportional to the magnitude of flexion torque at the knee. The unlocking issue can be resolved with an increased mechanical advantage for the pawl control pin, which can be achieved through various methods such as increasing the release lever arm or adopting a mooring hook mechanism (described in Section 2.4.3). The mechanical advantage of the system can then be adjusted and fine tuned to operate within the bounds of what is safe but not overly conservative.

2.4.1.4 Third Revision #2: One-Way Locking Gas Spring Knee

Another knee was developed in parallel with the one-way clutch knee that uses, instead, a one-way locking gas spring. As shown in Figure 2-23, the locking gas spring has a damper control pin, which when left fully extended, the spring is locked against compression while still being free to extend. On the other hand, when the damper control pin is fully depressed, the damper valve is opened and the gas spring simply operates as a gas spring with some residual damping coefficient. The locking gas spring knee operates in a similar fashion as the one-way clutch knee except that 1) there is some residual damping coefficient when unlocked, 2) the spring loaded extension is built-in, and most importantly, 3) the joint can be unlocked even under load. The one-way locking gas spring knee was designed by graduate student Michael McKinley and the reader is referred to [43] for more information on this design.

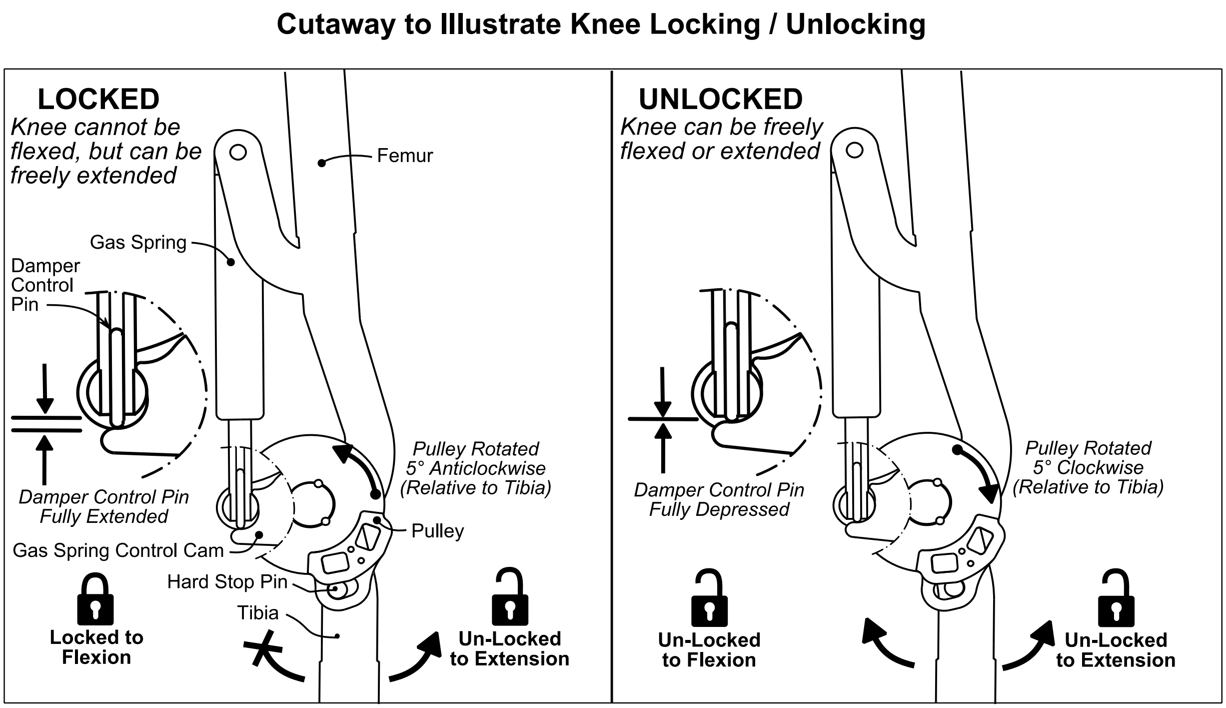

Figure 2-23: One-Way Locking Gas Spring Knee Operation
Figure from [43]

2.4.2 Coupling Mechanism Coupling Ratio

The 2-to-1 hip-knee coupling ratio of the coupling mechanism was designed based on a modified level-ground walking knee trajectory. Figure 2-24 plots Winter's hip-knee data with a modified knee trajectory based on the approximation that the knee remains fully extended and locked during the entire stance phase. This type of gait is commonly observed in passive orthotic users and double transfemoral amputees walking with passive prosthetic knees. As shown in Figure 2-24, on average, the knee flexes 66.5° during the Swing-Flexion phase while the hip flexes 30.5° in the same time interval. This results in a flexion ratio of 2.18. Similar analysis can be conducted with Kirtley and Linskell CGA data, which yields comparable results.

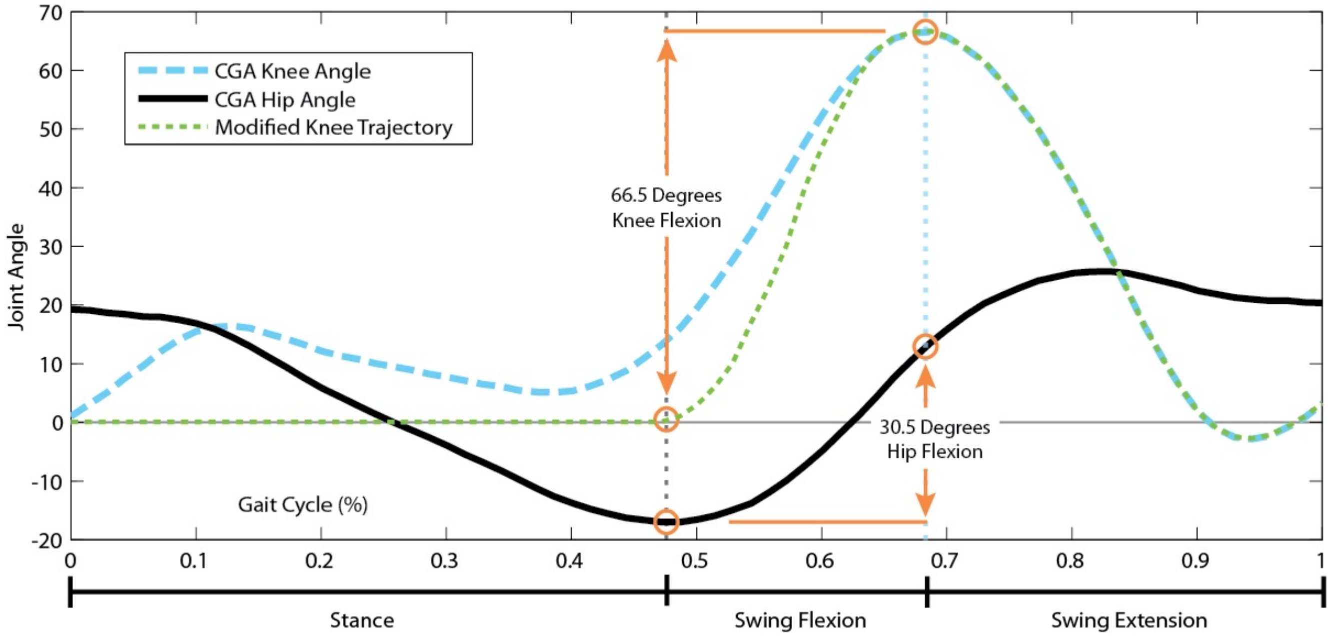

Figure 2-24: Winter's hip-knee data with an adjusted knee trajectory
Amount of hip and knee flexion during Swing-Flexion phase indicate a coupling ratio of 2.18

Although a fixed 2-to-1 coupling ratio has shown the capacity to generate a functional walking gait, it is possible to further improve the correspondence of the generated knee trajectory by implementing a progressively variable coupling ratio. Through modifying the circular hip and knee pulleys into specific cam profiles, each sub-segments of the Swing-Flexion phase can have a different coupling ratio, which results in more accurate knee trajectory tracking. For example, the Swing-Flexion phase can be further divided into two sub-segments. Using the same coupling ratio calculation method as before on each segment, the first portion can be assigned a coupling ratio of 4.13 while the second portion can be assigned a coupling ratio of 1.27. The generated knee trajectory by this two-phase coupling ratio system is plotted in Figure 2-25 and it is put in comparison with the trajectory generated by a single phase 2-to-1 coupling ratio system. It is important to note that the hip trajectory used in this analysis was simply the CGA hip data and this was done only for the sake of clarity and trajectory comparison. The actual hip trajectory used by the exoskeleton is modified to better accommodate the 2-to-1 coupling ratio so the system generates a smoother gait. Nevertheless, Figure 2-25 demonstrates that further subdivisions can be used to generate a variety of coupling trajectories.

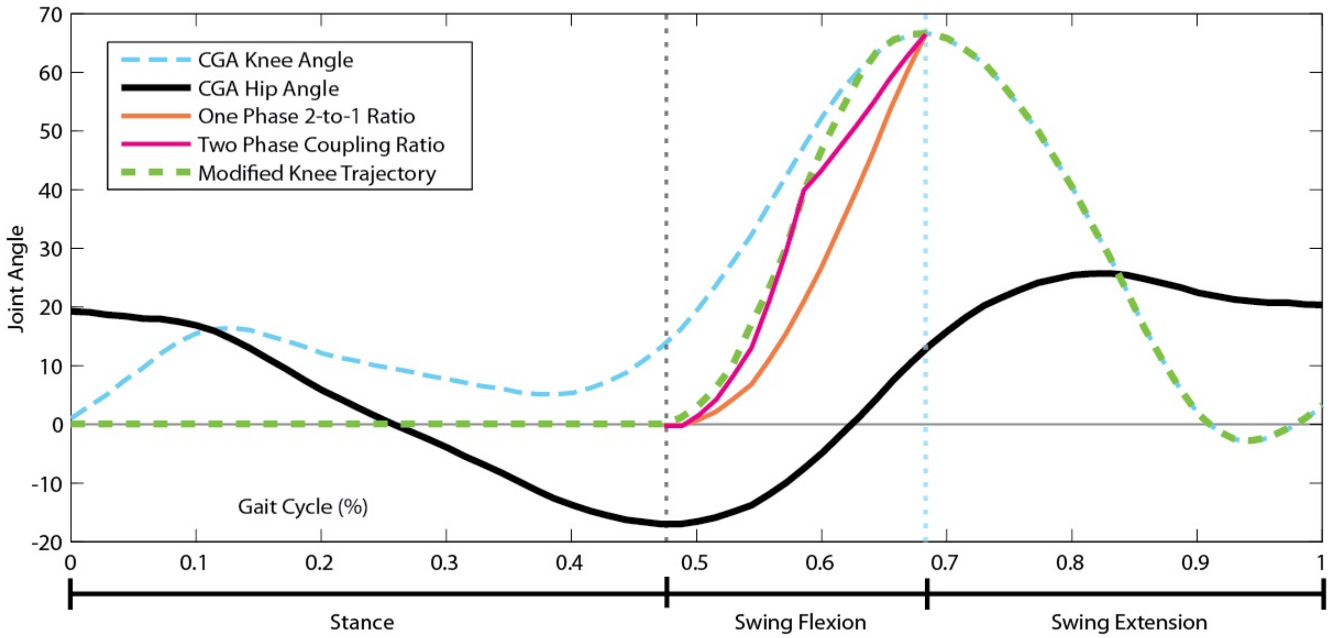

Figure 2-25: Single Phase 2-to-1 Coupling Ratio versus Two Phase Coupling Ratio

2.4.3 Pulley Engagement System – Gait Generator

As described in Section 2.2.4, the coupled motion of the exoskeleton leg is generated through fixating the hip pulley to the exoskeleton torso. This operation can be achieved through several methods. One of the most straightforward approaches would involve the implementation of a small servo or solenoid that activates and deactivates a breaking system that would fix the hip pulley on command. However, in the effort to completely minimize actuation, a purely mechanical pulley engagement system was designed.

The mechanical pulley engagement system locks and unlocks the hip pulley strictly as a function of hip angle. As shown in Figure 2-26, the system consists of a hip pulley tooth and a spring-loaded torso tooth. Starting at a standing position, the torso tooth is retracted and riding on the back of the hip pulley tooth. In this state, the hip pulley is unlocked and it rotates concurrently with the exoskeleton femur link since the knee is locked at full extension. When the hip is extended to a predetermined “toe-off” position (which was approximated to be -17° in Section 2.2.5), the torso tooth snaps into engagement with the hip pulley tooth and prevents rotation of the hip pulley. The coupling mechanism is now activated and the system is ready to proceed into the Swing-Flexion phase. The -17° engagement point is built into the system hardware and it can only be changed by modifying the relative positions of the engagement teeth.

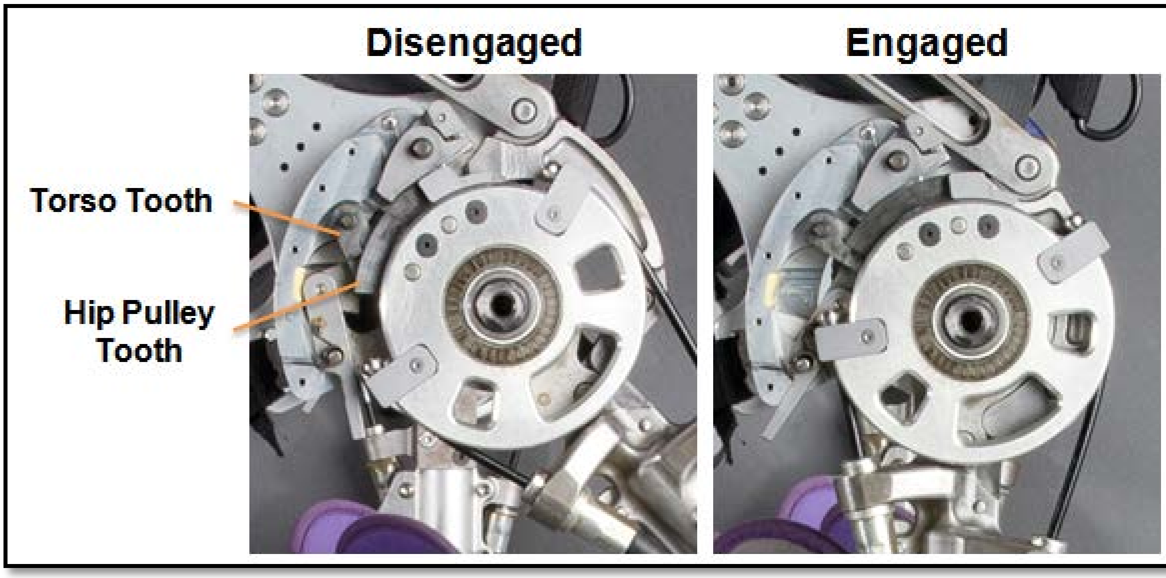

Figure 2-26: Mechanical Hip Pulley Engagement System Engaged and Disengaged Configuration

The gait transitions into Swing-Extension phase when a cam mounted on the exoskeleton femur retracts the torso tooth and releases the hip pulley (Figure 2-27). This disengagement cam is contoured so that the pulley is released at +13° hip flexion (Based on analysis from Section 2.2.5). The cam can also be rotated ±10° to modify the gait and to accommodate for different amount of desired knee flexion. The torso tooth is under a substantial amount of load at the point of release due to the weight of the shank and the knee extension spring. To guarantee that the torso tooth can be smoothly retracted under load, an over-the-center four-bar linkage construction was adopted. The torso tooth mechanism operates in a similar fashion as a quick release mooring hook, which uses geometric over-the-center mechanical advantage to minimize the proportional release force requirement. The mechanism was designed with a 1° over-the-center lock and a 2-to-1 lever arm advantage at the tooth link, which results in a combined tooth-release mechanical advantage of 114.6 times the pulley load.

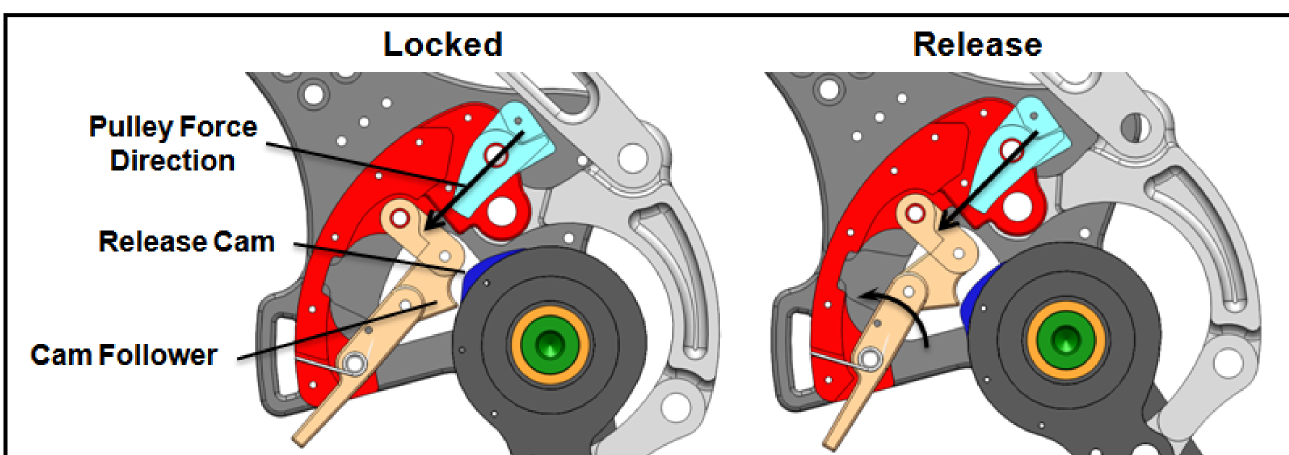

Figure 2-27: Illustration of the Mooring Hook and Release Cam

Once the torso tooth is disengaged, the leg can either be returned to the feet-together double stance position or be extended to -17° to begin the next step.

The sitting procedure can only be initiated when the exoskeleton is in the feet-together double stance state. In this state, the torso tooth on both legs is disengaged and the coupling engagement systems are in a configuration as shown in Figure 2-28. The sitting procedure begins with 45° of hip flexion, which brings the hip pulley into contact with a mechanical hard stop. A spring-loaded sitting tooth rotates into place and locks the hip pulley in the other direction (see Figure 2-28). With the hip pulley locked in both directions, the sitting process proceeds with the coupled hip and knee flexion. The pulley engagement system on both legs stays in this configuration while the user is seated. The reverse process then brings the exoskeleton back into a feet-together double stance.

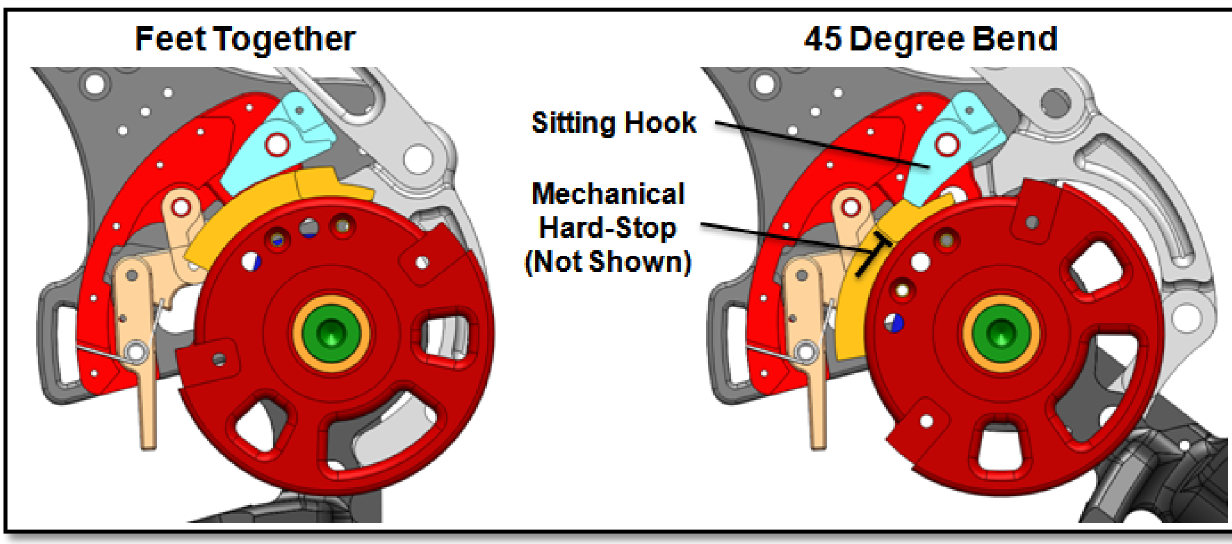

Figure 2-28: Mechanical Pulley Engagement System during Sitting and Standing

2.4.4 Exoskeleton Finite State Machine

The exoskeleton system operates as a finite state machine where the exoskeleton pilot operates two push-buttons to move from one state to another. Figure 2-29 illustrates the finite state machine of the exoskeleton.

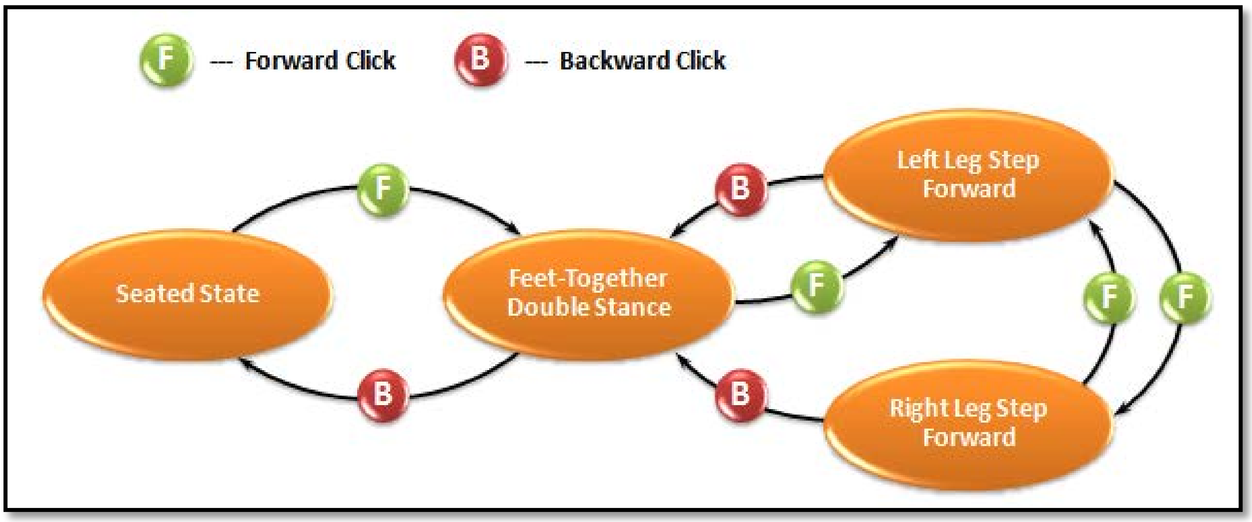

Figure 2-29: Exoskeleton Finite State Machine Diagram

The two push-buttons represent a forward and backward motion in the state machine. The exoskeleton always begins in the seated state in which the user puts on the device. A forward click in the seated state will command the hip actuators to rotate the exoskeleton femur to a vertical position, which, with the help of the coupling mechanism, brings the user to a feet-together double stance. Once in this double stance state, the user has the option of sitting back down with a backward click or step forward with a forward click. The first step from double stance was programmed to always begin with the left leg stepping forward. This step is executed by flexing the left leg to approximately +18° (for heel strike) and extending the right leg to -17° (for coupling engagement). Another forward click in this state will trigger the right leg to step forward which flexes the right leg to approximately +18° and extends the left leg to -17°. Each successive forward click triggers an alternating step and results in a forward walking gait. A backward click in either of these two states (either left leg forward or right leg forward) will bring both legs back into the feet-together double stance. The terminating step is executed by bringing the stance leg to 0° while cycling the swing leg to +18° and then back to 0°. The swing leg cycling for the terminating step is necessary to release the coupling engagement.

Chapter 3

Ryan Exoskeleton: Dynamic Joint Coupling

The Ryan Exoskeleton was conceptualized during the development process of the AustinExo. This system adopted a new knee actuation strategy in order to further simplify the device hardware and to minimize the overall device size and weight. Similar to the AustinExo, the Ryan also operates with the concept of joint coupling. However, instead of using a hardware-based joint coupling mechanism, it achieves joint coupling dynamically. The Ryan Exoskeleton utilizes dynamic joint coupling as the source of its knee actuation, that is, knee motion during ambulation is generated through deliberate swinging of the hip joint. This knee actuation strategy was inspired by the gait mechanics of bilateral above-knee amputees whose lower limbs can be modeled as double pendulums. Through utilizing the dynamic inertial response of the lower leg, the exoskeleton is able to generate 1) passive knee flexion with actuated hip flexion and 2) passive knee extension with actuated hip extension. This method of gait generation has also been referred to in the literature as ballistic walking. The combination of dynamic joint coupling with a function-specific knee design led not only to a more natural looking gait, but also to the development of the first powered exoskeleton system that weighs less than 20 pounds.

3.1 Inspiration: Bilateral Transfemoral Amputee Gait

Bilateral transfemoral amputees (BTFA) using unactuated knee-ankle prosthetics are commonly seen capable of attaining a high level of bipedal mobility and achieving an extremely independent lifestyle. Amongst the most popular prosthetic lower limbs is Ottobock's C-Leg which acts as a variable damping knee joint that allows free swing and locked stance. With such prostheses, BTFAs can perform many activities of daily living (level ground walking, walking on slopes, stair ascent/decent, etc) without the use of hand held stability aides such as walkers or crutches. Interest in the gait mechanics of BTFAs was initially developed in the effort to improve Austin Exoskeleton's ambulation stability and propulsion efficiency; however, observation of high levels of toe clearance and knee flexion despite the absence of knee actuation soon became profoundly enlightening. As shown in Figure 3-1, a BTFA is able to consistently achieve a healthy level of toe clearance through manipulating hip swing and pelvic tilt. This observation prompted the investigation of whether the same swing leg dynamics can be reproduced on a medical exoskeleton system, which would further eliminate the need for a hardware-based joint coupling mechanism.

Figure 3-1: Level-ground walking of a bilateral transfemoral amputee with unactuated knee-ankle prosthetics

The Austin Exoskeleton was modified to test the feasibility of utilizing dynamic joint coupling on an exoskeleton system. The mechanical coupling mechanism on the Austin system was temporarily disabled by removing the wire ropes connecting the hip and knee pulleys. Further, a small linear actuator was installed on each knee, see Figure 3-2. The miniature actuators are connected to the release pawl of the one-way clutch knee (described in Section 2.4.1.3) in order to lock the knee during stance and allow free flexion during swing. The actuator engagement timing is controlled by the exoskeleton's main computer, communicating via an electric cable. The actuator selected to perform this task was the Firgelli PQ12-30-12-P for its small size and high power density.

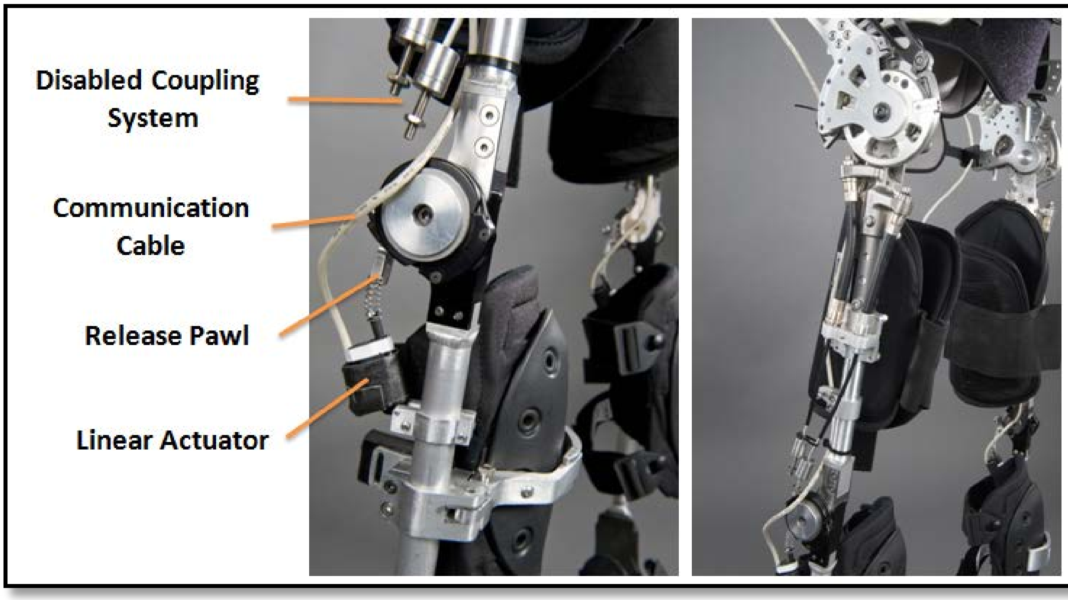

Figure 3-2: Austin Exoskeleton with disabled joint coupling mechanism

The modified Austin Exoskeleton yielded promising results. It showed that the utilization of dynamic joint coupling for paraplegic exoskeletons is highly feasible. Figure 3-3 shows the step sequences of a preliminary dynamic coupling gait trial (top) juxtaposed with Austin Exoskeleton's mechanical coupling gait (bottom).

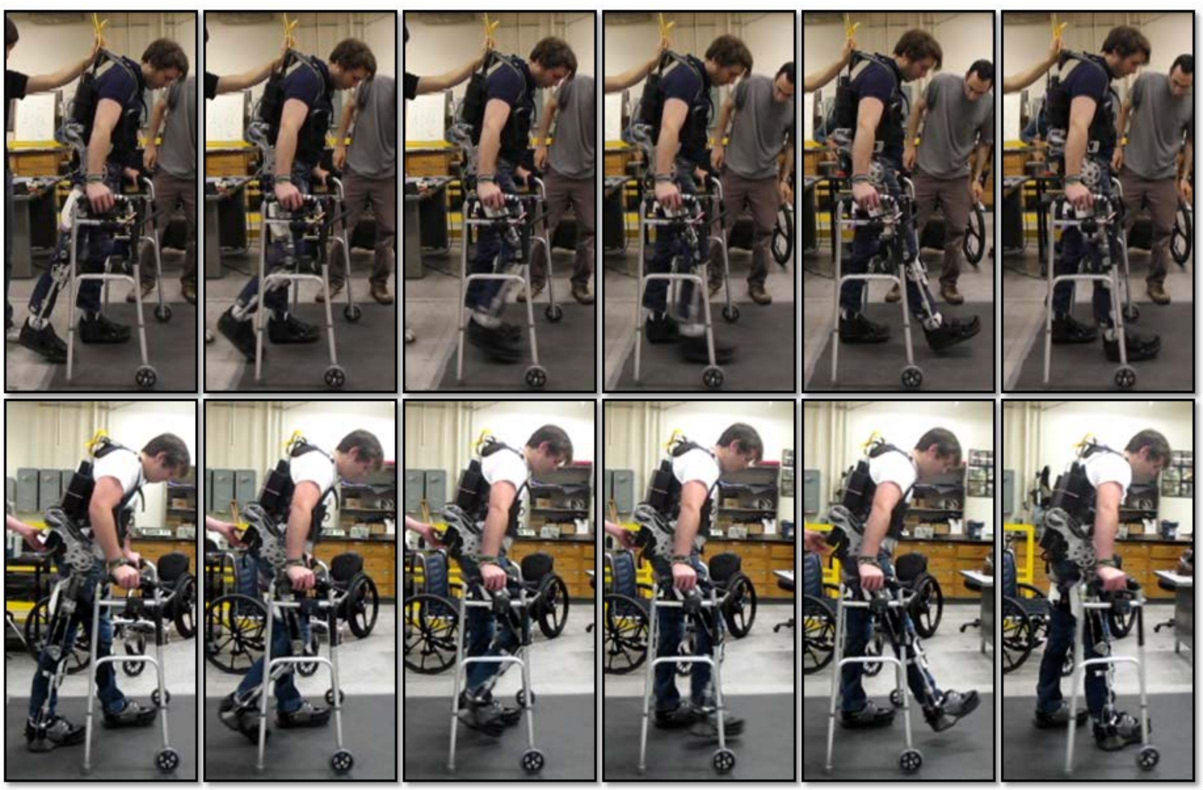

Figure 3-3: Dynamic joint coupling gait (top) Austin mechanical coupling gait (bottom)

The preliminary experiment showed that dynamic joint coupling generated a comparable amount of toe clearance and produced a similar gait pattern. The mechanical joint coupling gait still demonstrated a slightly larger amount of toe clearance, approximately 1.5 to 2 inches, while the dynamic joint coupling gait was generating approximately 0.5 to 1 inch of toe clearance. Nevertheless, this result was obtained prior to any swing dynamics optimization, that is, the hip trajectory used for this experiment was the same hip trajectory used for the Austin Exoskeleton.

The hip and knee joint angles for the dynamic coupling swing were obtained via point tracking. The data is plotted in Figure 3-4. The joint angles from the Austin Exoskeleton gait and the Winters CGA data were also plotted in the figure for comparison. It can be observed from the plot that this preliminary swing leg trajectory closely resembles the Austin Exoskeleton gait and generated almost the same amount of knee flexion as depicted by the Winters CGA data. This result suggests that very little knee power is required during the swing phase of able-bodied level ground walking and inertial force alone might be sufficient enough to achieve satisfactory toe clearance.

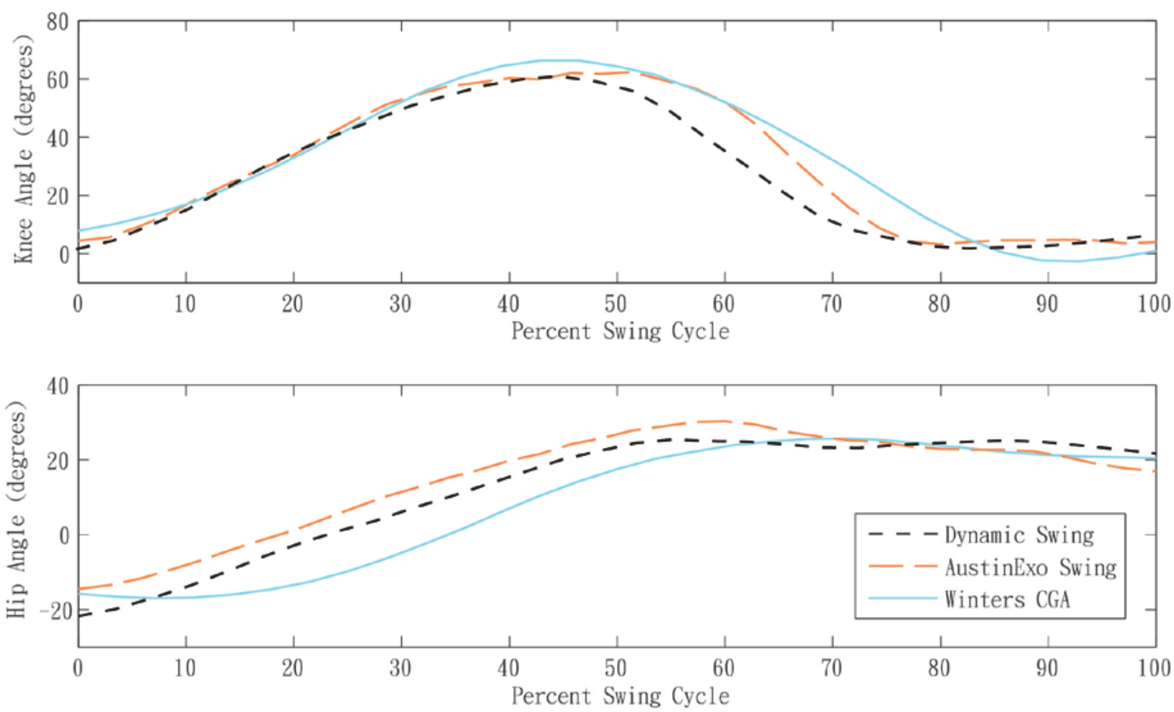

Figure 3-4: Experimental Dynamic Joint Coupling Swing Phase Gait Comparison

3.2 Knee Design Specifications

A pair of complementary mechanical knees with very specific functionalities is essential for the execution of the proposed ballistic gait model. The knee needs to have two basic functions. 1) It needs to act as a free joint with minimal rotational friction so the dynamic coupling knee motion can be generated with minimal impedance. 2) It also needs to be able to lock against flexion during stance. Through several knee design iterations, more advanced knee functions were specified and implemented. The reader is referred to Section 2.4.1 for more detailed description of each knee design revisions. A summary of the desired knee functions is described below.

1. The most basic knee design has two states. It locks at (and only at) the fully extended position during stance, and acts a free joint during swing.

2. A locking capability upgrade allows the knee to lock at all angles. This function is useful for stumbling recovery, which describes the unexpected scenario when the user's foot contacts the ground while the knee is not fully extended. This capability further enhances the overall safety of the device.

3. A complementary element for a joint that locks at all angles is the ability to freely extend while the joint is locked against flexion. The joint becomes analogous to a one-way-clutch which the locked bent-knee can still be straightened out, either manually or through hip actuation.

4. It was originally believed that (for the sake of safety) the knee should never be unlocked while it is under load. However, when this was executed to the extreme, the user had to completely unload the leg at toe off in order to proceed into the swing phase, which was extremely inefficient and unnecessary. It is therefore desirable to be able to unlock the knee while the leg is still carrying some amount of body weight.

5. It would also be valuable if the locking and unlocking property of the knee is instead a spectrum of variable damping. In other words, besides having the capability of being fully locked and completely free, the joint can also be used to generate some incremental damping torque values. This feature can be very useful for tasks such as sitting and descending stairs.

A wrap spring clutch knee was designed for this exoskeleton system due to its unique capacity to achieve the abovementioned features while retaining a compact size and a relatively low manufacturing cost. Detailed description of the wrap spring knee design is covered in Section 3.6.

3.3 Ryan Exoskeleton Hardware

The first revision of the Dynamic Joint Coupling Exoskeleton (also called the Passive Knee Exoskeleton and the Ryan Exoskeleton) is shown in Figure 3-5. The system was designed and customized to fit Test Pilot #2: A 28-year old male, 1.78 m (5’10”) tall, weighs approximately 150lbs, and has sustained a complete T12 injury 12 years prior to participating in this project.

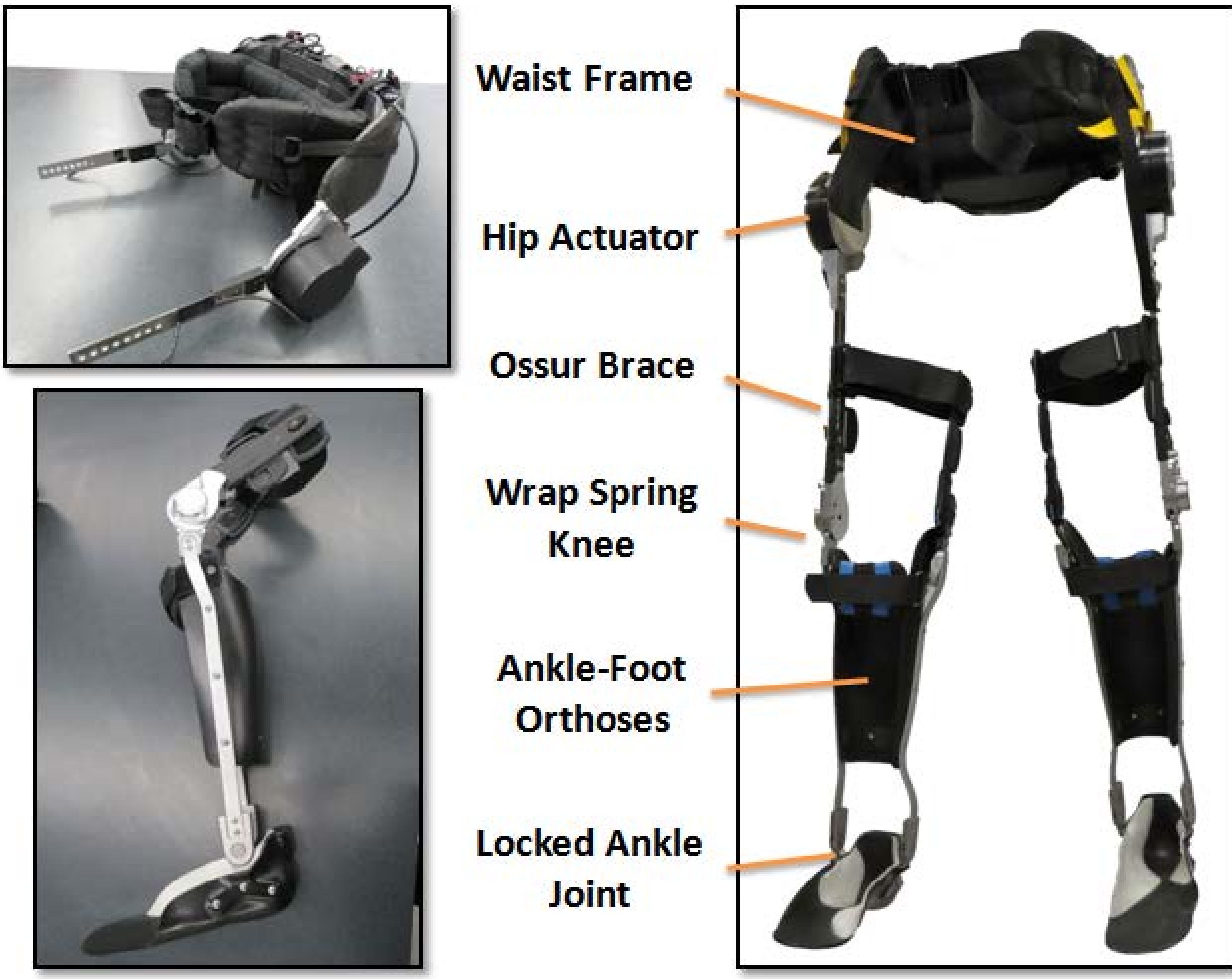

Figure 3-5: Overview of the first Ryan Exoskeleton

The suit consists of a custom molded carbon fiber waist frame, two hip actuators, and a pair of wrap spring knees which are connected to the test pilot’s custom fitted ankle-foot orthoses. A waist-frame design was chosen for this system because the test pilot has a high level of lower abdominal control, hence constraining the upper torso would not be necessary.

The hip actuator is composed of an Emoteq HT03000-J01-Z frameless electric motor, a Harmonic Drive (CSD-25-160-2A-GR-SP) 160-to-1 unhoused strain wave gearing transmission, and a Renishaw 16bit absolute magnetic encoder. These components are enclosed in a custom

4.5 inch diameter by 1.8 inch length cylindrical housing. The entire package weighs a total of 3.5 pounds. The actuators were designed to allow 152Nm of momentary peak torque (limited by the harmonic drive), 67Nm of maximum continuous torque, and a maximum no load speed of 1.4 radians per second. This actuation package was designed by Yoon Jeong, a Ph.D. student at UC Berkeley. This motor package was originally designed intended to be used on the Austin suit; however in order to speed up the prototype process, these motors were adopted onto the Passive Knee Exoskeleton system.

Meanwhile, a second hip actuation package was designed specifically for the dynamic joint coupling gait. This actuation module uses housed components that are off-the-shelf in order to facilitate manufacturing and assembly. As a tradeoff, adopting this module results in a 1 inch wider overall exoskeleton hip width. The actuator unit measures 3.5 inches in diameter, 2.3 inches in length, and weighs approximately 3 pounds. It consists of a Maxon EC-90-flat electric motor, a Harmonic Drive (SHD-20-100-2SH) 100-to-1 transmission, and a Renishaw 16bit absolute magnetic encoder. The actuator was designed to allow 95Nm of momentary peak torque, 49Nm of maximum continuous torque, and a maximum no load speed of 2.2 radians per second. This unit was specified to operate with higher speed and less torque, which allows for more desirable lower leg swing trajectory. Figure 3-6 shows an image of the two actuator assemblies.

Figure 3-6: Ryan Exoskeleton Hip Actuator. Emoteq (left) and Maxon (Right)

The hip actuator is connected to the wrap spring knee via an off-the-shelf Ossur knee brace, particularly, the femur component of the knee brace. The exoskeleton femur allows for 3 inches of adjustment to accommodate different user femur lengths. The interior exoskeleton femur and the interior exoskeleton knee joint are also components from the Ossur knee brace. The interior exoskeleton knee joint is simply a free joint with the purpose of providing additional out-of-plane joint support and a more secure thigh strap mount. See Figure 3-7 for a closer view.

Figure 3-7: Lower Leg Construction

The lower leg orthoses were taken from the test pilot's RGO. The ankle of the orthosis is locked at approximately 95 degrees with respect to the exoskeleton tibia (slight plantar flexion). This was done for several reasons.

1. Locking the ankle prevent foot drop, which would result in toe drag and difficulty in getting any toe clearance during swing.
2. The slightly plantar flexed ankle induces a torque that helps extend the knee when the foot is contacting the ground. This mechanism alleviates some breaking stresses on the knee joint during stance and also acts as a safety precaution in case of a knee failure.
3. At the point of toe-off, the locked ankle allows the user to transfer his weight onto the toes without further dorsiflexion. This mechanism simulates an activated ankle joint and assists with forward propulsion.

3.4 Experimental Evaluation

The following tests were conducted to evaluate the performance of the Passive Knee Exoskeleton:

1. Point tracking of ambulation joint trajectory
2. A series of 10-meter walk test (10MWT)
3. Quarter-mile speed test and speed comparison with other exoskeletons
4. Extended real-world-terrain walk test

These tests were performed by the device's first test pilot: Test Pilot #2. As previously mentioned, he is a 28-year old male, 1.78 m (5'10") tall, weighs approximately 150lbs, and has sustained a complete T12 injury 12 years prior to participating in these tests. The tests were conducted after the pilot had spent at least 10 hours in the suit and had gained a high level of confidence and familiarity with using the device.

3.4.1 Ambulation Point Tracking

Figure 3-8 and Figure 3-9 show the step sequence and point tracking data of Test Pilot #2 using the first revision of the Passive Knee Exoskeleton. The shown point-tracking plot is zoomed-in on the swing phase of the gait cycle (since the knee joint is simply locked during stance phase). As one can see from Figure 3-9, the implemented hip trajectory was exaggerated, it has a larger amount of hip extension and hip acceleration when comparing with the CGA data. The more aggressive hip motion was adopted in order to maximize the inertial force generated at lower limb which would increase the amount of knee flexion and toe clearance. It can be seen from Figure 3-9 that the resultant knee flexion generated through dynamic joint coupling exceeded that of which was observed from both the CGA data and the Austin Exoskeleton mechanical coupling gait. This result further demonstrates that knee actuation is not necessary for level-ground gait generation as long as appropriate hip actuation is present. It is important to note, however, that adopting this knee actuation strategy also means the exoskeleton will now provide less sit-to-stand assistance, since dynamic joint coupling cannot be utilized during standing.

Figure 3-8: Swing Sequence of the Ryan Exoskeleton

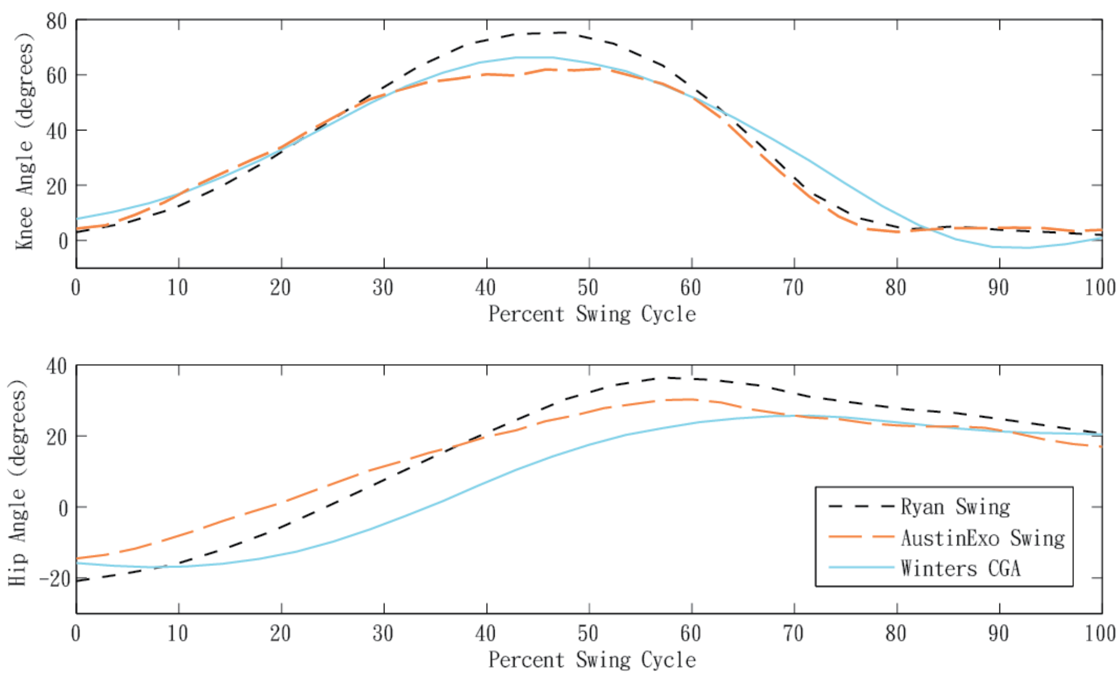

Figure 3-9: Point Tracking Data for the Swing Phase of the Ryan Exoskeleton

3.4.2 10-Meter Walk Test

The 10-meter walk test (10MWT) is a test that measures the time required for a patient to walk 10 meters at a self-selected pace. This test is a well-established functional mobility assessment tool commonly used in the clinical community to evaluate persons with neurological mobility impairment such as Parkinson's disease, stroke, and spinal cord injury [48–51]. In particular, the 10MWT has been considered as "the best tool to assess walking capacity in SCI subjects" [52] and "the most valid measure of improvement in gait and ambulation" of SCI patients [53,54]. For this reason, the 10MWT was administered to characterize the efficacy of the Passive Knee Exoskeleton.

The 10MWT was conducted on a flat and level track (as shown in Figure 3-10) with markers placed at the 0, 2, 8 and 10 meter positions along the direction of the walk path. The test pilot used the first 2 meters to accelerate before timing began at the 2-meter mark. The walk was then timed for the next 6 meters between the 2-meter and 8-meter marks. The final two meters was used for deceleration.

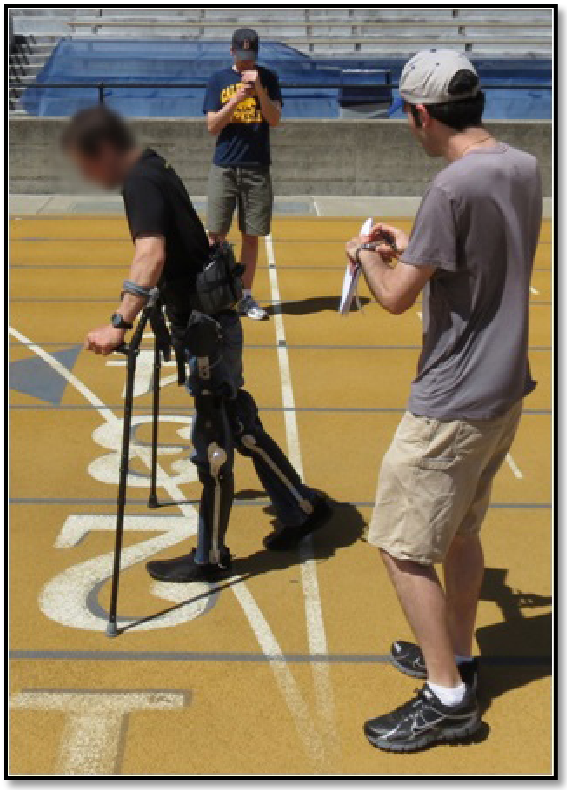

Figure 3-10: 10-Meter Walk Test

The test pilot performed three 10MWTs for each of the following six ambulation methods:

1. Exoskeleton with crutches
2. Exoskeleton with walker
3. Leg Braces with crutches, performing a swing-through gait[1]
4. Leg Braces with walker, performing a swing-through gait
5. Leg Braces with crutches, performing a reciprocating gait[2]
6. Leg Braces with walker, performing a reciprocating gait

[1] The swing-through gait is a method of ambulation where the person uses his or her arms to lift the entire body off the ground and swing forward like a pendulum, pivoting about the shoulder joints. For persons with paraplegia, use of leg braces is required to lock the knee joints.

[2] The reciprocating gait refers to the method of ambulation which the person manually swings one leg forward in a pendular manner while keeping the other leg planted on the ground. Similarly, for persons with paraplegia, use of leg braces is required to lock the knee joint that is weight bearing during this maneuver.

The results for the six sets of 10MWTs are presented below in Table 3-1.

	Speed (m/s)	Speed Ranking
Exoskeleton with Crutches	0.22 ± 0.01	2nd
Exoskeleton with Walker	0.20 ± 0.01	4th
Braces, Swing-through, Crutches	0.52 ± 0.01	1st
Braces, Swing-through, Walker	0.20 ± 0.02	4th
Braces, Reciprocating, Crutches	0.21 ± 0.02	3rd
Braces, Reciprocating, Walker	0.16 ± 0.01	6th

Table 3-1: 10MWT Timing Results with Change in Heart Beat Per Minute and Borg RPE

Of the six means of ambulation, walking with the exoskeleton (using crutches) clocked in at second place with an ambulation speed of 0.22 m/s (0.49 mph). The fastest means of ambulation remained to be the swing-through gait with crutches at a speed of 0.52 m/s (1.16 mph). The speedy performance of the swing-through gait was anticipated because 1) swinging about the shoulder joints covers approximately twice the distance per step when comparing to a regular reciprocating gait, and 2) the test pilot had several years of experience ambulating via the swing-though gait. On the other hand, when comparing to a passive reciprocating gait, the exoskeleton walk speed has shown to be faster, especially when walkers were use.

3.4.3 Quarter-Mile Speed Test

In order to quantify the steady-state walking speed of the Passive Knee Exoskeleton over long distances, a Quarter-Mile Speed Test was conducted at the U.C. Berkeley Edwards Stadium. The test pilot was also asked to perform this test using the swing-through gait (with crutches) for comparison. The test result is shown below in Table 3-2 along with the walk speed of other exoskeleton devices.

	Average Speed (m/s)	(mph)
Passive Knee Exoskeleton	0.27	0.60
Vanderbilt [55]	0.22	0.49
Ekso eLEGS [56]	0.19	0.43
Rex [57]	0.05	0.11
Swing-Through Gait with Crutches	0.59	1.32
Preferred Healthy Gait [58]	1.30	2.91

Table 3-2: Quarter-Mile Speed Test Result and Speed Comparison with Other Exoskeletons

3.4.4 *Extended Real-World-Terrain Walk Test*

Two extended real-world-terrain walk tests were conducted where the test pilot used the Passive Knee Exoskeleton to walk through the U.C. Berkeley campus. The routes taken are shown below in Figure 3-11.

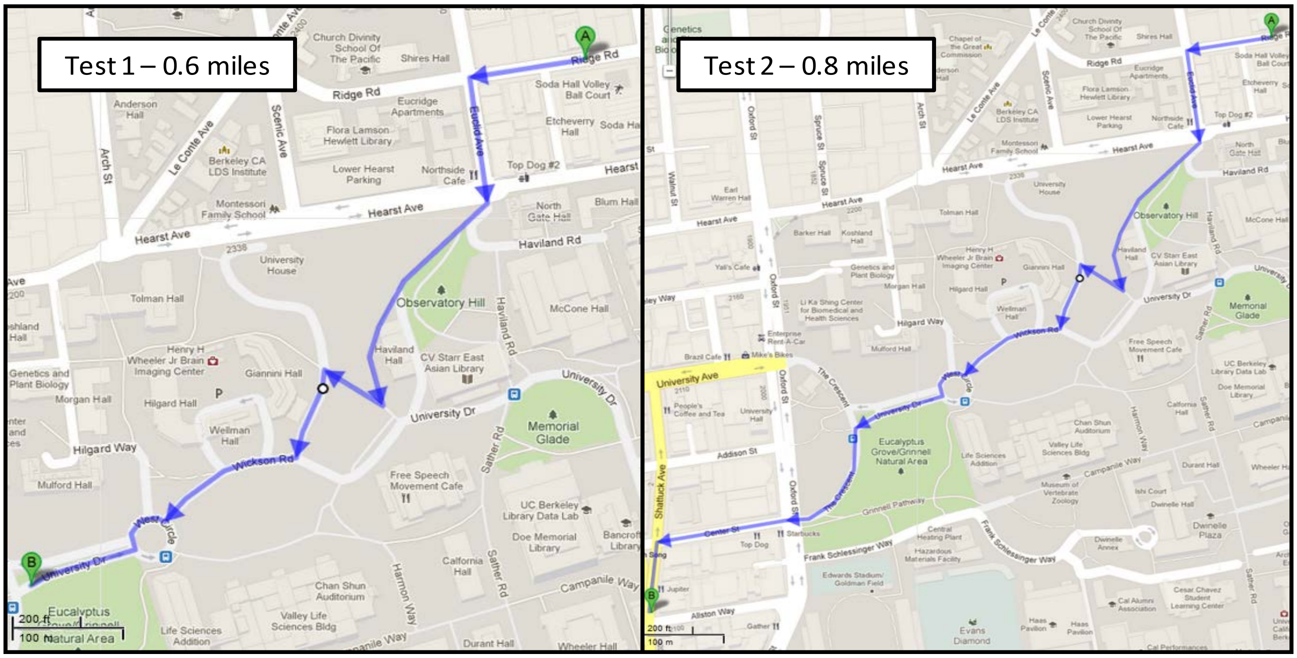

Figure 3-11: Routes of the Extended Walk Test Through the U.C. Berkeley Campus
Map Data from Goggle Maps and Image Adapted from [59]

The two tests were performed on two different days to ensure the test pilot was well rested prior to each test. The routes for the two days were 0.6 miles (~965 meters) and 0.8 miles (~1390 meters) long, respectively. The test pilot performed the walk at a comfortable self-selected pace and was free to take breaks whenever desired. The average speed of the first walk (including intermittent breaks) was 0.13 m/s or 0.29 mph. The average speed of the second walk (including intermittent breaks) was 0.17 m/s or 0.38 mph.

3.4.5 *Functional Ambulation Velocity and Distance Requirements*

Robinett et al. [60] have conducted a study defining the ambulation distances and velocities that individuals need to be able to achieve in order to function independently in their community. The study showed that for an individual to be able to visit commonly-visited public venues (e.g., stores, post offices, banks, and medical buildings) the individual needs to be able to walk approximately 289 meters to 505 meters depending on the size of the community. As proven by the real-world-terrain walk tests presented in Section 3.4.4, this distance requirement is easily achievable with the Passive Knee Exoskeleton.

As for functional ambulation velocity requirements, an updated study conducted by Andrews et al. [61] indicated a mean ambulation velocity of 0.49 m/s is necessary to safely cross streets. Referencing the test results from the Quarter-Mile Speed Test, at an ambulation speed of 0.27 m/s, the exoskeleton currently still falls short of the specified functional community walk speed.

3.5 Testing with Different Subjects

The Dynamic Joint Coupling Exoskeleton system was tested by several different patients with different levels of injury, physiques, upper body strength, and experience with crutch usage. Modifications were made to the exoskeleton to accommodate different users as new parameters were being identified through experiments. In the following subsections, some of the major system modifications will be discussed.

3.5.1 <u>Test Subject Overview</u>

Test Subject #1 – is primarily the test subject for the Austin Exoskeleton system. As previously mentioned, he is a 21-year-old male (6’2”, 200 pounds) with a complete T12 injury sustained 3 years prior to testing. The subject has been in a wheelchair since initial injury and has not had any previous training on orthotic usage or standing practice. He has a moderate amount of muscle tone, which facilitates with exoskeleton padding and decreases the likelihood of developing pressure sores. The subject didn’t show any signs of spasticity, but has some amount of joint contracture in the left knee.

Test Subject #2 – is the first test pilot for the Ryan Exoskeleton. He is a 28 year old male, 5’10” tall, weighs 150lbs, and has sustained a complete T12 injury 12 years prior to the experiment. He is exceptionally experienced with using leg braces and has been doing a swing-through gait as his primary method of transportation (as opposed to using a wheelchair) for approximately 8 years. The subject has a moderate amount of muscle tone but shows no signs of spasticity or joint contracture.

Test Subject #3 – is a 26 year old male, 6’ tall and weighs 120lbs. He has a T10 complete injury eight years prior to our first experiment. The subject has significant amount of muscle atrophy, which means his knee joints have minimal muscle tone resistance. Although he was fitted for leg braces and had done rehab with them, he discontinued use about six years ago due to the excessive amount of physical exertion. From then on, the subject stayed primarily in a wheelchair and might have shown signs of exhibiting slight amounts of joint contracture. This test pilot also has a good amount of abdominal control.

Test Subject #4 – is a 21 year old male, 6’1” tall and weighs 130lbs. He has an incomplete T9 injury three years prior to trying on the exoskeleton. The subject has very high levels of spasticity that lock up the knee joints and induce forceful hip adduction when in a standing position. A high level of clonus is also observed especially across the ankle joint.

Test Subject #5 – is a 24 year old female, 5'2" tall and weighs 140 pounds. Her injury level is T5, which makes her injury the highest amongst the five test subjects. This also means that she has very little to almost no abdominal control. She has a comparatively high amount of muscle tone and fat tissue, which facilitates with exoskeleton padding, but slightly hampers knee joint rotation. She is currently participating in a stem cell clinical trial and is testing with the exoskeleton as a potential method for rehabilitation.

3.5.2 Knee Spring Damper

As described in Section 3.4, the Passive Knee Exoskeleton adopted an exaggerated hip swing trajectory in order to increase the amount of knee flexion and toe clearance. However, as a result, an overly aggressive knee re-extension motion was observed at the end of the swing phase. At that instant, the pendular forward swing of the lower leg, combined with change of direction at the hip, generates a whipping motion of the lower limp. Because of the high terminal velocity and the lack of knee joint damping, when the exoskeleton knee reaches maximum extension, the residual momentum creates a rather violent jerking motion that propagates across test pilot's entire body.

In the effort to minimize this undesirable knee thrust, it was hypothesized that the extra knee extension energy could be captured with a spring element and be reutilized for more exaggerated knee flexion and more toe clearance. The author sets up a preliminary spring damper system as shown in Figure 3-12a, where bungee cords were used as the energy storage element. Preliminary experiments showed that the spring was able to successfully dampen swing-extension and generate a slight amount of extra toe clearance. This test result prompted further investigation by Tai I. (Nick) Um, a M.S. student at U.C. Berkeley, to develop an add-on knee joint spring damper (see Figure 3-12b and c). The final add-on device was able to reduce unwanted peak acceleration by 67% and increase ground clearance by 75% while adding only 11 oz of total hardware weight and without increasing the overall profile of the knee. The reader is referred to Nick's Master's thesis [62] for additional information on the spring damper system.

Figure 3-12: (a) Preliminary Swing-Extension Energy Capture Setup (b) Knee Spring Damper Add-on (c) Close-up view

3.5.3 Anatomic Joint Damping, Spasticity, and Joint Contracture

Aggressive knee swing extension was, however, not observed across all test subjects. After testing with several different patients, it was concluded that the user's anatomic knee damping plays a critical role in defining the knee joint swing trajectory. For example, when the hip trajectory used for Pilot #2 is implemented on Pilot #3, no violent knee extension was observed due to the fact that Pilot #3 has a higher coefficient of damping at his anatomic knee. Additionally, despite the dampened knee extension, approximately the same amount of toe clearance was obtained with Test Subject #3, which suggests that joint damping can be direction dependent and nonlinear. Particularly, Test Subject #3 showed no signs of additional knee damping in the direction of knee flexion and an increased joint damping only at the end portion of full knee extension. This result suggests that the extra knee damping is likely a result of joint contracture and/or residual uncontrolled muscle tone. Both of these conditions are not uncommon among SCI patients. In fact, Test Subject #2's exceptionally low knee joint resistance throughout the entire range of motion is likely the result of the extensive amount of standing exercises he has been doing after his injury which has accustomed his knees to be in a fully extended position. Nevertheless, it is much more common for SCI patients to not be as active in practicing standing and spend majority of their time in a seated position, which results in joint contracture and decreased joint range of motion. Minute signs of joint contracture have been observed in Test

Subject #3; however it was not significant enough to hamper the performance of the dynamic gait. Test Subject #1's left knee, on the other hand, had significant joint contracture that was enough to prevent the knee from reaching full extension. In this case, an external gas spring can be installed to counter the resistance from the user's knee. However, the spring force needs to be tuned to also not hinder knee swing flexion.

Another mechanism which has been observed to induce extrinsic knee torques is the patient's muscle tone. This mechanism is only present in patients with intact motor neurons and reflex arcs, which is the case for subjects #1, #4, and #5. SCI patients with intact reflex arcs are often characterized as having more muscle mass, whereas patients with severed reflex arcs frequently have acute muscle atrophy. From the perspective of exoskeleton control and application of dynamic joint coupling, it is much easier to work with individuals without muscle tone because it eliminates a lot of external factors and the knee joint can simply be modeled as a free pendulum. The dynamic joint coupling strategy still works for most SCI patients with muscle tone, such as Test Subject #1 and Test Subject #5, except that the hip swing trajectory will need to be modified to match their specific physical conditions. There are, however, individuals with significant amount of stretch reflex and spasticity to the point where the knees almost completely lock up when in a standing position. Test Subject #4 falls into this citatory and the exoskeleton did not work for him.

It should be appreciated that although individuals with intact reflex arcs and considerable amount of stretch reflex are less ideal candidates for the dynamic joint coupling system, they are viable FES candidates and therefore it is possible to incorporate FES to compensate for the additional joint resistance, or even assist with knee flexion.

3.5.4 Full Torso Frame

A full torso frame for the Ryan Exoskeleton was developed for users with lesser abdominal control, which is commonly associated with higher injury levels. The extended torso frame adopted elements from the Austin Exoskeleton system where an aluminum exoskeleton "spine" and shoulder straps were incorporated onto the exoskeleton. Figure 3-13 shows the extended torso module. The spine of the module can be adjusted in length and in stiffness to accommodate different user preferences. Furthermore, the new torso frame can also be adjusted for different user hip widths. An optional corset can be attached onto the exoskeleton spine for even more trunk support if necessary. However, so far none of the test pilots needed to use the corset. Test Subject #5 (who has the highest level of injury, at T5, and the least amount of abdominal control amongst the five test pilots) initially began using the exoskeleton with the corset. However, after several days of testing, she decided the corset was unnecessary and demonstrated that the shoulder straps and the waist belt were sufficient.

Figure 3-13: Extended Torso Frame for the Ryan Exoskeleton (Left)
Demonstration of use of the corset and walker (Right)

The design and fabrication of the full torso frame was done in collaboration with Patrick Barnes, a Masters student at U.C. Berkeley who worked in the Human Engineering Laboratory. The reader is referred to Patrick's Master's thesis for additional information on the design details of the extended torso module [63].

3.5.5 Adjustable Leg Module

An adjustable leg module was developed for the Ryan system to fit test pilots who do not have custom molded leg braces. The length of the leg module can be adjusted at the femur link and at the tibia link so that the device can be worn by users ranging from 5-foot tall to 6-foot-2. The module can also be adjusted for different amounts of hip rotation and ankle plantar flexion and dorsiflexion. The human-machine interface of the leg module consists of a thigh brace, a calf brace, and an exoskeleton shoe. Figure 3-14 shows the modular leg system.

Figure 3-14: Adjustable Leg Module for Different User Heights

3.5.5.1 Human-Machine Interface: Thigh Brace

For thigh bracing, a similar posterior thigh support solution as used for the Austin Exoskeleton system was adopted. However, contrary to the compliant plastic thigh braces on the Austin device, the new braces were made to be rigid through carbon fiber reinforcement. The thigh braces are detachable from the femur link and two sizes were made (a large and a small). They are contoured to fit a generic thigh shape and rely on additional padding for fine fitting. Additionally, the braces can be adjusted up-and-down, front-and-back, and be rotated along the axis collinear with the femur link. The posterior thigh support was chosen for two reasons (as oppose to anterior thigh support).

1. It eases the donning and doffing of the exoskeleton.
2. The rigid thigh braces, when properly positioned to be right below the buttocks, are effective in preventing the pilot from slipping out of the suit.

3.5.5.2 Human-Machine Interface: Shin Guard and Calf Brace

Securing and aligning the knee joint with the exoskeleton has long been regarded as one of the most critical aspect of exoskeleton operation. The Austin Exoskeleton used a rigid frontal "shin guard" design (see Figure 3-15a), which swings open during donning and latches shut when the pilot is in the suit. The rigid frontal shin support is effective in aligning the knee and preventing the user from falling out of the device. A similar shin guard design was implemented on the Ryan Exoskeleton as shown in Figure 3-15b.

(a) (b) (c)

Figure 3-15: Human-Machine Interface for the Legs
(a) Austin Exoskeleton. (b) Ryan Exoskeleton Shin Guard Design. (c) Ryan Calf Brace Design.

Figure 3-15c shows an alternative solution where a rigid posterior calf brace is used in conjunction with soft strapping in the front (a method commonly used by traditional orthotic leg braces). The exoskeleton calf brace was first modeled based on a generic calf contour. A plastic mold was then created with fused deposition modeling (FDM), which was later carbon fiber reinforced and padded (see Figure 3-16). Three different sizes were made (small, medium, large) and they can be interchanged depending on the user's level of muscle atrophy and calf diameter. So far, the calf brace solution is preferred over the shin guard solution due to its higher level of adjustability.

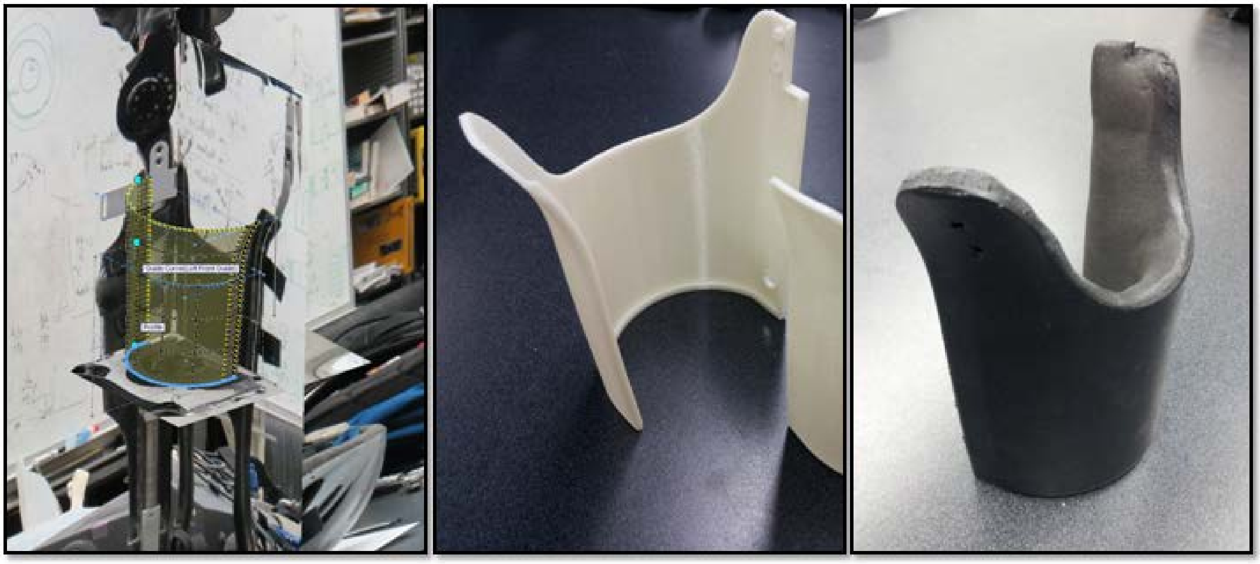

Figure 3-16: Exoskeleton Calf Brace Fabrication Procedure

3.5.5.3 Human-Machine Interface: Exoskeleton Shoe

Exoskeleton foot interface can be separated into two categories: internal and external. As previously mentioned, prior to having an adjustable leg module, the Ryan Exoskeleton exclusively used custom molded leg braces, which includes an ankle-foot-orthosis (AFO). The AFO is worn inside of the shoe as shown in Figure 3-17(a). An internal foot-interface solution is advantageous for the following reasons.

1. It is minimalistic. It does not add a lot of weight or bulk to the foot.
2. The internal orthosis is thin and does not add too much extra thickness to the sole.
3. It is a proven and widely used technology. It is safe.
4. The ankle flexion adjustment component is small and effective.

Despite the aforementioned benefits of an internal foot brace, it was decided that an external solution would be more reasonable for a module that needs to be used by a variety of different users with very different foot shapes. It was decided that having a generic internal orthotic foot brace would be too risky since an improperly contoured orthosis has a high chance of causing pressure sores on the foot. For this reason, an external exoskeleton shoe was designed and adopted as shown in Figure 3-17(b). The exoskeleton shoes are usually worn outside of the user's personal shoes, but it is also possible to wear them directly over the user's feet if preferred. There are two sizes available as shown in Figure 3-17(c). The two sizes so far have been able to accommodate shoe sizes ranging from female size 6 to male size 11. An adjustable ankle joint is also adopted on the foot module as shown in Figure 3-17(c).

(a) (b) (c)

Figure 3-17: (a) Internal Foot Interface (b) External Exoskeleton Shoes (c) Sizes Large and Small

3.5.5.4 <u>Adjustable Leg Module Concluding Remarks</u>

As expected, the adjustable leg setup presented in this section is heavier and more cumbersome than the personalized and custom molded leg bracing solution. However, the module's adjustable sizing element makes it more ideal for quick testing with multiple subjects and for clinical settings.

3.6 Wrap Spring Clutch Knee Design

The wrap spring clutch in its most basic form consists of two concentrically rotating arbors and a spring. These three components are assembled in a configuration as shown in Figure 3-18, where the spring sits across the interface of the two arbors. When the arbors are rotated in the direction of which the spring is wound, the spring wraps down onto the arbors, gripping the two components so that torque can be transferred from one component to the other. Putting this description in the context of a knee design, one of the arbors will correspond to the femur link and the other corresponds to the tibia link. As shown in Figure 3-19, the spring will be wound in the direction of the knee flexion so that the spring can wrap down on the arbors and lock the knees during flexion.

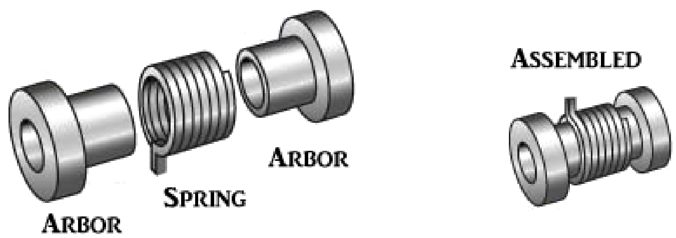

Figure 3-18: Basic Wrap Spring Clutch Assembly
Image adapted from [64]

In the case for knee extension, the arbors will be rotating in the opposite direction of the spring winding, also shown in Figure 3-19. This has an unraveling effect on the spring, which loosens the grip and allows the arbors to slip. The mechanism described so far portrays a knee that locks against flexion while permitting extension, which is ideal during stance.

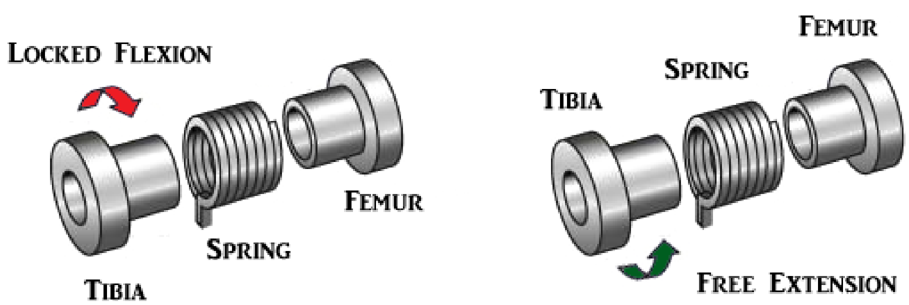

Figure 3-19: Wrap Spring – Locked Flexion and Free Extension. Adapted from [65]

In the swing phase of the gait, the knee has to be free in both directions. The spring of the clutch assembly can be manually unraveled and disengaged by pushing on the tang of the spring, as shown in Figure 3-20. The tang needs to be pushed in the opposite direction of the spring winding, and when this is done, the tibia arbor becomes free to rotate in both directions. In the knee design, a linear servo is mounted on the femur link to control the disengagement of the wrap spring. It is important to note that successful disengagement of the wrap spring is only possible if the opposite end of the spring is fixated to the arbor. Otherwise, the entire spring will simply slip and rotate instead of unraveling.

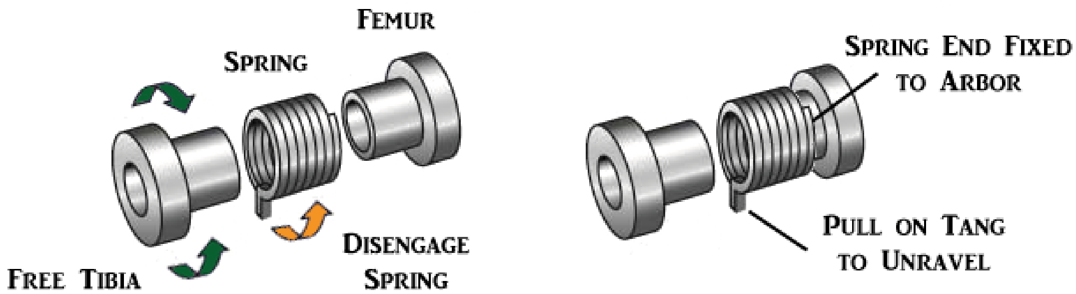

Figure 3-20: Wrap Spring – Free Swing Operation. Adapted from [65]

3.6.1 Hardware Overview

Based on the simplest wrap spring description presented in the previous section, a variety of different wrap spring arrangements can be designed to comply with specific application needs. Two different knee configurations were designed for this exoskeleton system with the following objectives, which are ranked by priority:

1. Minimize Joint Width
2. Minimize Joint Diameter
3. Minimize Joint Weight
4. Ease of Assembly/Disassembly

Figure 3-21 shows the first revision of the wrap spring knee. The knee measures 3.6in (9.2cm) by 2.5in (6.3cm) by 1.3in (3.4cm) and weighs 0.8lbs (0.36kg). Figure 3-22 shows the knee component arrangement and a section view.

Figure 3-21: Wrap Spring Knee – First Revision

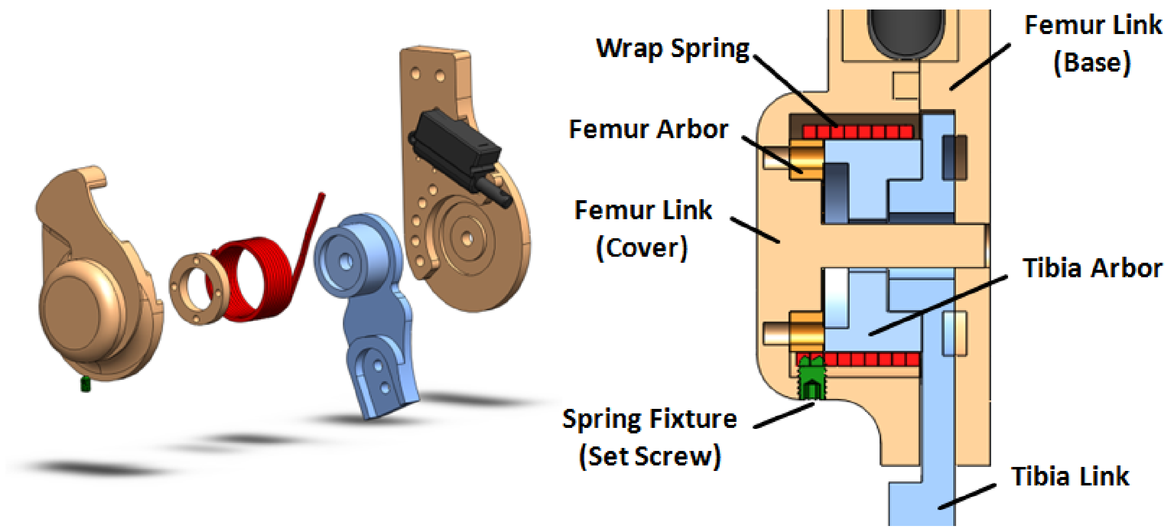

Figure 3-22: Wrap Spring Knee – First Revision. Assembly and Section View

3.6.1.1 <u>Femur Construction</u>

The femur link of this knee revision is made of two components: 1) a base-plate that gets connected to the femur of the exoskeleton and 2) a front cover that is rigidly connected to the base-plate. This two-piece design was chosen for three reasons.

1. The two-piece femur sandwiches the tibia link and double supports the axis of rotation.
2. This construction allows the femur plane to sit right next to the tibia plane, which eliminates unnecessary out-of-plane joint torquing and provides a more streamline and compact construction. Since it is unavoidable for the two arbors to be on the opposite ends

of the wrap spring, many single-supported assemblies tend to have large load-plane offsets that are more than an inch apart.

3. The two-sided femur link is effective in preventing the separation of the two arbors, which can damage the spring and cause a catastrophic failure of the spring clutch. The femur cover provides axial loading for the assembly and facilitates the incorporation of thrust needle-bearings. This allows smoother joint rotation even with the presence of off-axis moments.

3.6.1.2 Spring Fixture

The wrap spring is fixed to the femur link by a few set screws located on the femur cover, as shown in Figure 3-22. The set screws are threaded into the femur cover and used to secure the coil spring against the femur arbor. Fixing the spring to the femur link is essential for two reasons.

1. As mentioned in the previous section, during the swing phase of the gait, the knee needs to be free to rotate in both directions, which is achieved by unraveling wrap spring. Pushing on one of the tangs of the spring without fixing the other end will simply rotate the spring, and hence the set screws are critical for effective spring disengagement.
2. Since the torque transmission capacity of the spring clutch is dictated by the number of spring coil engagement with the arbor, the locking capacity of the knee can only be as high as the arbor with the lesser spring engagement would allow. That is, the clutch will begin to slip on whichever arbor that has fewer spring coil engagement. Therefore, the design is generally optimized when the number of coil wrappings on the two arbors is the same. This description, however, is only true for constructions in which both ends of the wrap springs are left unconstrained. In the effort to minimize the thickness of the knee joint, one end of the wrap spring is fixed to the femur arbor, which allows for a reduced number of coil engagements on the femur arbor while obtaining the same overall performance. Notice in Figure 3-22, the number of spring coils wrapped around the femur arbor is significantly fewer than then number of coils wrapped around the tibia arbor. The reader is referred to Section 0 for more detailed explanation of this topic.

3.6.1.3 Actuator Placement

The linear actuator shown in Figure 3-21 is used to push on the tang of the wrap spring in order to unravel the spring when free flexion of the knee is wanted. This actuator has to be mounted on the same body as which the wrap spring is fixed to – in this case, the femur link. If the disengagement actuator was mounted on the opposite rotating body, the tibia link, then the disengagement actuation will become a function of knee angle, which introduces unnecessary complexity for joint control. To get a better understanding of this, imagine the linear actuator mounted in the same configuration as shown in Figure 3-21, but now rotates with the tibia link instead. During operation, suppose the linear actuator is extended just enough to disengage the spring, however, as the knee flexes, the actuator also moves away from the spring tang. This hypothetical construction would require the linear actuator to continue to extend as the knee flexes, which becomes unrealistic and not optimal. Similarly, one can imagine another scenario which the linear actuator is mounted on the femur link in the same configuration, however, the wrap spring is now fixed to the tibia link. Any knee flexion would result in the spring tang rotating closer to the actuator, which can either damage the spring or requires a large amount of actuator contraction in order to avoid contact with the spring tang.

3.6.1.4 Material Selection and Assembly

All of the machined components in the knee are made out of 6061-T6 aluminum alloy with the exception of the two arbors. The arbors are made out of 8620 steel and case hardened in order to minimize wear at the spring interface. The arbors are fixed to their corresponding links by dowel pins.

The optimal assembly procedure for this design is to:

1. First assemble the tibia arbor with the tibia link with dowel pins.
2. Put the thrust bearing into the groove inside the tibia arbor and place the femur arbor over the thrust bearing.
3. Install the wrap spring over the two arbors at the desired orientation.
4. Secure the femur cover onto the femur arbor with dowel pins.
5. Install the linear actuator into the femur cover, place the thrust bearing on the back of the tibia link and enclose the entire assembly with the femur link.
6. Adjust the orientation of the wrap spring and tighten the spring fixture setscrews.

3.6.2 Wrap Spring Design Equations

3.6.2.1 Output Torque Capacity

Wrap spring clutches operate under the classic capstan torque amplification principle, that is, the torque transmission capacity of each successive coil of wire is amplified exponentially by the frictional forces of the previous coils. In the design of a classical external[3] wrap spring clutch, the inner diameter of the free wrap spring is always smaller than the diameter of the arbor so there is a diametric interference before assembly. Upon assembly, the spring is forced to expand slightly to fit over the arbor. The expansion of the spring generates a pressure at the mating interface, which develops a proportional friction force at the contact surface. This initial friction force becomes the Energizing Torque of the system and it is amplified through each successive coil of wire when the arbors are turned in the winding direction.

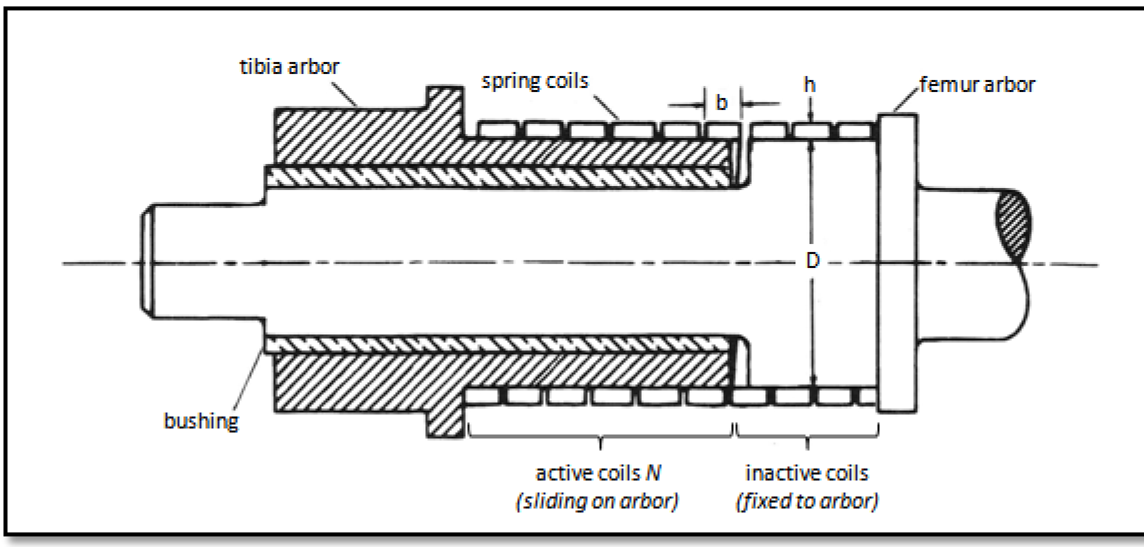

Figure 3-23: Pictorial Illustration of Wrap Spring Design Parameters. Adapted from [66]

The locking capacity of the spring clutch, as shown in Figure 3-23, can be expressed as [66]

$$T_o = \frac{p_0 b D^2}{4}(e^{2\pi\mu N} - 1) \tag{3.1}$$

[3] External wrap spring clutch describes the most common wrap spring clutch setup of which an external coil spring sits on the arbor shafts, as shown in Figure 3-23. It is also possible to use an internal coil spring in conjunction with hollow arbors to achieve the same torque amplification. Internal wrap spring clutch has its pros and cons, and the reader is referred to [71] for more information.

where

T_o	=	Output Torque (total torque transmission capacity)
p_0	=	Initial Pressure (between the spring and the arbor)
b	=	Spring Wire Width
D	=	Arbor Diameter
μ	=	Coefficient of Friction (between spring and arbor)
N	=	Number of Spring Coil Engagement (with the active arbor[4], i.e. the tibia arbor)

The initial pressure p_0 developed between the spring and the arbor is a function of the coil's flexural rigidity EI, the amount of diametric interference Δ, and the diameter of the friction surface D. The initial pressure of the system is derived in [66] as

$$p_0 = \frac{8EI\Delta}{b(D+h)^4} \mp p_c \tag{3.2}$$

where

E	=	Modulus of Elasticity of the wire
I	=	Moment of Inertia of area in bending
Δ	=	Diametric interference before assembly
h	=	Wire height
p_c	=	Pressure induced by the centrifugal force

(Circular Wire)	$I = \frac{\pi}{4} r^4$	$r = wire\ radius$
(Rectangular Wire)	$I = \frac{bh^3}{12}$	$b = wire\ width$ $h = wire\ height$

The p_c term only becomes significant at high rotational velocity when centrifugal force comes into play. The centrifugal force pushes the spring coil outwards and has a countering affect to the interference pressure, hence the negative sign before the p_c term. For an application as a knee joint, the p_c term can be ignored due to its slow rotational speed.

Combining Equations (3.1) and (3.2) while setting the p_c term to zero gives

$$T_o = \frac{2EI\Delta D^2}{(D+h)^4} \left(e^{2\pi\mu N} - 1\right) \tag{3.3}$$

---

[4] "Active" arbor refers to the arbor that allows for sliding with the spring in the overrunning direction. That is, the "Inactive" arbor refers to the arbor that is fixed to the spring.

Equation (3.3) can be viewed as having two components. The first part of the equation represents the initial Energizing Torque, which is a function of the coil's flexural rigidity *EI*, the diametric interference *Δ*, and the diameter of the friction surface *D*. The second part of the equation represents the exponential torque amplification factor, which is a function of number of coil wraps *N* and the coefficient of friction μ.

$$T_o = \underbrace{\frac{2EI\Delta D^2}{(D+h)^4}}_{\substack{Energizing \\ Torque}} \quad \underbrace{(e^{2\pi\mu N} - 1)}_{\substack{Coil \\ Amplificiation \\ Factor}}$$

Equation (3.3) can be rewritten as:

$$T_o = T_e \; (e^{2\pi\mu N} - 1) \tag{3.4}$$

where T_e is the Energizing Torque.

The torque in the i-th coil of the wrap spring can be expressed as

$$T_i = T_e \; (e^{2\pi\mu i} - 1) \tag{3.5}$$

Figure 3-24 illustrates the torque carrying capacity of each spring coil in a hypothetical wrap spring clutch design. The coefficient of friction is assumed to be 0.15 for this figure.

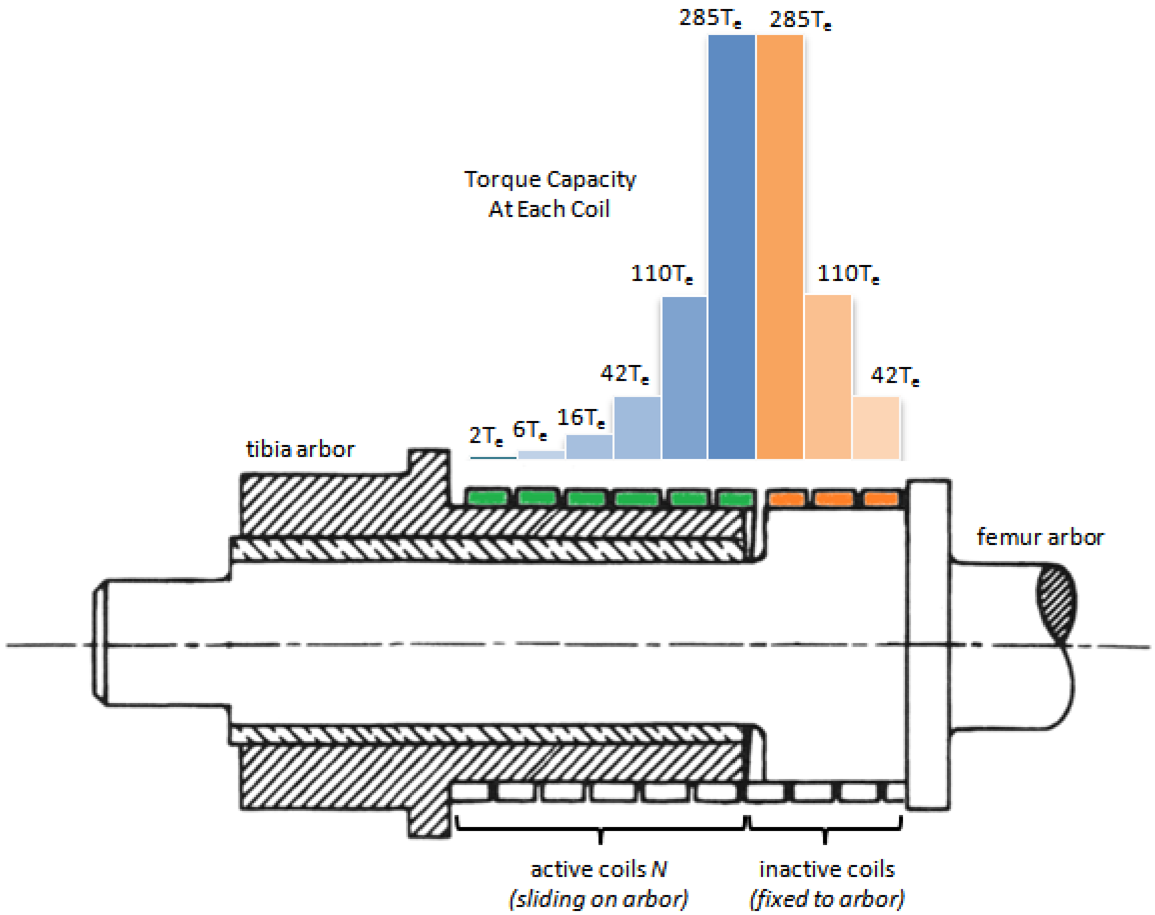

Figure 3-24: Successive Spring Coil Torque Carrying Capacity.

After six coil wraps, the torque carrying capacity of the clutch is amplified 285 times the initial Energizing Torque. Any torque higher than $285T_e$ will cause the clutch to slip. It is critical for the side of the spring with only three coil engagements to be fixed to the arbor (i.e. the femur arbor) in order to obtain the maximum locking capacity. If both ends of the spring are left free to rotate, then the clutch will begin to slip on the side with the fewer number of coil wraps (which in this given example, only has three coils of torque amplification and hence the clutch will only be capable of generating a maximum locking torque of $16T_e$, as shown in Figure 3-24). If both ends of the spring have six coils engaged, then neither sides of the spring need to be fixed to obtain the $285T_e$ locking capacity, however, this will obviously result in a ticker clutch assembly.

The fixed end of the spring can, in fact, have less than one coil engagement. However, such system will need to have a spring fixture mechanism that is capable of handling the entire torque capacity. For example, in the case of the knee design presented in Section 3.6.1 where the spring fixation is done by setscrews, the setscrews will need to provide enough holding force to provide and match the $285T_e$ locking torque. However, if an additional coil of wire is used for spring fixture, then the setscrews will only need to hold $110T_e$ (see Figure 3-24) and can rely on capstan torque amplification to reach the final $285T_e$ locking capacity. With each additional coil of wire, the spring fixture mechanism will need to provide less locking force, and when the number of coil engagement on both arbors are the same, the fixture component is no longer necessary.

It is important to note that several different wrap spring clutch analyses are available in existing literature. The equations presented in this section as well as equations derived in [67,68] are based on a simplified assumption that the initial pressure between the spring and the arbor is uniform throughout the entire spring coil. A more exact analysis [69] takes into account of the concentrated force at the end of the spring, however the result shows no significant difference in the calculated torque.

The wrap spring clutch torque equation can be written in various forms. Another common representation of Equation (3.3) is used in [70] and expressed as

$$T_o = EIR_A \frac{R_{SA} - R_{SF}}{R_{SF}{R_{SA}}^2} \left(e^{2\pi\mu N} - 1\right) \tag{3.6}$$

where

E	=	Young's Modulus of Spring Material
I	=	Area Moment of inertia of the wrap spring
R_A	=	Radius of the Clutch Arbor
R_{SF}	=	Radius of the Neutral axis of the free wrap spring
R_{SA}	=	Radius of the Neutral axis of the wrap spring when fitted over the arbor

While the variables in the two presented equations are different, the underlying principal is the same. Equation (3.6) can also be represented in a similar two-component format and the only difference between the two equations is the representation of the spring-arbor interference.

$$T_o = \underbrace{EIR_A \frac{R_{SA} - R_{SF}}{R_{SF}{R_{SA}}^2}}_{\substack{Energizing \\ Torque}} \quad \underbrace{\left(e^{2\pi\mu N} - 1\right)}_{\substack{Coil \\ Amplificiation \\ Factor}}$$

3.6.2.2 ***Unwinding (Overrunning) Torque Equation***

An unwinding torque, also known as the Overrunning Torque, is present in the clutch when the arbors are rotated in the unwinding direction of the spring. From Equation (3.1), the sign of the coefficient of friction μ is reversed to obtain the unwinding torque T_U

$$T_U = \frac{p_0 b D^2}{4}\left(1 - e^{-2\pi\mu N}\right) \tag{3.7}$$

When the spring clutch is used in a knee joint application, this unwinding torque represents the resistance during knee extension. Equation (3.7) can be rewritten in terms of Energizing Torque T_e as:

$$T_U = T_e(1 - e^{-2\pi\mu N}) \quad (3.8)$$

As shown in Table 3-3, the unwinding torque rapidly converges to the Energizing Torque as the number of coils increases. It is important to emphasize that this unwinding torque represents the resistance to knee extension when the spring tang is left untouched by the linear actuator. The actual knee extension resistance can be increased via pulling on the spring tang in the winding direction, which has the effect of decreasing the spring inner diameter and hence increasing the friction forces at the spring-arbor interface. Conversely, the knee extension resistance can also be decreased via pushing on the spring tang in the unwinding direction, which has the effect of increasing the spring inner diameter and therefore decreasing the friction forces at the spring-arbor interface.

Number of Coils	Unwinding Torque	Output Torque
1	0.61 T_e	1.57 T_e
2	0.85 T_e	5.59 T_e
3	0.94 T_e	15.90 T_e
4	0.98 T_e	42.38 T_e
5	0.99 T_e	110.32 T_e
6	1.00 T_e	284.68 T_e
7	1.00 T_e	732.15 T_e
8	1.00 T_e	1880.50 T_e
9	1.00 T_e	4827.54 T_e
10	1.00 T_e	12390.65 T_e

Table 3-3: Unwinding Torque and Output Torque as a function of Number of Coils. In terms of Energizing Torque T_e

3.6.2.3 <u>Design Optimization: Minimize Overrunning Torque</u>

One of the design considerations for a wrap spring clutch knee is to minimize the joint's Overrunning Torque so that there is minimal knee extension resistance and the joint allows better "free extension" performance. As shown in Table 3-3, the Overrunning Torque is essentially the same as the Energizing Torque, and therefore it is ideal to minimize the

Energizing Torque from the perspective of attaining a more uninhibited joint extension. As shown by Equation (3.4), which is repeated below for convenience,

$$T_o = T_e \ (e^{2\pi\mu N} - 1),$$

minimizing the Energizing Torque T_e while maintaining the same output torque T_o specification requires an increase in number of coil engagement. It can therefore be concluded that a spring clutch optimized for low-resistance knee extension should have a large number of coil wraps and a small Energizing Torque. (See Section 3.6.2.1 on Energizing Torque)

It is also possible to further minimize the clutch Overrunning Torque through modifying the shape of the spring or the arbor. For example, a designer can change the shape of the arbor so that only the outer spring coils interfere with the arbor and a slight clearance is left for the inner coils (see Figure 3-25). In this configuration, the overall torque capacity is largely unaffected since the inner coils will contract and achieve full engagement during operation. However, in the overrunning direction, the effective number of coil engagement can be drastically decreased with this method. Similarly, the same performance can be achieved with a varying diameter spring. This method was however not adopted for the current knee revision due to the added cost and complexity of such designs. The reader is referred to [71] for more information on this topic.

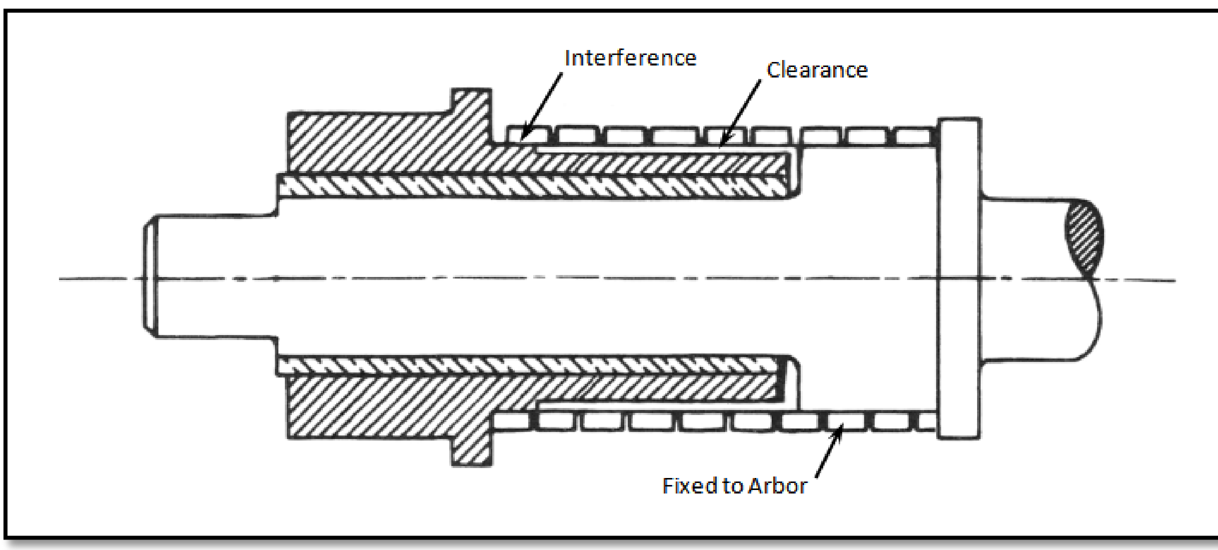

Figure 3-25: Arbor Modification to Decrease Overrunning Torque

3.6.2.4 *Variable Damping for Wrap Spring Clutches*

Traditionally, wrap spring clutches are most commonly used in pure locking and unlocking applications. Rarely are the clutches used to allow slippage and generate variable resistive torques. As described in Section 3.2, there are several advantages for having a knee joint that could generate a variable amount of damped flexion for activities such as sitting and descending stairs.

Referring to Equation (3.3) as shown below,

$$T_o = \frac{2EI\Delta D^2}{(D+h)^4} \left(e^{2\pi\mu N} - 1\right)$$

one can see that although a wrap spring clutch is self-energizing, it is not self-locking. That is, the spring coil amplification mechanism produces a finite breaking torque value (as oppose to an infinite breaking value), one of which when exceeded, will allow the joint to slip. This characteristic is significant because it demonstrates that the breaking torque can be manipulated and the spring clutch can be used as a variable resistive torque generator instead of a simple locking and unlocking device.

The output torque T_o of the spring clutch can be adjusted during operation through pushing or pulling on the wrap spring tang. As previously described, pushing on the spring tang in the unraveling direction has the effect of increasing spring diameter, which results in a drop in the Energizing Torque T_e and subsequently causes the release of the clutch. However, if the spring tang can be controlled and deflected in micro-steps by a linear actuator, then the Energizing Torque can be finely adjusted, which ultimately results in a controllable torque output.

3.6.2.5 Design Optimization: Maximize Variable Damping Controllability

The precision of which the output torque can be controlled is an important design parameter. Due to the large torque amplifying coefficient of the spring clutch, the resolution of damping adjustment can be quite low. In other words, the resultant output torque can be very sensitive to any incremental deflection of the spring tang. That is, in extreme cases, it is possible that any infinitesimal deflection of the spring tang will instantaneously transition the clutch from being locked to completely free. To more clearly illustrate this point, the reader is referred back to Equation (3.3), which is repeated below for convenience.

$$T_o = \underbrace{\frac{2EI\Delta D^2}{(D+h)^4}}_{\substack{Energizing \\ Torque}} \quad \underbrace{\left(e^{2\pi\mu N} - 1\right)}_{\substack{Coil \\ Amplificiation \\ Factor}}$$

As previously described in Section 3.6.2.4, the output torque limit of the spring clutch can be adjusted by micro-deflecting the spring tang, which in Equation (3.3) represents a change in the diametric spring interference Δ. The resolution of the actuator that deflects the spring tang, therefore, ultimately determines the controllability of the Energizing Torque, and hence the output torque. However, notice from Equation (3.3), even with high Energizing Torque controllability, if combined with a large amplification factor, the output torque control resolution would be lost. Consequently, from the viewpoint of maximizing damping controllability, it is ideal to minimize the number of active coils and compensate with a higher nominal Energizing Torque.

3.6.2.6 Overrunning Torque vs. Damping Controllability

Based on the analysis of Section 3.6.2.3 and Section 3.6.2.5, one can see that there is a tradeoff relationship between minimizing Overrunning Torque and maximizing damping controllability. That is, when one attempts to lower the Overrunning Torque of the clutch (via specifying a smaller nominal Energizing Torque and a higher number of active coils), he is at the same time losing damping controllability. This performance tradeoff relationship is very important and will come into play in the process of specifying design variables such as spring-arbor interference and number of coil engagements. The reader is referred to a later section (Section 3.6.4.4) for more information on this topic.

3.6.3 Stress Calculation for Knee Components

Stresses on several clutch components must be evaluated and taken into account of in the design process. This section will examine the stresses in the spring coil and the arbor.

3.6.3.1 Spring Coil Stresses

The stresses in the spring coil consist of several components. The most dominant element is an axial tensile stress in the direction of the wire created by the tangential force which is responsible for the clutch's torque carrying capacity. A second component includes the bending stress generated when the smaller diameter spring is fitted over the larger diameter arbor. This bending stress is almost always significantly smaller than the axial tensile stress and for that reason can be neglected for most applications. A third bending stress component caused by additional contraction of the spring can also be introduced under the special circumstance of which additional clearance is left for the inner coils, as previously discussed in Section 3.6.2.3. This special construction is unnecessarily costly and complex for our application, and therefore was not adopted.

The axial tensile stress at each segment of the spring is directly proportional to the torque capacity of the said segment. Remember from Section 0, the torque capacity of the i-th coil of the wrap spring can be calculated with Equation (3.5), as shown below.

$$T_i = T_e \left(e^{2\pi\mu i} - 1\right)$$

With Equation (3.5), the axial tensile stress in the spring can be derived.

$$\sigma_{SAi} = \frac{F_i}{A} = \frac{T_i}{A \cdot R_c} \qquad (3.9)$$

where

σ_{SAi}	=	Axial Stress in the i-th coil of the spring [psi]
F_i	=	Axial Load in the i-th coil of the spring [lb]
A	=	Spring cross sectional area [in^2]
T_i	=	Torque in the i-th coil of the Wrap Spring [lb.in]
R_c	=	Radius to the centroid of the wrap spring when fitted over the arbor [in]

Since the torque capacity of the clutch reaches maximum at the interface of the two arbors, the "crossover" coil will have the highest axial loading and therefore the highest axial stress, assuming that the cross sectional area of the spring and the radius of the spring on the arbor stay constant. The maximum axial stress at the crossover coil can be expressed as:

$$\sigma_{SAmax} = \frac{F_o}{A} = \frac{T_o}{A \cdot R_c} \qquad (3.10)$$

where

$$T_o = T_e \left(e^{2\pi\mu N} - 1\right)$$

3.6.3.2 Internal Spring Construction and Fatigue Loading

It is important to point out that the axial stress discussed in this section is in tension if the spring is wrapped outside of the arbor. It is possible to construct a spring clutch with an internal spring, that is, the arbors are hollow hoops which the spring is fitted inside of (See Figure 3-26). In such construction, the spring's outer diameter should be slightly larger than the inner diameter of the hoop so that the spring is contracted slightly when installed. The resultant axial stress for this setup then becomes compressive, which is more advantageous from the standpoint of fatigue loading.

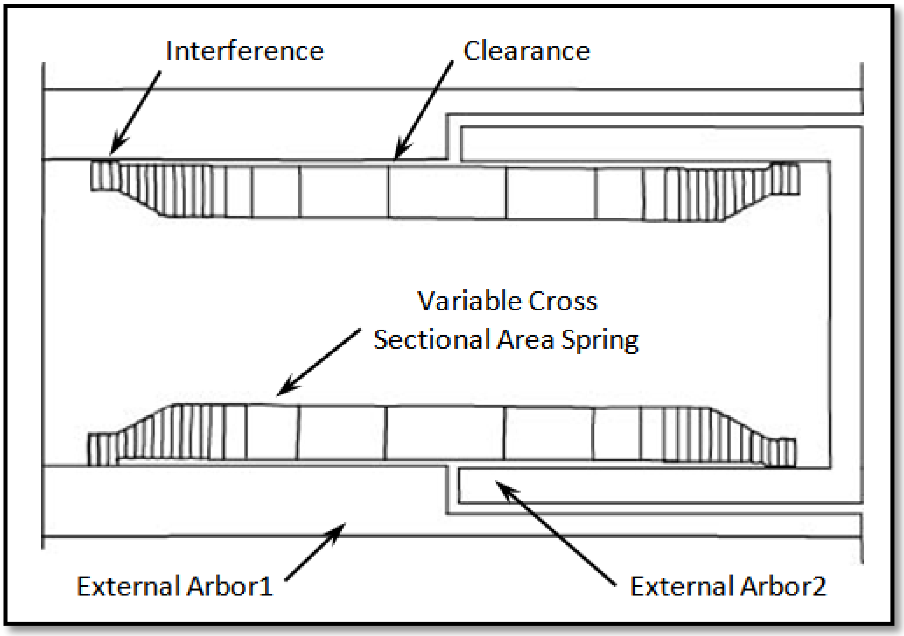

Figure 3-26: Example of Internal Wrap Spring Clutch Design. Adapted from [71]

External spring construction was adopted for the current knee design due to its much more straightforward construction and assembly procedure. However for this reason, the axial load is in tension and it is desirable to specify a spring that is operating under the endurance limit of the spring material to avert fatiguing.

3.6.3.3 Arbor Stresses

A compressive stress is induced onto the arbor during clutch operation when the spring constricts down onto the arbor. This pressure can be calculated with knowledge of the tangential component of the torque and the projected area of the spring [71]. The compressive pressure on the arbor can be derived as:

$$P_{Ai} = \frac{2F_i}{A_{AP}} = \frac{2\,T_i/R_c}{b \cdot 2R_A} = \frac{T_i}{b \cdot R_A R_c} \tag{3.11}$$

where

P_{Ai}	=	Pressure on the Arbor at the i-th coil of the spring [psi]
F_i	=	Axial Load in the i-th coil of the spring [lb]
A_{AP}	=	Projected area of the spring coil [in^2]
T_i	=	Torque in the i-th coil of the Wrap Spring [lb.in]
R_c	=	Radius to the centroid of the wrap spring when fitted over the arbor [in]
R_A	=	Radius of the Arbor [in]
b	=	Coil Width or Coil Diameter [in]

Figure 3-27 provides a pictorial explanation of the variables.

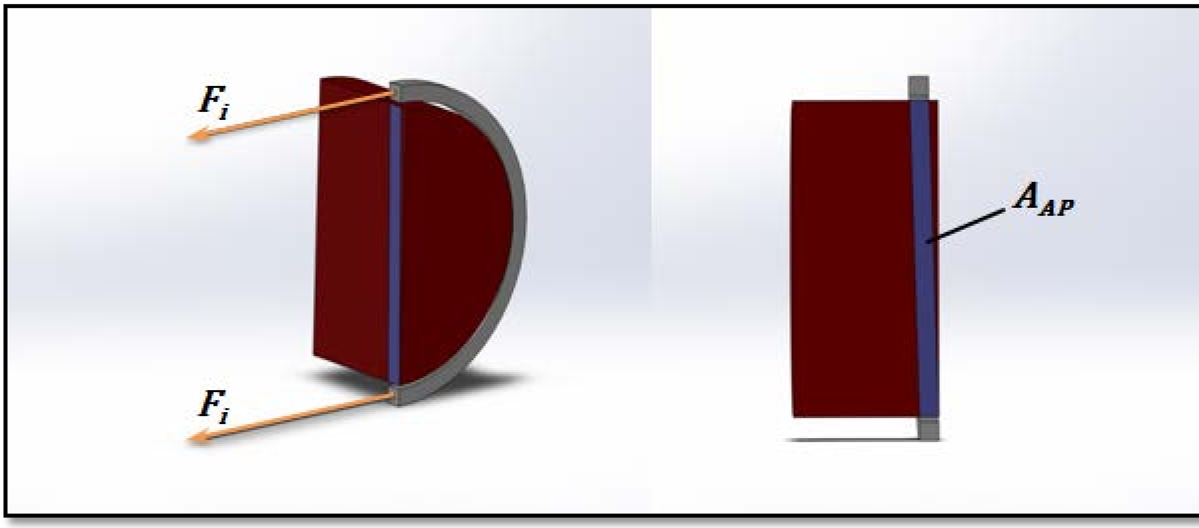

Figure 3-27: Pictorial Depiction of Variables used in Equation (3.11)

Maximum arbor pressure is, once again, induced by the spring coil with the highest torque capacity, which is at the crossover coil. The maximum arbor pressure, therefore, can be written as,

$$P_{Amax} = \frac{T_o}{b \cdot R_A R_c} = \frac{T_e\ (e^{2\pi\mu N} - 1)}{b \cdot R_A R_c} \tag{3.12}$$

This maximum pressure value is only valid when the spring coil width b is constant throughout the entire spring. There are more elaborate spring designs where the coil width gets progressively larger so that the pressure on the arbor is more evenly distributed. However, once again, this approach was not adopted since such custom springs would be too costly to fabricate.

With a known external pressure, the radial stress σ_r and the tangential stress σ_t in the arbor can be calculated using thick-walled cylinder stress formula, as shown below [72].

$$\begin{aligned} \sigma_{At} &= \frac{p_i r_i^2 - p_o r_o^2 - r_i^2 r_o^2 (p_o - p_i)/r^2}{r_o^2 - r_i^2} \\ \sigma_{Ar} &= \frac{p_i r_i^2 - p_o r_o^2 + r_i^2 r_o^2 (p_o - p_i)/r^2}{r_o^2 - r_i^2} \end{aligned} \tag{3.13}$$

Referring to Figure 3-28, the variables are defined as follows,

r_i	=	Inside Radius [in]
r_o	=	Outside Radius [in]
p_i	=	Internal Pressure [psi]
p_o	=	External Pressure [psi]
r	=	Radius to the location of stress calculation [in]

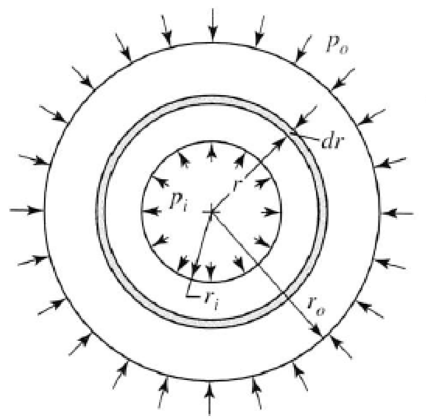

Figure 3-28: Thick-Walled Cylinder Stress.
Image adapted from [72]

The presented thick-walled cylinder equation can only be used when the wall thickness is more than one-twentieth of the cylinder radius. Otherwise, a thin-walled equation needs to be used. However, the arbors are generally not recommended to be made with thin walls. It is also worth noting that although the arbor shown in Figure 3-27 is represented as a solid cylinder, it is much more common for the arbor to be in the form of a hollow cylinder and hence the presented equation. Equation (3.13), however, can be adapted to represent a solid cylinder by equating the inside radius r_i to zero. Furthermore, Equation (3.13) is a generic formula that can be used for designs with either internal or external springs. For our current configuration, only an external pressure p_o is present and the internal pressure p_i is zero. Eliminating the internal pressure p_i term results in,

$$
\begin{aligned}
\sigma_{At} &= \frac{-p_o r_o^2 - r_i^2 r_o^2 (p_o)/r^2}{r_o^2 - r_i^2} = \frac{-p_o r_o^2}{r_o^2 - r_i^2}\left(1 + \frac{r_i^2}{r^2}\right) \\
\sigma_{Ar} &= \frac{-p_o r_o^2 + r_i^2 r_o^2 (p_o)/r^2}{r_o^2 - r_i^2} = \frac{-p_o r_o^2}{r_o^2 - r_i^2}\left(1 - \frac{r_i^2}{r^2}\right)
\end{aligned}
\tag{3.14}
$$

As usual, positive stress value indicates tension and negative stress values indicate compression. Equation (3.14) illustrates that the stresses in the arbor is always in compression and therefore have no effect on the fatigue life of the component. Furthermore, comparing

Equations (3.10), (3.12), and (3.14) shows that the maximum stress in the arbor is almost always significantly lower than the maximum stress in the spring. Therefore, in conclusion, stress consideration for arbor design is generally less of a concern in the design process.

3.6.4 Design Procedure and Parameter Specification

As depicted by Equation (3.3), there are several critical design parameters that need to be specified by the designer so that the spring clutch performance is optimized to match the specific application needs. The design variables that need to be determined are shown in Table 3-4.

Design Parameter	Corresponding Variable
Arbor Diameter	D
Diametric Interference	Δ
Number of Coil Engagement	N
Wire Geometry	I, h
Wire Material	E

Table 3-4: Wrap Spring Equation Variables

Equation (3.3) is repeated below for reader's convenience.

$$T_o = \underbrace{\frac{2EI\Delta D^2}{(D+h)^4}}_{\substack{Energizing \\ Torque}} \underbrace{(e^{2\pi\mu N} - 1)}_{\substack{Coil \\ Amplificiation \\ Factor}} \tag{3.3}$$

Determining the optimal combination of these parameters can be a challenging task. Hence, this section is dedicated to go through the steps taken by the author in the design process and explain how and why various design parameters were chosen. Figure 3-29 below shows a summary of the design procedure.

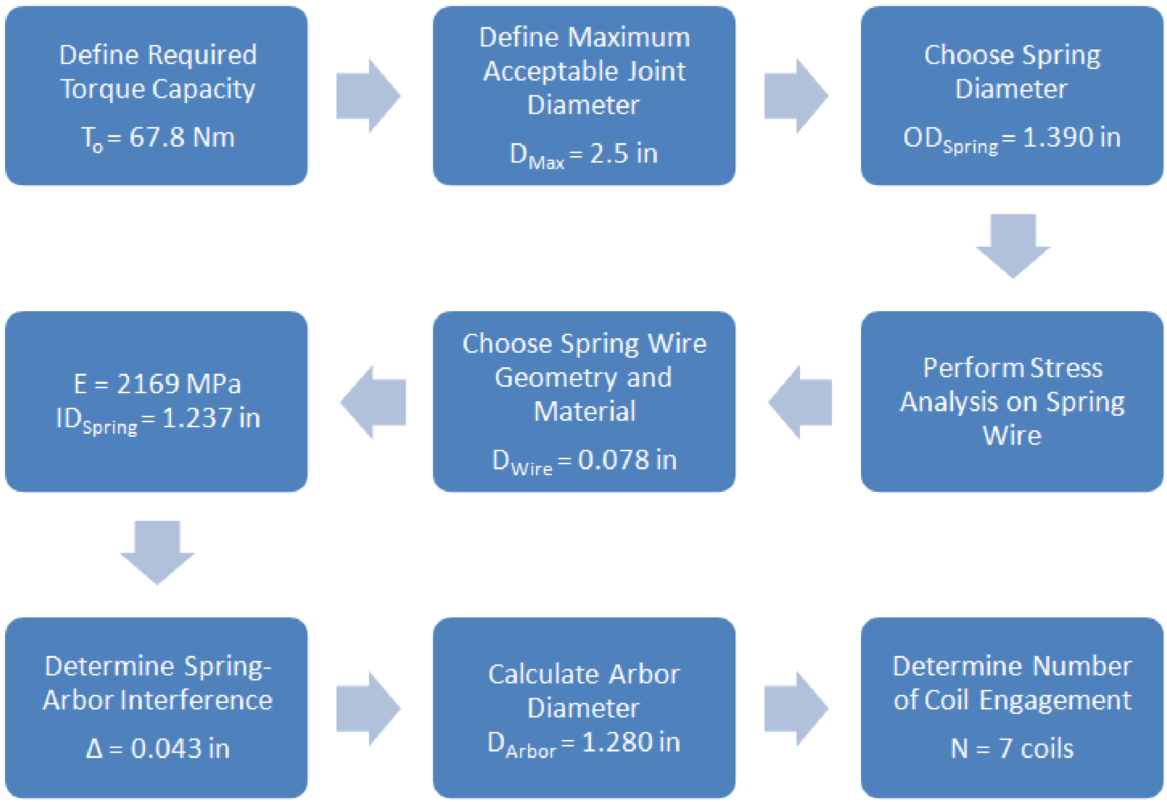

Figure 3-29: Design Procedure Flow Chart

Table 3-5 summarizes the final values chosen for the wrap spring clutch design parameters

Design Parameter	Chosen Value
Arbor Diameter	1.280 in
Diametric Interference	0.043 in
Number of Coil Engagement	7 coils
Wire Diameter	0.078 in
Wire Young's Modulus	2169 MPa

Table 3-5: Values Chosen for the Rev1 Wrap Spring Clutch Design Variables

3.6.4.1 Define Torque Capacity

The first step in the design process of the spring clutch knee is to define the torque capacity necessary at the joint. This torque specification can be based on 1) CGA joint torque data, 2) prior arts, and 3) pose estimation.

1. CGA data by Winter, Kirtley, and Linskell indicate that the maximum knee damping torque during level ground walking is approximately 45.2 Nm (400 lb-in), 16.9 Nm (150 lb-in), and 62.1 Nm (550 lb-in), respectively [44–47].
2. Goldfarb and Durfee specified a knee torque capacity of 50 Nm for their hybrid FES orthosis [30]. Irby et. al. specified a torque capacity of 56.5 Nm for their knee-ankle-foot orthosis used in a similar application. Veneman et. al. specified a maximum torque of 65 Nm for their gait rehabilitation device [73]. Average maximum knee torque for transfemoral amputee ambulation was measured by Seroussi et. al. to be approximately 60 Nm [74].
3. Lastly, as verification, resistive knee torques can be calculated based on body poses. Two potentially critical postures that were investigated are: single-stance right at toe off and feet-together backward lean prior to sitting. The calculation was based on anthropometry data of a 200 lb male who is 6 foot and 2 inches tall. The pose estimation resulted in a maximum torque capacity of approximately 67.8Nm (600 lb-in).

From the literature searches and the analysis above, a conservative resistive torque capacity of 67.8Nm (600 lb-in) was chosen for the exoskeleton knee design.

3.6.4.2 Define Maximum Acceptable Joint Diameter

The second step of the design process is to define a maximum acceptable joint diameter. This step is important because it is almost always preferred to use the largest spring possible; since the larger spring diameter would help minimize the axial stresses in the spring, minimize the pressure on the arbors, and also minimize the amount of wear at the arbor-spring interface. Equations (3.10) and (3.12) demonstrate these effects numerically.

The knee joint was originally conceptualized to be small enough to be worn inside of pants and, therefore, it was specified to be less than 2.5 inches in diameter and preferably no more than 1.5 inches in thickness. With this diametric constraint established, the largest allowable spring outer diameter was determined to be approximately 1.5 inches. A low-cost commercially available torsion spring with an outer diameter of 1.390 inches was found and chosen as a potential spring candidate. The spring is made out of music wire with a wire diameter of 0.078 inches. In the next section, stress analysis will be performed on the spring wire to guarantee no failure. After that, the spring-arbor diametric interference will be determined (hence the Energizing Torque) as well as the corresponding number of coil engagements N.

3.6.4.3 Determining Wire Geometry

With a chosen torque capacity, spring diameter, and spring material, minimum spring wire geometry can be estimated based on the stress analysis equation presented in Section 3.6.3. Using a modified Equation (3.10) along with the following values,

1. Torque capacity of 67.8 Nm (600 lb-in). [T_o]
2. Spring diameter of 3.53 cm (1.390 in). [$2R_c$]
3. Minimum tensile strength of 2169 MPa (314.5 ksi), assuming music wire [75]. [σ_{SAmax}]

$$A = \frac{T_o}{\sigma_{SAmax} \cdot R_c}$$

estimates a minimum spring wire cross section area of 0.002745 in^2, or a 0.059 inch wire diameter. In other words, this equation helps define the thinnest wire diameter that can be used; however it is probably preferred to use a larger wire diameter for higher safety factor.

The next step is to check the safety factor for the 0.078 inch wire diameter spring we have previously found readily available. Once again, using Equation (3.10), we calculate the maximum stress in the wire to be approximately 181 ksi (1248 MPa), which corresponds to a 1.74 safety factor. It would be ideal to attain a safety factor that is above 2 which would also greatly improve the fatigue resistance of the spring. Since the minimum tensile strength of music wire can range from 230 to 399 ksi (1586 to 2751 MPa), it would be beneficial to make sure that the spring wire has a tensile strength that is above 362 ksi.

As a design rule for specifying spring wire diameter, it is more desirable to minimize the spring wire cross sectional area (while keeping the stresses within allowable limits) since this would also minimize the overall clutch size and weight. Additionally, excessively large spring wires would also make the spring element too stiff for the frictional forces between the spring and the arbor to further contract the spring during operation, which prohibits torque amplification. This, however, is generally more of a concern in applications with very high torque requirements, which is not the case for this application [71].

Also note that for a given wire cross sectional area, rectangular wire height and width can be optimized to attain a specific coil flexural rigidity EI (which ultimately affects the clutch Energizing Torque). However, such custom rectangular spring would incur extra manufacturing time and cost. Therefore, a more standardized spring wire geometry was chosen for this design.

3.6.4.4 Determining Spring-Arbor Interference and Number of Coil Engagement

The previous three sub-sections serve as a guide for spring selection. They can help the reader define a suitable spring diameter, spring wire geometry, and find the corresponding stresses in the spring. With a proper spring selected, the next step is to determine an appropriate arbor size so that the spring-arbor interference generates a suitable Energizing Torque, which ultimately defines the torque capacity of the clutch. As previously mentioned in Section 3.6.2.6, two variables (the Energizing Torque and the coil engagement count) can be manipulated to produce the specified torque capacity. However, because these two variables have a direct tradeoff relationship – that is, a higher Energizing Torque (which corresponds to a lower coil engagement count) is beneficial for damping controllability but hurts free joint extension – determining the optimal balance for these two variables can be challenging.

An upper bound on the maximum number of coil engagements allowable can be set by imposing the constraint of maximum clutch thickness. Based on a joint thickness limit of 1.5 inches and a wire diameter of 0.078 inch, the maximum allowable number of active coils was calculated to be 9.3 turns. Using Equation (3.4) with the following values,

$$T_o = T_e \left(e^{2\pi\mu N} - 1\right) \tag{3.4}$$

1. Output torque [T_o] of 600 lb-in (67.8 Nm)
2. Coil engagement count [N] of 9.3
3. Friction coefficient[5] of 0.15

calculates a minimal Energizing Torque [T_e] of 9.367e-2 lb-in, which corresponds to a 0.001503 inch diametric interference. Obviously, this engineering tolerance will be nearly impossible to achieve since machining tolerance limit is commonly in the range of 0.001 inch. There are two main issues with having a high tolerance fitting between the arbor and the spring:

1. When there is an unattainable geometric tolerance, the designer has to always err on the safe side and create an output torque capacity overshoot. For example, with the calculated diametric interference of 0.001503 inch, the actual interference has to be increased to the closest thousandths inch (namely a diametric interference of 0.002 inch). This results in an Energizing Torque of 0.1245 lb-in, which corresponds to a 33 percent output torque capacity overshoot. Having a large torque capacity overshoot generally hampers damping controllability.

---

[5] The friction interface being examined is between the surfaces of the 8620 hardened steel arbor and the music wire of the spring. Existing literature indicates the coefficient of static friction for steel on steel ranges from 0.15 to 0.74 and the coefficient of kinetic friction ranges from 0.09 to 0.60 [80]. As a safety precaution, use of the kinetic friction coefficient is recommended. The coefficient of kinetic friction between music wire and steel was also experimentally determined to be approximately 0.15 to 0.17. This result prompted the use of 0.15 friction coefficient in our calculations.

2. Secondly, the design with a diametric interference of 0.001503 inch will be more likely to fail and have a shorter operation life due to its high precision manufacturing requirements. For example, if the setup with the 0.001503 inch diametric interference had a 0.001 inch diametric wear or manufacturing error, the resultant output torque would have dropped by 66.5 percent. On the other hand, if a nominal diametric interference of 0.050 inch was used instead, the same 0.001 inch diametric wear would cause less than 2 percent drop for the output torque capacity.

Based on these observations, one can see that using the maximum geometric permissible coil engagement number of 9.3 is not ideal due to the excessively high machining tolerance requirement.

Next, a lower bound for coil engagement count can be determined through defining the maximum permissible Overrunning Torque. Ideally, the Overrunning Torque should be zero in order to achieve minimal extension impedance during Swing-Extension. However, while zero Overrunning Torque is ideal, small amounts of extension resistance generally will not greatly affect the gait. A maximum allowable Overrunning Torque was empirically determined to be approximately 5 lb-in, which corresponds to a coil engagement count of 5.1 and a diametric interference of 0.092 inch.

With the upper and lower bounds defined, the designer can now specify a coil count and interference combination best suited for the application. The first revision wrap spring knee was designed to have 7 coil engagements and a diametric interference of 0.043 inches. This setup produces an Energizing Torque of 2.52 lb-in and a maximum torque capacity of 1840 lb-in.

3.6.5 Knee Design Discussion

3.6.5.1 Caution with Exponential Terms

It should be noted that when calculating the torque capacity of the clutch using Equation (3.4), extra care should be taken when dealing with the coefficient of friction μ and the number of coil engagement N. Due to the exponential nature of these two terms, slight variation in them can have a dramatic effect on the calculated result. For example, using the specifications of the first knee design, if the coefficient of friction is changed from 0.15 to 0.20, the resultant torque capacity would have increased by more than 900 percent. Similarly, an increase of coil engagement from 7 to 7.5 would produce a 160 percent increase in output torque. Of the two exponential terms, uncertainty in the coil engagement count is generally less of an issue since design accommodations can be made so that coil sliding across the arbors is minimized. On the other hand, determining the precise value of the friction coefficient during operation is often much more challenging and can be the cause of large disparity between the calculated torque value and the actual torque value.

3.6.5.2 Variable Damping Discussion

Because slight variations in the coefficient of friction can have a very significant impact on the clutch torque capacity, the designer is compelled to assume a more conservative coefficient value to avoid unexpected buckling of the knee. Consequently, the actual joint torque capacity is frequently significantly higher than the specified torque capacity and can fluctuate greatly depending on the coefficient of friction. These two characteristics hamper the resolution of the system's damping control. For this reason, the variable damping feature is currently only being used to a limited fashion. Particularly, damped knee flexion is used only during sitting and only one pre-calibrated resistive torque value is used. When the sitting procedure is triggered by the user, the linear actuator is moved to a predetermined position so that the spring tang is deflected to some intermediate position between full engagement and full release. The optimal amount of spring deflection is derived experimentally and it can vary from user to user. The relationship between spring deflection and generated resistive torque is, as expected, not entirely consistent across different joints (due to discrepancies in initial spring orientation, arbor machining tolerance, spring diameters, friction surface conditions, and etc.), and therefore, the amount of spring deflection for each joint during sitting is recommended to be derived experimentally.

More sophisticated damping control strategies are possible with the incorporation of a knee joint encoder. For example, with real time knee angle measurement, the linear actuator can be controlled in a feedback loop that tracks a specific knee joint angular velocity. That is, the linear actuator is incrementally extended to release the spring if the current joint angular velocity is below a prespecified value, and similarly, the linear actuator is retracted if the joint angular velocity is higher than the prescribed value. This control method bypasses issues associated with hardware inconsistencies and might not require the experimental calibration as previously described. Future work for this type of control method still needs to be done.

3.6.5.3 Kinetic and Static Friction Transition

As with some of the most common potential spring and arbor material combinations, the static friction coefficient is typically higher than the kinetic friction coefficient. Having a large difference in the kinetic and static friction coefficient can make it more difficult to generate a smooth damping motion due to the sudden drop of resistive torque when the joint begins to rotate (a stick-slip phenomenon). In other words, when the exoskeleton user is sitting with the damping knee, the resistive torque is the highest at the beginning before the joint beings to rotate and will suddenly drop to a lower resistive torque capacity when the user begins the sitting motion. Ideally, the torque profile should be the other way around, where the resistive torque is initially low and gradually increases as the person gets closer to a sitting position.

A moderate amount of stick-slip behavior has been observed in the proposed spring clutch joint, however its magnitude, although not ideal, will not completely incapacitate the damping motion. The stick-slip behavior has been observed to be more pronounced at higher torque capacities, which is consistent with the observation from [76]. Therefore, is possible to implement a damping scheduling scheme where the joint motion begins with a small resistive torque (which is beneficial for static and kinetic friction transition) and gradually increases as the knee becomes more bent. The issue with stiction can also be solved through selecting a different spring-arbor material combination or modifying the mechanics of the contact interface. Stephen McKinley, a graduate student at U.C. Berkeley, investigated this topic for his Master's thesis and the reader is referred to [77].

3.6.5.4 Component Wear

Wear at the interface of the spring and the arbor is traditionally not an issue for wrap spring clutches due to the absence of slippage during operation, i.e., the clutch is traditionally used only for locking and unlocking applications. However, if the spring clutch is used as a resistive torque generator that allows for damped joint rotation, then wear will become present at the slip interface. Adhesive wear at the contact surface can be quantified as:

$$V = K\frac{L \cdot x}{3H} \tag{3.15}$$

where

V	=	Wear Volume of the Softer Material (in^3)
K	=	Wear Coefficient
L	=	Radial Load at the Spring-Arbor Interface (lbf)
x	=	Slip Distance (in)
H	=	Material Hardness of the Softer Surface (psi)

As shown by Equation (3.15), the wear volume is directly proportional to the load and the slip distance. Since maximum loading is at the crossover coil, maximum wear is also present under the crossover coil. The wear coefficient K can range from 10^{-7} to 10^{-3} depending on interface material compatibility and interface lubrication[78]. For metal on metal with average lubrication, the wear coefficient is roughly $2x10e^{-5}$. Material hardness H can be approximated as three times the material tensile strength. Wearing of the harder surface also occurs and the wear volume of the harder surface can be calculated using Equation (3.16).

$$\frac{V_{hard}}{V_{soft}} = \left(\frac{H_{soft}}{H_{hard}}\right)^2 \tag{3.16}$$

Concerns for wear first came into light with the alpha prototype of the spring clutch knee, which had arbors made out of 17-4PH stainless steel with an approximate Rockwell hardness of HRC 35. After several months of testing, visible wear marks on the arbor were found underneath the first quarter of the crossover coil. For this reason, an 8620 steel arbor case hardened to HRC 60-62 was adopted in order to decrease wear rate of the arbor. In addition to using harder contact materials, several other design modifications can be adopted to curb wear rate.

1. The radial load L at the spring-arbor interface can be decreased by using a larger diameter arbor and spring combination. The increased diameter results in a larger moment arm, which allows the generation of the same amount of torque capacity with less interface forces.
2. It is also beneficial to use springs made of rectangular wires instead of round wires because this allows for more surface contact area between the spring and the arbor. Although this modification would not change the overall wear volume rate, but due to the increased contact surface area, the wear depth rate is decreased. Slowing down wear depth is important for maintaining the proper spring-arbor interference, and hence the torque capacity.
3. The wear coefficient K can also be decreased through using better lubrication or change contact material compatibility. For example, if the arbor is made out of non-metal such as ceramic or plastic, then the K value can be decreased to $5 \text{x} 10e^{-6}$, or $2 \text{x} 10e^{-6}$ if with excellent lubrication.

3.6.6 Second Knee Design

A second wrap spring knee was designed with the following modifications and improvements.

1. A larger diameter arbor and spring was adopted to decrease component wear and stress. The objective was to redesign the hardware assembly so that a larger diameter arbor can be used without increasing the overall size of the joint.
2. A rectangular spring wire was adopted to help with wear problems.
3. A rotary magnetic encoder was added to the joint.
4. The new design also intended to further ease assembly
5. A more reliable spring fixture was incorporated to replace the setscrews.

Some of the design features of the second knee joint were adapted from [79]. Figure 3-30 shows the second revision of the wrap spring knee. The knee measures 3.7in (9.3cm) in length, 2.5in (6.3cm) in width, 1.2in (3.1cm) in thickness, and weighs 1.14lbs (0.52kg). As comparison, the first knee design was 3.6in (9.2cm) by 2.5in (6.3cm) by 1.3in (3.4cm) and weighs 0.8lbs

(0.36kg). The overall size of the joint stayed roughly the same, but the weight increased by 44 percent due to the larger arbor diameter. Figure 3-31 shows the knee component assembly and a section view.

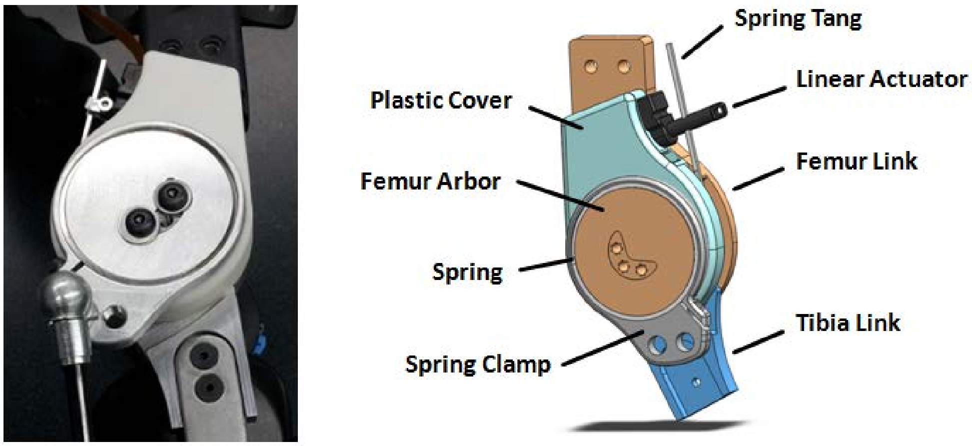

Figure 3-30: Wrap Spring Knee – Second Revision

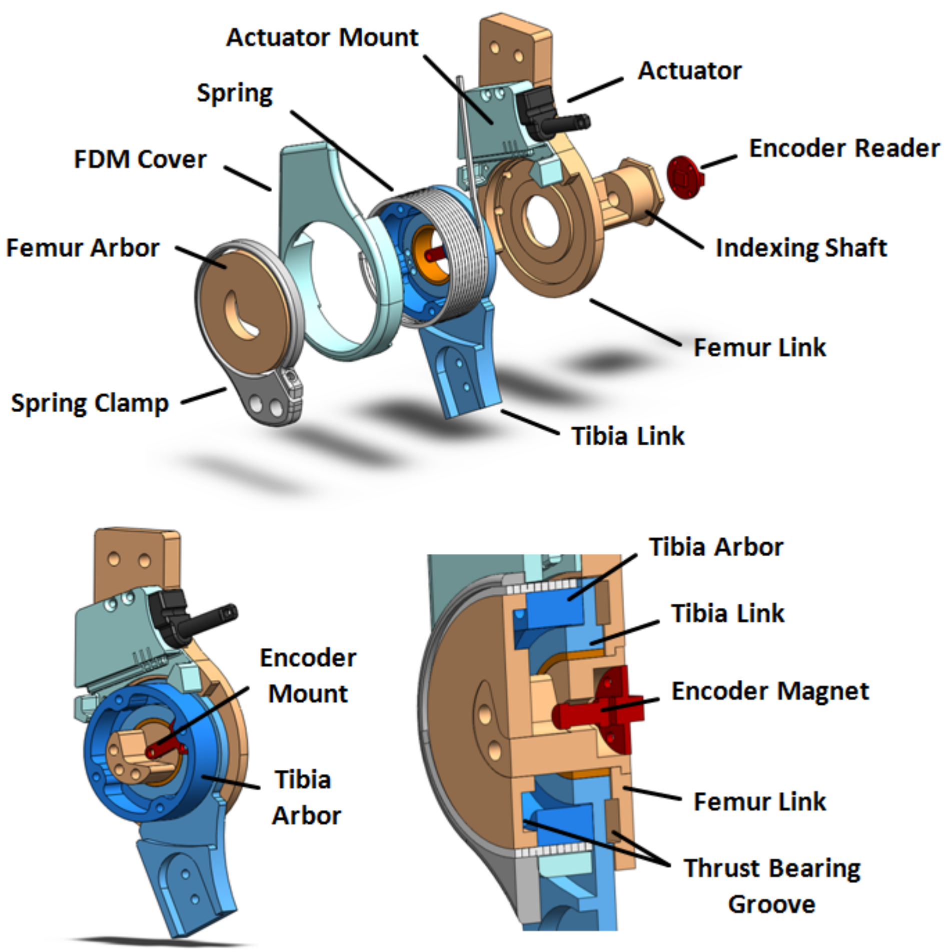

Figure 3-31: Wrap Spring Knee – Second Revision. Assembly and Section View

3.6.6.1 Femur Construction

As discussed Section 3.6.1, it is desirable to line up the tibia link as closely as possible with the femur link in order to minimize off-axis torque and streamline the assembly. However, since it is inevitable that the two arbors need to sit on the opposite sides of the spring, some “bridging” component is necessary to connect the femur arbor to the femur link. In the first knee revision, this bridging component is the femur link cover, which rigidly connects the femur arbor to the femur link externally. This external component encloses the spring, acts as a cosmetic cover, and is structurally load bearing. In the second knee revision, the load bridging is done internally through the shaft. The steel shaft which the tibia link rotates on is constrained rotationally to the femur link by a hexagonal boss. The shaft goes inside the spring and gets connected to the femur arbor with a mating extrusion.

3.6.6.2 Increasing Arbor and Spring Diameter

Connecting the femur arbor with the femur link internally means that the external casing no longer needs to be load bearing. This allows the outer cover to be thinner and serves purely as a cosmetic cover and as a dust barrier. This construction permits the use of a larger diameter arbor and spring combination without increasing the overall size of the knee assembly. As previously mentioned, the larger diameter arbor and spring translates into higher locking capacity, lower stresses, and lower component wear.

3.6.6.3 Magnetic Knee Encoder

A Renishaw 16bit rotary magnetic absolute encoder was incorporated into the second knee design. An encoder mount is fixed to the tibia link inside the inner diameter of the tibia arbor. The indexing shaft is shaped to allow the encoder mount to freely rotate within the 135 degrees of knee motion range. The encoder magnet goes through the center of the indexing shaft and rotates next to the encoder reader fixed on the medial end of the shaft.

3.6.6.4 Spring Clamp

In the first knee design, the coil spring was fixed to the femur link through the use of set screws. However, because of the round spring wire, the set screws were not very effective in securing the spring to the femur arbor. In addition, access to the spring was fairly challenging due to the presence of the femur cover, which further obstructs the process of securing the spring to the femur. As a result, the knee joint has been observed to occasionally slip below torque capacity. To amend this issue, a spring clamp as shown in Figure 3-30 was adopted. This clamp acts as a shaft collar which significantly increases the locking surface area to include the entire perimeter of the femur arbor. Additionally, using a coil spring made with rectangular wire also further enhances the locking capacity through increasing the locking surface area.

3.6.6.5 Assembly and Adjustment

One of the most challenging assembly procedures of the first knee design was the installation of the coil spring. The spring assembly procedure is difficult largely because the femur cover blocks off access to the spring and the femur arbor. This makes the adjustment of spring orientation and lateral spring position much more difficult. Through eliminating the structural femur cover, access to the spring and the arbors becomes always available.

Furthermore, it is important to point out that the gap at the interface of the two arbors should be kept at a minimum. Although a small gap at the interface is desirable for low friction rotation, excessively large gap will cause the coil spring to constrict into the gap and cause permanent damage to the spring. It is therefore important to not only minimize the gap at the interface but also provide enough axial compression and load the thrust bearing at the arbor interface to make sure that the arbors do not separate during operation. The second knee design allows the adjustment of the axial compression force though simply tightening the screws located on the indexing shaft. The arbor interface gap and the amount of loading no longer depend on the thickness tolerance of machined components.

3.6.6.6 Component Fabrication and Material Selection

The most complicated component to machine in the first knee revision was the femur cover because it was used as an arbor bridge, a linear actuator mount, and a cosmetic cover. When the femur arbor bridging is done internally, the external casing becomes much easier to fabricate. In the second knee revision, both the cosmetic cover and the linear actuator mount are made out of ABS plastic with a Fused Deposition Modeling (FDM) machine. Nonetheless, the simplified cover construction comes with a tradeoff. The joint shaft becomes slightly more complicated to machine because it now has two indexing bosses to mate with the femur link and the femur arbor. Overall, the second knee revision is simpler and is preferred.

All of the machined components in the second knee design are made out of 6061-T6 aluminum alloy with the exception of the tibia arbor and the indexing shaft. The femur arbor does not need to be made out of steel because the spring does not slip on it. The tibia arbor is once again made out of 8620 steel and case hardened for minimizing wear at the spring interface.

3.6.6.7 Design Parameters

The spring clutch parameter values for the second knee were determined using the same procedure as described in Section 3.6.4. Table 3-6 summarizes the values chosen for the second wrap spring clutch design.

Design Parameter	Chosen Value
Arbor Diameter	2.000 in
Diametric Interference	0.018 in
Number of Coil Engagement	7.5 coils
Wire Height & Width	0.071 in
Wire Young's Modulus	2169 MPa

Table 3-6: Values Chosen for the Rev1 Wrap Spring Clutch Design Variables

Chapter 4

Concluding Remarks

This dissertation described the design and operation of two different minimally actuated medical exoskeleton devices capable of providing ambulation assistance for individuals with lower body paralysis. Special emphasis is placed on the term “minimal actuation” since one of the main research objectives of this work is to explore alternative methods of exoskeleton actuation that could potentially result in a device that is lightweight, compact, user-friendly, and more commercially affordable. The two presented devices use electric DC motors to provide powered hip assistance and rely on two different types of hip-knee joint coupling systems to generate the desired knee motion.

The Austin Exoskeleton uses a mechanical joint coupling mechanism. The system has been proven to be successful in assisting a T12 complete paraplegic subject to walk, sit, and stand. Through replacing knee actuators with the joint coupling mechanism, the exoskeleton legs achieved a lower profile and a slight weight reduction. However, the added complexity of the joint coupling mechanism also makes the actual increased affordability criterion debatable. In the end, while the mechanical coupling concept of the Austin Exoskeleton serves as a good alternative method of actuation, the actual improvement it provides in terms of device weight, size, and cost might not be significant enough to be considered as having a decisive advantage over the traditional hip-knee actuation paradigm. It is, however, important to recognize that the Austin joint coupling mechanism was designed to meet the more stringent design requirement of assisted sitting and standing, which required more complicated components and more substantial hardware. That is, if the exoskeleton was designed purely for ambulation assistance then the mechanical joint coupling approach is very likely to have a more significant advantage over the four-actuator system designs.

The Passive Knee Exoskeleton (Ryan Exoskeleton) uses dynamic joint coupling, which is a method of generating knee rotation through utilizing the momentum created by the hip actuator.

This system has been validated by several SCI test pilots with injury levels ranging from T5 to T12. Dynamic joint coupling has been proven to be quite effective especially for newly injured individuals who have not yet developed significant amounts of joint contracture or sustain high levels of spasticity. The exoskeleton has been well received by test subjects despite the fact that its sit-to-stand assistance is not as pronounced as what traditional hip-knee actuation exoskeletons can offer. It is clear that there is a demand for such simple and lightweight ambulation-centric assistive devices that do not have very elaborate actuation schemes and functionalities. It is believed that such devices, despite their inherent inability to perform more complex joint motions, actually end up providing higher levels of freedom and maneuverability due to their lighter weight and higher adaptability.

Future work in the field of medical exoskeletons will most likely revolve around two fields: performance improvement and safety enhancement. Currently, at an average ambulation velocity of 0.27 m/s, the exoskeleton is traveling at approximately half of the speed required for an individual to be considered as a functional community walker. As echoed by the test pilots, increasing the ambulation speed will definitely make the exoskeleton much more practical for daily use. In the effort to increase ambulation velocity, work is currently being done on implementing an adaptive controller that can modify step parameters (e.g., step length, torso tilt, and joint velocity) as a function of the user's current velocity. In other words, instead of having a single step pattern that is repeated from the first step to the last, the system will be able to gradually accelerate and potentially reach a higher steady-state speed as the user becomes more experienced with the system. It is hoped that the medical exoskeleton technology will continue to mature and will soon allow paralyzed individuals to achieve the same level of mobility independence as prior to their injury.

Bibliography

[1] NSCISC, 2012, “Spinal Cord Injury Facts and Figures at a Glance.,” **35**(4) [Online]. Available: https://www.nscisc.uab.edu.

[2] Cao Y., Chen Y., and DeVivo M. J., 2011, “Lifetime Direct Costs After Spinal Cord Injury,” Topics in Spinal Cord Injury Rehabilitation, **16**(4), pp. 10–16.

[3] Brown-Triolo D. L., Roach M. J., Nelson K., and Triolo R. J., 2002, “Consumer perspectives on mobility: implications for neuroprosthesis design.,” Journal of rehabilitation research and development, **39**(6), pp. 659–69.

[4] L. Phillips, M. Ozer, P. Axelson and J. F., 1987, Spinal cord injury: A guide for patient and family, Raven Press.

[5] Eng J. J., Levins S. M., Townson A. F., Mah-jones D., Bremner J., and Huston G., 2001, “Research Report Use of Prolonged Standing for Individuals With Spinal Cord Injuries,” pp. 1392–1399.

[6] Harvey L. a, Newton-John T., Davis G. M., Smith M. B., and Engel S., 1997, “A comparison of the attitude of paraplegic individuals to the walkabout orthosis and the isocentric reciprocal gait orthosis.,” Spinal cord, **35**(9), pp. 580–4.

[7] Baardman G., IJzerman M. J., Hermens H. J., Veltink P. H., Boom H. B., and Zilvold G., 1997, “The influence of the reciprocal hip joint link in the Advanced Reciprocating Gait Orthosis on standing performance in paraplegia.,” Prosthetics and orthotics international, **21**(3), pp. 210–21.

[8] Johnson W. B., Fatone S., Hons B. P. O., and Gard S. A., 2009, “Walking mechanics of persons who use reciprocating gait orthoses,” **46**(3), pp. 435–446.

[9] Center for Orthotics Design, 2013, “Isocentric RGO” [Online]. Available: http://www.centerfororthoticsdesign.com/isocentric_rgo/index.html. [Accessed: 05-Jan-2013].

[10] Bernardi M., Canale I., Castellano V., Di Filippo L., Felici F., and Marchetti M., 1995, “The efficiency of walking of paraplegic patients using a reciprocating gait orthosis.,” Paraplegia, **33**(7), pp. 409–15.

[11] Harvey L. a, Davis G. M., Smith M. B., and Engel S., 1998, “Energy expenditure during gait using the walkabout and isocentric reciprocal gait orthoses in persons with paraplegia.,” Archives of physical medicine and rehabilitation, **79**(8), pp. 945–9.

[12] Sykes L., Edwards J., Powell E. S., and Ross E. R., 1995, “The reciprocating gait orthosis: long-term usage patterns.,” Archives of physical medicine and rehabilitation, **76**(8), pp. 779–83.

[13] Vukobratovic M., Hristic D., and Stojiljkovic Z., 1974, “Development of active anthropomorphic exoskeletons,” Medical and Biological …, (January), pp. 66–80.

[14] Townsend M. a, and Lepofsky R. J., 1976, “Powered walking machine prosthesis for paraplegics.,” Medical & biological engineering, **14**(4), pp. 436–44.

[15] Ruthenberg B. J., Wasylewski N. a, and Beard J. E., 1997, “An experimental device for investigating the force and power requirements of a powered gait orthosis.,” Journal of rehabilitation research and development, **34**(2), pp. 203–13.

[16] Kawashima N., Sone Y., Nakazawa K., Akai M., and Yano H., 2003, “Energy expenditure during walking with weight-bearing control (WBC) orthosis in thoracic level of paraplegic patients.,” Spinal cord, **41**(9), pp. 506–10.

[17] Yano H., Kaneko S., Nakazawa K., and Bettoh A., 1997, “Prosthetics and Orthotics International.”

[18] Ohta Y., Yano H., Suzuki R., Yoshida M., Kawashima N., and Nakazawa K., 2007, “A two-degree-of-freedom motor-powered gait orthosis for spinal cord injury patients,” Proceedings of the Institution of Mechanical Engineers, Part H: Journal of Engineering in Medicine, **221**(6), pp. 629–639.

[19] Zoss A. B., Kazerooni H., and Chu A., 2006, “Biomechanical Design of the Berkeley Lower,” **11**(2), pp. 128–138.

[20] Lower B., Exoskeleton E., Chu A., Kazerooni H., and Zoss A., 2005, “On the Biomimetic Design of the,” (April), pp. 4345–4352.

[21] Kazerooni H., Racine J., Huang L., and Steger R., 2005, “On the Control of the Berkeley Lower Extremity Exoskeleton (BLEEX),” (April), pp. 4353–4360.

[22] Strausser K., Swift T., and Zoss A., 2011, “Mobile Exoskeleton for Spinal Cord Injury: Development and Testing,” ASME 2011 Dynamic Systems and Control Conference.

[23] Goffer A., 2006, “Gait-locomotor apparatus,” US Patent 7,153,242.

[24] Farris R., 2011, “Preliminary Evaluation of a Powered Lower Limb Orthosis to Aid Walking in Paraplegic Individuals,” Neural Systems and ….

[25] Quintero H. a, Farris R. J., and Goldfarb M., 2011, “Control and implementation of a powered lower limb orthosis to aid walking in paraplegic individuals.,” IEEE ... International Conference on Rehabilitation Robotics : [proceedings], **2011**, p. 5975481.

[26] Little R., and Irving R., 2011, “Self contained powered exoskeleton walker for a disabled user,” US Patent App. 12/801,809.

[27] Bionics R., “Rex Bionics” [Online]. Available: http://www.rexbionics.com/. [Accessed: 10-Jan-2013].

[28] Lynch C. L., and Popovic M. R., “Functional Electrical Stimulation,” IEEE Control Systems Magazine, pp. 40–50.

[29] Winslow J., Jacobs P. L., and Tepavac D., 2003, “Fatigue compensation during FES using surface EMG,” Journal of Electromyography and Kinesiology, **13**(6), pp. 555–568.

[30] Goldfarb M., and Durfee W. K., 1996, “Design of a controlled-brake orthosis for FES-aided gait.,” IEEE transactions on rehabilitation engineering : a publication of the IEEE Engineering in Medicine and Biology Society, **4**(1), pp. 13–24.

[31] To C., and Kobetic R., 2008, “Design of a variable constraint hip mechanism for a hybrid neuroprosthesis to restore gait after spinal cord injury,” Mechatronics, IEEE/ …, **13**(2), pp. 197–205.

[32] Kumamoto M., Oshima T., and Yamamoto T., 1994, “Control properties induced by the existence of antagonistic pairs of bi-articular muscles—Mechanical engineering model analyses,” Human Movement Science, **13**, pp. 611–634.

[33] Wells R., and Evans N., 1987, “Functions and recruitment patterns of one-and two-joint muscles under isometric and walking conditions,” Human movement science, **6**, pp. 349–372.

[34] Zajac F. E., Neptune R. R., and Kautz S. a, 2002, “Biomechanics and muscle coordination of human walking. Part I: introduction to concepts, power transfer, dynamics and simulations.,” Gait & posture, **16**(3), pp. 215–32.

[35] Morrison J., 1970, “The mechanics of muscle function in locomotion,” Journal of biomechanics, (December).

[36] Van Ingen Schenau G. J., Boots P. J., de Groot G., Snackers R. J., and van Woensel W. W., 1992, “The constrained control of force and position in multi-joint movements.,” Neuroscience, **46**(1), pp. 197–207.

[37] Voigt M., and Simonsen E., 1995, “Mechanical and muscular factors influencing the performance in maximal vertical jumping after different prestretch loads,” Journal of …, **28**(3).

[38] Winter D. a, 1983, “Moments of force and mechanical power in jogging.,” Journal of biomechanics, **16**(1), pp. 91–7.

[39] Schenau G. van I., 1989, “From rotation to translation: constraints on multi-joint movements and the unique action of bi-articular muscles,” Human Movement Science, **8**, pp. 301–337.

[40] Doorenbosch C. a, Harlaar J., Roebroeck M. E., and Lankhorst G. J., 1994, “Two strategies of transferring from sit-to-stand; the activation of monoarticular and biarticular muscles,” Journal of biomechanics, **27**(11), pp. 1299–307.

[41] Van Ingen Schenau G. J., Bobbert M. F., and Rozendal R. H., 1987, “The unique action of bi-articular muscles in complex movements.,” Journal of anatomy, **155**, pp. 1–5.

[42] Sutherland D. H., Kaufman K. R., and Moitoza J. R., 1994, “Kinematics of normal human walking.,” Human walking, Williams & Wilkins, pp. 23–44.

[43] Mckinley M. G., 2011, “Design of a Novel Orthotic Knee Joint for Use in an Assistive Exoskeleton for Paraplegics,” University of California at Berkeley.

[44] Winter D. A., “2D Gait Data,” International Society of Biomechanics. Biomechanical Data Resources. [Online]. Available: http://isbweb.org/data/.

[45] Winter D. A., 1990, Biomechanics and Motor Control of Human Movement, 2nd ed., John Wiley & Sons.

[46] Kirtley C., “CGA Normative Gait Database,” Hong Kong Polytechnic University, 10 Young Adults. [Online]. Available: http://guardian.curtin.edu.au/cga/data/.

[47] Linskell J., “CGA Normative Gait Databse,” Limb Fitting Centre, Dundee, Scotland, Young Adult. [Online]. Available: http://guardian.curtin.edu.au/cga/data/.

[48] Smith M., and Baer G., 1999, “Achievement of simple mobility milestones after stroke,” Archives of physical medicine and rehabilitation, **80**(April), pp. 442–447.

[49] Van Hedel H. J., Wirz M., and Dietz V., 2005, “Assessing walking ability in subjects with spinal cord injury: validity and reliability of 3 walking tests.,” Archives of physical medicine and rehabilitation, **86**(2), pp. 190–6.

[50] Schenkman M., Cutson T., Kuchibhatla M., Chandler J., and Pieper C., 1997, “Reliability of impairment and physical performance measures for persons with Parkinson’s disease,” Physical Therapy, **77**, pp. 19–27.

[51] Rossier P., and Wade D. T., 2001, “Validity and reliability comparison of 4 mobility measures in patients presenting with neurologic impairment.,” Archives of physical medicine and rehabilitation, **82**(1), pp. 9–13.

[52] Van Hedel H. J. a, Wirz M., and Dietz V., 2008, “Standardized assessment of walking capacity after spinal cord injury: the European network approach.,” Neurological research, **30**(1), pp. 61–73.

[53] Scivoletto G., Tamburella F., Laurenza L., Foti C., Ditunno J. F., and Molinari M., 2011, “Validity and reliability of the 10-m walk test and the 6-min walk test in spinal cord injury patients.,” Spinal cord, **49**(6), pp. 736–40.

[54] Jackson A. B., Carnel C. T., Ditunno J. F., and Read M. S., 2008, “Outcome measures for gait and ambulation in the spinal cord injury population,” Journal of Spinal Cord Medicine, **31**, pp. 487–499.

[55] Farris R. J., 2012, “Design of a Powered Lower-Limb Exoskeleton and Control for Gait Assistance in Paraplegics,” Vanderbilt University.

[56] Swift T., 2011, “Control and Trajectory Generation of a Wearable Mobility Exoskeleton for Spinal Cord Injury Patients,” University of California, Berkeley.

[57] Exoskeleton, 2011, “Rex Bionics” [Online]. Available: http://www.exoskeleton-suit.com/RexBionics.html . [Accessed: 26-May-2013].

[58] Mohler B. J., Thompson W. B., Creem-Regehr S. H., Pick H. L., and Warren W. H., 2007, “Visual flow influences gait transition speed and preferred walking speed.,” Experimental brain research. Experimentelle Hirnforschung. Expérimentation cérébrale, **181**(2), pp. 221–8.

[59] Reid J. I., 2012, “Control Strategies for a Minimally Actuated Medical Exoskeleton for Individuals with Paralysis,” University of California, Berkeley.

[60] Robinett C. S., and Vondran M. a, 1988, “Functional ambulation velocity and distance requirements in rural and urban communities. A clinical report.,” Physical therapy, **68**(9), pp. 1371–3.

[61] Andrews A. W., Chinworth S. A., Bourassa M., Garvin M., Benton D., and Tanner S., 2010, “Update on distance and velocity requirements for community ambulation,” Journal of Geriatric Physical Therapy, **27244**, pp. 128–134.

[62] Um T. I., 2012, “Passive Impedance Control for Medical Exoskeleton Knees Using Gas Spring,” University of California, Berkeley.

[63] Barnes P. E., 2012, “Design of a Modular Human Exoskeleton Torso,” University of California, Berkeley.

[64] “Spring Clutches,” Tiny-Clutch Helander Products, Inc. [Online]. Available: http://www.tinyclutch.com/spring-clutches/.

[65] “Spring Clutches,” Tiny-Clutch Helander Products, Inc.

[66] Burr A. H., and Cheatham J. B., 1995, Mechanical Analysis and Design, Prentice-Hall, Inc., Upper Saddle River, NJ.

[67] Wiebusch C. F., 1939, “The Spring Clutch,” Trans. ASME, **61**, pp. A103–A108.

[68] Kaplan J., and Marshall D., 1956, “Spring Clutches,” Machine Design, **28**, pp. 107–111.

[69] Wahl A. M., 1940, “Discussion of Wiebusch’s Paper,” Trans. ASME, **62**, pp. A89–A91.

[70] Irby S. E., Kaufman K. R., Wirta R. W., and Sutherland D. H., 1999, “Optimization and application of a wrap-spring clutch to a dynamic knee-ankle-foot orthosis.,” IEEE transactions on rehabilitation engineering : a publication of the IEEE Engineering in Medicine and Biology Society, **7**(2), pp. 130–4.

[71] Kish J., 1977, Helicopter Freewheel Unit Design Guide, Stratford.

[72] Shigley J. E., and Mischke C. R., 2001, Mechanical Engineering Design, McGraw-Hill, New York.

[73] Veneman J. F., Kruidhof R., Hekman E. E. G., Ekkelenkamp R., Van Asseldonk E. H. F., and van der Kooij H., 2007, "Design and evaluation of the LOPES exoskeleton robot for interactive gait rehabilitation.," IEEE transactions on neural systems and rehabilitation engineering : a publication of the IEEE Engineering in Medicine and Biology Society, **15**(3), pp. 379–86.

[74] Seroussi R., and Gitter A., 1996, "Mechanical work adaptations of above-knee amputee ambulation," Archives of physical …, **77**(November).

[75] Ace Wire Spring and Form Company, 2005, "Properties of Common Spring Materials," **30**(207) [Online]. Available: http://www.tribology-abc.com/calculators/properties_of_common_spring_materials.pdf. [Accessed: 12-May-2013].

[76] Hwang D.-H., and Zum Gahr K.-H., 2003, "Transition from static to kinetic friction of unlubricated or oil lubricated steel/steel, steel/ceramic and ceramic/ceramic pairs," Wear, **255**(1-6), pp. 365–375.

[77] McKinley S., 2012, "Design and Control of a Continuously Variable Brake for use in an Assistive Orthotic Device," University of California at Berkeley.

[78] Komvopoulos K., 1998, Fundamentals of Tribology and Contact Mechanics, University of California, Berkeley, Berkeley.

[79] Irby S., and Kaufman K., 2004, "Electromechanical joint control device with wrap spring clutch," US Patent 6,834,752.

[80] Chen E., and Elert G., 2004, "Coefficients of Friction for Steel" [Online]. Available: http://hypertextbook.com/facts/2005/steel.shtml. [Accessed: 24-Mar-2013].